Fall 2007

Mechanical integrity and behavior of thin films and their applications in MEMS

Gang Duan

Department: Mechanical and Aerospace Engineering

MECHANICAL INTEGRITY AND BEHAVIOR OF THIN FILMS AND THEIR APPLICATIONS IN MEMS

by

GANG DUAN

A DISSERTATION

Presented to the Faculty of the Graduate School of the

UNIVERSITY OF MISSOURI-ROLLA

In Partial Fulfillment of the Requirements for the Degree

DOCTOR OF PHILOSOPHY

In

MECHANICAL ENGINEERING

2007

_____	_____
K. T. Wan, Advisor	L. R. Dharani
_____	_____
K. Chandrashekhara	B. A. Miller

_____

M. N. Rahaman

PUBLICATION DISSERTATION OPTION

This dissertation consists of the following three papers that have been published or submitted as follows:

Pages 4-39 have been published in the ASME JOURNAL OF APPLIED MECHANICS (Vol. 74, 2007).

Pages 40-65 have been submitted for publication to the ASME JOURNAL OF APPLIED MECHANICS.

Pages 66-84 have been submitted for publication to the ASME JOURNAL OF APPLIED MECHANICS.

ABSTRACT

This dissertation, consisting of three papers, presents the mechanical integrity and behavior of thin films and their applications in Micro-electromechanical Systems (MEMS). In the first paper, a solid-mechanics model is derived for the electromechanical deformation of a thin film in a capacitive MEMS-RF-switch and the associated "pull-in" phenomenon for both a 1-D rectangular bridge and a 2-D axisymmetric plate. The ratio of film-pad gap to film thickness (g/h) is found to play a significant role in the device behavior. The proposed analytical solution has some advantages over the existing models in formulating the design criteria.

In the second paper, an elastic model is constructed to account for "pull-in" in terms of the applied voltage, the residual stress, and the film-pad gap for a 2-D axisymmetric film. The new model determines the validity range of the classical solution and accounts for the deviation for large elastic strain and high membrane stress. Both tensile and compressive residual stresses are allowed. New design criteria are derived for MEMS devices.

In the third paper, an elastic model is constructed to account for the phenomena for ranges of film-pad gap, residual stress, and fringing field effects for a 1-D rectangular bridge. The results compare favorably with finite element analysis (FEA) in the literature, and possess much advantage over other available closed-form solutions.

In Appendix A, a rigorous theoretical model is constructed for the contact mechanics of the transition from pre- to post- "pull-in" and the elastic recovery of the film at the removal of external electrostatic potential. The contact mechanics theory is extended for the design criteria of microstructure presented in Appendix B.

ACKNOWLEDGMENTS

I would like to give my thanks to two groups of people who have contributed much to me in the past four years during my doctoral program – those who helped me in my academic development, and those who helped me in my personal life.

First of all, I want to express my sincere gratitude to my advisor, Dr. Kai-tak Wan, for providing guidance and constant encouragement throughout the past four years during my PhD program. I will never forget the countless hours of discussions with Dr. Wan. He provided a good working environment and supported me in every aspect beyond my research. I also want to express my appreciation to group member Mr. Mingfung Wong's discussions and suggestions, and Dr. Nathan Ravi and Dr. Paul Hamilton from School of Medicine, Washington University in St. Louis, for guiding me to the biomechanics field. Appreciation is extended to my advisory committee members for their valuable time, efforts and review of this dissertation. In particular, Dr. Dharani taught me Fracture Mechanics and Fatigue Analysis at the beginning of my PhD program, which is useful to my later research; Dr. K. Chandrashekhara introduced me to the Finite Element Analysis; Dr. Miller and Dr. Rahaman gave me many useful suggestions during the preparation of this dissertation. Financial support from NSF CMS-0527912, University of Missouri Research Board (#2428), and Department of Mechanical and Aerospace Engineering are gratefully acknowledged.

Finally, I want to express my deep appreciation to my wife, Lan Ren, sisters, Benxia Duan, Bencui Duan, and Yan Duan, especially my parents, Xingwen Duan and Maozhen Zhang, for their endless encouragement, patience and support.

TABLE OF CONTENTS

Page

LIST OF ILLUSTRATIONS

LIST OF TABLES

INTRODUCTION

Electric actuated thin films are widely used in micro-electromechanical systems (MEMS) such as radio frequency switches (RF-switches), micro-pumps and valves, and electrostatic actuators. This dissertation will focus on the operation of a MEMS-RF-switch. In a typical MEMS-RF-switch, a mechanically suspended 1-D rectangular or 2-D axisymmetric thin film is pulled by an electrostatic voltage (V_0) applied to an electrode-pad directly underneath. When V_0 exceeds a certain "pull-in" threshold, V_0^*, the thin film makes direct contact with the pad so that either an "on" or "off" signal is induced, and when the voltage is removed, the thin film resumes its original undeformed configuration. To understand the device operation and to optimize the design parameters (e.g., dimension of the thin film), it is necessary to construct a rigorous elastic model for the electromechanical interaction.

One major difficulty in formulating the exact electromechanical behavior is the nonlinear governing solid-mechanics equation, which forbids an analytical solution. To simplify this problem, the classical "lumped model" in the literature assumes a rigid rectangular plate with one surface attached to an elastic recoil spring, while another surface interacts with a rigid substrate via the attractive electrostatic forces. This simple model predicts a "pull-in" deflection when the mid-span of the film deforms to reach 1/3 of the film-pad gap. More sophisticated closed-form models are available in the literature to account for the fringing field as a result of the finite thin film width (1-D rectangular case) and residual stress due to fabrication and operation. Other numerical approaches using variational method with series of predetermined orthogonal trial functions and finite element analysis (FEA) are devised to solve for the device "pull-in" voltage.

Several limitations are noted: (i) all these solutions in literature are inconsistent with one another, because some models are based on pure plate-bending of the thin film, some on pure membrane-stretching and some on some well-defined mathematical functions, (ii) the thin film profile takes on a fixed shape that is unable to account for changes due to mixed plate-bending and membrane-stretching, (iii) the numerical procedures must be repeated for new design in device geometry and dimension, and (iv) the coupled electromagnetic and mechanical parameters do not lead to well-defined design criteria.

In this dissertation, the electromagnetic and mechanical components of the MEMS-RF-switch are decoupled based on an assumption that the electrostatic field in the narrow film-pad gap is uniform, resulting in an exact analytical solution. The new solution is capable of formulating new design criteria, as the film dimensions vary over wide ranges of thickness and span. The critical operational parameters, such as pull-in voltage and critical film-pad gap, are also derived. Deviation resulting from the uniform field assumption is assessed. The fringing field effects due to finite film width are considered (1-D rectangular case).

It is common for thin films to suffer from tensile / compressive residual stress during device fabrication and operation due to mismatch of the thermal expansion coefficients of the film and the substrate. Extreme residual stresses in thin films can lead to buckling, cracking, and even failure of the device. In this dissertation, the “pull-in” phenomena for a 1-D rectangular or a 2-D axisymmetric thin film are also derived incorporating the intrinsic film tensile / compressive membrane stress. The results are useful in formulating design criteria and in assessing the device performance.

When the applied electrostatic potential exceeds a certain threshold, V_0^*, the film makes direct contact with the pad, leading to "pull-in" or an "on" state. If the applied electrostatic potential is turned off, the thin film is supposed to return its undeformed shape or "off" state. But the thin film may adhere to the pad even without the external electric field due to the van der Waals interactions, stray charges left at the interface, and meniscus formation due to water condensation. In this dissertation, a rigorous theoretical model is constructed for the contact mechanics of the transition from pre- to post- "pull-in" and the elastic recovery of the film at the removal of external electrostatic potential. A critical film-pad gap, g/h, is determined to prevent device stiction failure. The theoretical results have significant impacts on the design and fabrication of many MEMS devices and nano structures.

PAPER I

Analysis of 1-D and 2-D Thin Film "Pull-in" Phenomena under the Influence of an Electrostatic Potential

Gang Duan and Kai-Tak Wan

Mechanical Engineering, University of Missouri-Rolla, Rolla, MO 65409-0050

Abstract

A thin 1-D rectangular or 2-D axisymmetric film is clamped at the perimeter. In the presence of an electrostatic potential (V_0^*) applied to a pad directly underneath the film leads to a "pull-in" phenomenon. The electromagnetic energy stored in the capacitive film-pad dielectric gap is decoupled from the mechanical deformation of the film using the Dugdale-Barenblatt-Maugis cohesive zone approximation. The ratio of film-pad gap (g) to film thickness (h), or, (g / h), is found to play a crucial role in the electromechancial behavior of the film. Solution spanning a wide range of (g/h) is found such that $V_0^* \propto (g/h)^{3/2}$ for (g/h) < 0.5 and $V_0^* \propto (g/h)^{5/2}$ for (g/h) > 5. The new model leads to new design criteria for MEMS-RF-switches.

Keywords: MEMS, RF-switch, electrostatic potential, surface forces, pull-in phenomena

1. Introduction

When a thin film clamped at the perimeter is subjected to an external force (e.g. electrostatic potential, long-range intersurface forces), "pull-in" occurs when a tunable

surface force reaches a threshold or when the film is brought into close proximity of a substrate. There are numerous applications of this phenomenon, e.g. micro-actuators [1, 2], micro-pumps [3-5], and strain gauges [6]. In this paper, we will focus on the operation of a MEMS device and will allude to measurement of the range and magnitude of intersurface forces. In a typical MEMS-RF-switch, a mechanically suspended bridge is pulled by an electrostatic voltage (V_0) applied to an electrode-pad directly underneath (Figure 1) [7-11]. When V_0 exceeds a certain "pull-in" threshold, V_0^*, the bridge makes direct contact with the pad so that either an "on" or "off" signal is induced; and when the voltage is removed, the bridge resumes its original undeformed configuration that induces the complementary signal. Note that the electrode-pad falls short of the bridge span in virtually all actual RF-switches, but the assumption of the same length is the most common adopted by literature. There is also a 2-D version of this switch where a circular bridge is clamped at the perimeter. To understand the device operation and to optimize the design parameters (e.g., dimension of the bridge), it is necessary to construct a rigorous elastic model for the electromechanical interaction.

The rudimentary "lumped model" assumes a rigid rectangular plate with one surface attached to an elastic recoil spring while another surface interacts with a rigid substrate via the attractive electrostatic forces. This simple parallel-plate capacitor model predicts a "pull-in" event (i.e. a spontaneous collapse of the bridge onto the electrostatic pad) to occur when the mid-span of the bridge reaches 1/3 of the bridge-pad gap [12, 13]. More sophisticated models become available recently to account for the fringing field as a result of the finite bridge width, residual stress due to fabrication and thermal expansion, and inclusion of air-cushion etc [14-16]. One major difficulty in formulating the exact

electro-mechanical behavior is the *nonlinear* governing solid-mechanics equation which forbids an analytical solution. In the literature, numerical approaches using variational method with series of predetermined orthogonal trial functions and finite element analysis (FEA) are devised to solve for the bridge profile and the associated device behavior [2, 12, 13, 15, 17, 18]. Several limitations are noted: (i) these solutions do not agree with one another, because some models are based on pure plate-bending of the bridge, some on pure membrane-stretching and some on some well-defined mathematical functions, (ii) since the normalized bridge profile takes on a fixed shape that is unable to account for changes due to mixed plate-bending and membrane-stretching, (iii) the numerical routine must be repeated for new design in device geometry and dimension, (iv) the coupled electromagnetic and mechanical parameters do not lead to well defined design criteria. A latest approach [19] is to adopt the Galerkin method where the electrostatic potential is expressed in a Taylor series with the terms higher than w^4 ignored. The method is also limited to a specific set of dimension and working parameters and might need to be repeated to cover a range of bridge stiffness and thickness. A comparison between the Galerkin method and our new model will be discussed.

In this paper, the electromagnetic and mechanical components will be *decoupled* based on an assumption that the electrostatic field in the bridge-pad gap is uniform, resulting in an *exact* analytical solution. Despite the inevitable inaccuracy involved, the new solution is capable of formulating new design criteria as the bridge gets thinner and shorter. The critical operational parameters such as pull-in voltage and critical bridge-pad gap will also be derived. Deviation resulting from the uniform field assumption will be

assessed. Edge effects due to finite bridge width and anticlastic deformation are also ignored. The 1-D model will be extended to 2-D.

2. Theory

Figure 1 shows a rectangular bridge mechanically clamped at the two opposite ends and suspended above an electrostatic pad which is a distance, g, below and has identical length as the bridge. The bridge is assumed to be free of pre-stress or residual stress and possesses a unit width, length, 2ℓ, thickness, h, elastic modulus, E, Poisson's ratio, ν, and flexural rigidity, $\kappa = Eh^3/12(1-\nu^2)$. An electrical potential, V_0, is applied to the pad to set up a uniform electric field. The bridge is compelled and deformed by bending and a longitudinal membrane stress, σ, to a profile, $w(x)$, governed by the classical von Karman equation [20, 21]:

$$\underbrace{\underbrace{-\kappa\,\nabla^4 w}_{\substack{\text{Plate-}\\\text{bending}}} + \underbrace{(\sigma h)\,\nabla^2 w}_{\substack{\text{Membrane-}\\\text{stretching}}}}_{\text{Mechanical deformation}} = \underbrace{-\left(\frac{\varepsilon_0 V_0^{\,2}}{2}\right)\frac{1}{(g-w)^2}}_{\text{Electrostatic force}} \qquad (1)$$

where ε_0 is the permittivity of free space, and ∇^2 is the Laplacian operator in the rectilinear or curvilinear coordinate systems. The right hand side of (1) denotes the electrostatic force on the bridge, while the left hand side represents the mechanical response of the bridge in terms of the two deformation modes of plate-bending and membrane-stretching. Since $w(x)$ appears on both sides of (1), the coupled electro-mechanical equation leads to nonlinearity and thus forbids an analytical solution. To decouple the two components, the Dugdale-Barenblatt-Maugis cohesion zone approximation [22] is adopted here. The electrostatic force is replaced by a uniform

mechanical pressure, p, which is related to the applied voltage by averaging the traction over the bridge span. Equation (1) will first be solved for a 1-D rectangular switch, followed by an extension to a 2-D axisymmetric film where (1) remains valid for the radial profile, $w(r)$.

2.1. A 1-D rectangular switch

For a 1-D switch, a rectangular film is clamped at the opposite ends. A set of normalized parameters is defined in Table 1. Note that β gauges the ratio of membrane stress to film rigidity such that (i) $\beta \approx 0$ corresponds to a plate-bending dominant deformation in a thick and stiff bridge and (ii) $\beta \to \infty$ refers to membrane-stretching dominant deformation in a thin and flexible bridge. A few boundary conditions are noted:

(i) At the clamped ends, $w_{x=0} = 0$, or, $\omega_{\xi=0} = 0$;

$(\partial w/\partial x)_{x=0} = 0$, or, $(\partial \omega/\partial \xi)_{\xi=0} = 0$;

(ii) At the center, $(\partial w/\partial x)_{x=\ell} = 0$, or, $(\partial \omega/\partial \xi)_{\xi=1} = 0$.

Applying the cohesive zone approximation, (1) becomes

$$-\kappa \nabla^4 w + (\sigma h) \nabla^2 w = -p, \quad \text{or,} \quad \frac{d^4\omega}{d\xi^4} - \beta^2 \frac{d^2\omega}{d\xi^2} = \rho \tag{2}$$

with the equivalent pressure

$$p = \frac{\varepsilon_0 V_0^2}{4\ell} \int_0^{2\ell} \frac{1}{[g - w(x)]^2}\, dx, \quad \text{or,} \quad \rho = \upsilon_0^2 \int_0^1 \frac{1}{[\gamma - \omega(\xi)]^2} d\xi \tag{3}$$

Equation (2) can be reduced to a second order linear differential equation [23] that leads to an *exact* analytical bridge profile

$$\omega = \rho\left(\frac{1}{\beta^3}\right)\left\{\frac{1}{\tanh\beta}[\cosh(\beta\xi)-1]-\sinh(\beta\xi)+\beta\left(\xi-\frac{\xi^2}{2}\right)\right\} \tag{4}$$

with a central deflection, $\omega_0 = \omega(\xi=1)$,

$$\omega_0 = \rho\left(\frac{1}{\beta^3}\right)\left\{\frac{1}{\tanh\beta}(\cosh\beta-1)-\sinh\beta+\frac{\beta}{2}\right\} \tag{5}$$

Note that (4) is a rigorous solution of (2), rather than a pre-determined profile as in most variational methods in the literature (c.f. Table 3). Figure 2 shows the changing bridge profiles for a range of β. The volume of the reduced dielectric space between the bridge and pad is found by integrating (4),

$$V = \int_0^{2\ell} w\ dx, \quad \text{or,} \quad \vartheta = \int_0^1 2\omega\ d\xi\ = \rho\left(\frac{2}{\beta^4}\right)\left(1+\frac{\beta^2}{3}-\frac{\beta}{\tanh\beta}\right) \tag{6}$$

The uniform membrane stress on the bridge can be found by elementary elasticity [23, 24]

$$\sigma = \frac{1}{2\ell}\left(\frac{E}{1-\nu^2}\right)\int_0^{2\ell}\frac{1}{2}\left(\frac{dw}{dx}\right)^2 dx, \text{ or,} \quad \beta^2 = 6\int_0^1\left(\frac{\partial\omega}{\partial\xi}\right)^2 d\xi \tag{7}$$

Substituting (4) into (7) yields

$$\rho = \frac{\beta^4\sinh\beta}{\left[(6+\beta^2)\cosh(2\beta)-9\beta\cosh\beta\sinh\beta-6-4\beta^2\right]^{1/2}} \tag{8}$$

By eliminating β from (5) and (8), the mechanical response, $\rho(\omega_0)$ can be obtained, though it is a mathematically formidable task because of the transcendental functions sinh(*x*) and cosh(*x*). An alternative to derive the *exact* form of $\rho(\omega_0)$ is to trace a parametric plot of $\rho(\omega_0)$ by taking β as a varying parameter since both ρ and ω_0 are functions of β (Figure 3). The bending to stretching transition can be expressed in an alternative manner as

$$\rho = k(\beta)\,\omega_0^{\,n(\beta)} \tag{9}$$

where both $k(\beta)$ and $n(\beta)$ are well defined functions of β. If $\rho(\omega_0)$ is shown in a log-log plot, $n(\beta)$ is the gradient and is defined as

$$n = \frac{d(\log\rho)}{d(\log\omega_0)} = \frac{\omega_0}{\rho}\left(\frac{d\rho}{d\omega_0}\right) \tag{10}$$

The exact form of $n(\beta)$ can be found by Mathematica™, though it is too lengthy to be given here. Figure 4 shows n as a function of β with $1 \le n \le 3$.

Deformation of the bridge is bounded by two limiting cases. In case of a thick and stiff bridge, the deformation is small ($\omega_0 < 0.5$), the membrane stress is negligible ($\sigma \approx 0$ and $\beta \approx 0$), and only plate-bending is present. It can be easily shown that (4), (5), (6) and (10) reduce to $\omega_{bend} = (\rho/24)\,\xi^2(\xi - 2)^2$, $\rho = 24\omega_0$, $\vartheta = (16/15)\,\omega_0$, and $n = 1$ respectively, which is consistent with the classical Timoshenko's *linear* solution [24] shown in Figures 2-4 as asymptotes. In case of a thin and flexible bridge with a zero bending inertia ($\kappa = 0$), the deformation is large ($\omega_0 > 5$), the normalized membrane stress becomes infinite ($\beta \to \infty$) and only membrane-stretching is present. The bridge behavior now becomes $\omega_{stretch} = (\rho/\beta^2)(\xi - \xi^2/2)$, $\rho = 16\omega_0^3$, $\vartheta = (4/3)\,\omega_0$, and $n = 3$. Note that $\omega_{stretch}$ is parabolic such that $(\partial\omega/\partial\xi)_{\xi=1} = 0$ and $(\partial\omega/\partial\xi)_{\xi=0} \to \infty$, which violates boundary condition (i). However, a film with zero flexural rigidity does not require a differentiable profile at the clamped edges. Figures 2-4 show the membrane-stretching asymptotes. Note that $\rho(\omega_0)$ for membrane-stretching is *cubic* (Figure 3) and is consistent with our earlier results for rectangular film deformed by a central line load [23, 25]. When the deformation is intermediate ($0.5 < \omega_0 < 5$), mixed bending-stretching must be considered. The transition

can be arbitrarily taken as the intersection between the two limiting cases in Figure 3 and is roughly $\omega_0 \approx 1.20$. Here $1 < n < 3$ and $16/15 < (\vartheta/\omega_0) < 4/3$.

There are two ways to investigate the electromechanical behavior of the RF-switch: (i) The first and most common method is to balance the mechanical force due to bridge deformation (c.f. (5) and (8)) and the electrostatic attraction due to applied voltage (3), and (ii) a balance of electromagnetic and mechanical energy involved. The stretching limit is chosen in this section to demonstrate the general behavior that is applicable also to mixed bending-stretching films. Figure 5 shows the mechanical and electrostatic forces for a range of applied voltage. When the applied voltage increases from null, there are two distinct intersections between the force curves at A and B as shown. It will become apparent that A corresponds to a *stable* configuration while B is *unstable*. As υ_0 increases further, $(\omega_0)_A$ and $(\omega_0)_B$ move closer until they converge to C. Further increase in $\upsilon_0 > \upsilon_0^*$ (with the superscript asterisk denoting "pull-in" hereafter) leads to "pull-in", i.e. spontaneous collapse of the bridge onto the electrode-pad. The electromechanical force balance is maintained along path OAC.

The device behavior can be further scrutinized by a simple energy balance. The total energy of the system is given by $U_T = U_C - U_E$, where U_C and U_E are the energies stored in the capacitive dielectric medium at the bridge-pad gap and in the elastic bridge respectively,

$$U_E = -\int p\, dV\,, \qquad \text{or,} \qquad \Sigma_E = -\int_0^{\beta} \rho(\beta)\, \frac{\partial \vartheta}{\partial \beta}\, d\beta \tag{11}$$

$$U_C = -\frac{\varepsilon_0 V_0^2}{2} \int_0^{2\ell} \frac{1}{g - w(x)}\, dx\,, \quad \text{or,} \quad \Sigma_C = -2\upsilon_0^2 \int_0^1 \frac{1}{\gamma - \omega(\beta, \xi)}\, d\xi \tag{12}$$

Figure 6 shows the energetics of the device. Since the bridge is bounded by the gap, $0 \le w_0 \le g$, or, $0 \le (\omega_0/\gamma) \le 1$. As υ_0 increases from null, the bridge deforms. Therefore, both Σ_E and Σ_C are monotonic decreasing in (ω_0/γ), and $\Sigma_T = \Sigma_C - \Sigma_E$ is shown as OABC. At a non-zero υ_0, the bridge moves to a stable equilibrium at A where Σ_T is minimal. An unstable equilibrium is found at B. Figures 7a and 7b show $\Sigma_T(\omega_0)$ for a range of fixed υ_0 and $\Sigma_T(\upsilon_0, \omega_0)$ respectively. As υ_0 increases, $(\omega_0)_A$ and $(\omega_0)_B$ move close to each other and eventually merge at C corresponding to a neutral equilibrium. Further increase in υ_0 leads to "pull-in". Energy balance is maintained along path OAA′C. The branch CB′B is obtained mathematically but is inaccessible physically. The stable equilibrium at A can be found by putting $(\partial\Sigma_T / \partial\omega_0) = 0$ and $[\partial^2 \Sigma_T / \partial(\omega_0)^2] < 0$. At "pull-in" at C, $[\partial^2\Sigma_T / \partial(\omega_0)^2] = 0$, resulting in a point of inflexion. Exact solution for the pull-in parameters ω_0^* and υ_0^* can be derived for the limiting cases of bending and stretching only, while the mixed bending-stretching behavior requires numerical integration.

The switch behavior depends significantly on the bridge-pad gap. Figure 8 shows (ω_0^*/γ) as a function of the bridge-pad gap γ. In theory, the force and energy balance should yield identical results. However, the cohesive zone approximation leads to a small inconsistency as shown in the shaded region, which cannot be resolved by the present model. Pull-in is expected anywhere within this zone. In fact, Figure 5 shows $\upsilon_0^* = 1.02$ (force balance) while Figure 7 shows $\upsilon_0^* = 0.92$ (energy balance) for the stretching limit. A bending-stretching transition occurs roughly at $g \approx 1.2\ h$, i.e. when the bridge-pad gap is twice the bridge thickness. A thick and stiff bridge combined with a small gap with $g < 0.5\ h$ leads to a bending dominant mode, while a thin (and flexible) bridge with a large

gap with $g > 5h$ leads to a stretching dominant behavior. Bridges with the intermediate thickness and gap ($0.5\ h < g < 5\ h$) requires the full bending-stretching solution. Force balance requires $0.455 \le (w_0^*/g) \le 0.679$ and energy balance requires $0.397 \le (w_0^*/g) \le 0.658$, with the lower and upper limits referring to the pure bending and pure stretching modes, respectively.

Figure 9 shows the pull-in voltage υ_0^* as a function of the bridge-pad gap. It can be easily shown that $\upsilon_0^* \propto \gamma^{3/2}$ in the plate-bending limit and $\upsilon_0^* \propto \gamma^{5/2}$ in the membrane-stretching limit. A small difference between force and energy balances is found as shown by the narrow shaded strip. In the bending limit, $\upsilon_0^* = 2.342\ \gamma^{3/2}$ (force balance) and $\upsilon_0^* = 2.101\ \gamma^{3/2}$ (energy balance). In the stretching limit, $\upsilon_0^* = 1.023\ \gamma^{5/2}$ (force balance) and $\upsilon_0^* = 0.916\ \gamma^{5/2}$ (energy balance). Bending-stretching transition occurs roughly at $g \approx 2.5\ h$ when the limiting cases intersect.

2.2. A 2-D axisymmetric switch

Figure 10 shows a 2-D axisymmetric MEMS-RF-switch clamped at the circular perimeter. The set of normalized parameters is redefined as in Table 2. The elastic deformation equation (1) remains valid, though the exact solution to the axisymmetric problems requires a nonlinear von Karman equation in cylindrical coordinates to be solved. To avoid the mathematical complexity, an average stress approximation is adopted (i.e. $\sigma = \sigma_r = \sigma_t$) in association with the cohesive zone approximation. The boundary conditions are given by:

(iii) At the clamped circumference, $w_{r=a} = 0$, or, $\omega_{\xi=1} = 0$;

$(\partial w/\partial r)_{r=a} = 0$, or, $(\partial \omega/\partial \xi)_{\xi=1} = 0$;

(iv) At the center, $(\partial w/\partial r)_{r=a} = 0$, or, $(\partial \omega/\partial \xi)_{\xi=1} = 0$.

Equation (1) is reduced to the modified Bessel equation [23] with the profile gradient given by

$$\xi^2 \frac{d^2\theta}{d\xi^2} + \xi \frac{d\,\theta}{d\xi} - \left(1+\beta^2\xi^2\right)\theta = \rho\,\xi^3 \tag{13}$$

with the apparent mechanical pressure on the film is given by

$$p = \frac{\varepsilon_0 V_0^2}{2\pi a^2} \int_0^a \frac{2\pi r}{[g - w(r)]^2}\, dr, \quad \text{or,} \quad \rho = \upsilon_0^2 \int_0^1 \frac{\xi}{[\gamma - \omega(\xi)]^2}\, d\xi \tag{14}$$

Equation (14) can be solved analytically to yield the film profile

$$\omega = \rho \left(\frac{1}{\beta^3 I_1(\beta)}\right)\left\{\frac{\beta}{2}\left(1-\xi^2\right) I_1(\beta) + I_0(\beta\xi) - I_0(\beta)\right\} \tag{15}$$

with a central deflection, $\omega_0 = \omega(\xi = 0)$,

$$\omega_0 = \rho \left(\frac{1}{\beta^3 I_1(\beta)}\right)\left\{\frac{\beta}{2} I_1(\beta) - I_0(\beta) + 1\right\} \tag{16}$$

The corresponding average membrane stress is given by

$$\sigma = \frac{1}{2a^2}\left(\frac{E}{1-\nu^2}\right) \int_0^a \left(\frac{dw}{dr}\right)^2 r\,dr, \text{ or,} \quad \beta^2 = 6\int_0^1 \left(\frac{\partial\omega}{\partial\xi}\right)^2 \xi\, d\xi \tag{17}$$

which yields a relation between pressure and membrane stress

$$\rho = \frac{\beta^{7/2} I_1(\beta)}{\{(9\beta/2)\, I_1(\beta)^2 - 3I_2(\beta)\, [\beta\, I_0(\beta) + 4I_1(\beta)]\}^{1/2}} \tag{18}$$

The volume of the reduced dielectric space is found to be

$$V = \int_0^a w\; 2\pi r\, dr, \quad \text{or,} \qquad \vartheta = \int_0^1 2\omega\xi\; d\xi \tag{19}$$

The mechanical response, $\rho(\omega_0)$, can be obtained by eliminating β from (16) and (18). The bending to stretching transition $\rho = k(\beta)\,\omega_0^{n(\beta)}$ is similar to the 1-D counterpart with $1 \le n \le 3$. The limiting plate-bending solution becomes $\omega_{bend} = (\rho/32)(1-\xi^2)^2$, $\rho = 32\omega_0$, $n = 1$, and $\vartheta = (1/3)\,\omega_0$. The limiting membrane-stretching solution becomes $\omega_{stretch} = (\rho/2\beta^2)(1-\xi^2)$, $\rho = 12\omega_0^3$, $n = 3$, and $\vartheta = (1/2)\,\omega_0$.

The energetics and "pull-in" phenomenon for a 2-D film is derived by the similar energy balance method as in the 1-D model. Figures 11a and 11b show $\Sigma_T(\omega_0)$ for a range of fixed υ_0 and $\Sigma_T(\upsilon_0, \omega_0)$ respectively. The trajectory OAA′C traces the energy balance locus, and "pull-in" occurs at C. Figure 12 shows (ω_0^*/γ) as a function of γ. A shaded region of uncertainty is found because of the discrepancies due to the average membrane stress approximation and the cohesive zone approximation. Figure 13 shows $\upsilon_0^*(\gamma)$. Similar to the 1-D model, $\upsilon_0^* \propto \gamma^{3/2}$ is expected in the bending limit and $\upsilon_0^* \propto \gamma^{5/2}$ in the stretching limit. In summary, $\upsilon_0^* = 4.483\,\gamma^{3/2}$ (force balance) and $\upsilon_0^* = 3.773\,\gamma^{3/2}$ (energy balance) in the bending limit ($\gamma < 2$); $\upsilon_0^* = 1.591\,\gamma^{5/2}$ (force balance) and $\upsilon_0^* = 1.338\,\gamma^{5/2}$ (energy balance) in the stretching limit ($\gamma > 4$); and the bending-stretching transition at $\gamma \approx 3$.

3. Discussion

A solid-mechanics model is derived for the electromechanical deformation of a bridge in a capacitive MEMS-RF-switch and the associated "pull-in" phenomenon for both 1-D and 2-D. The analytical solution has some advantages over the existing models in formulating the design criteria. Firstly, the combinatorial influences on the device are

derived analytically [26] in terms of (i) materials parameters: elastic modulus, Poisson ratio, and flexural rigidity of bridge; (ii) geometrical parameters: bridge-pad gap separation, bridge length and thickness; and (iii) structural index: mixed bending-stretching deformation, and the limiting cases of pure bending and pure stretching. Secondly, the ratio of gap to bridge thickness (g / h) is found to play a critical role in determining the pull-in voltage. The relations for a bending bridge ($\upsilon_0^* \propto \gamma^{3/2}$) and a stretching bridge ($\upsilon_0^* \propto \gamma^{5/2}$) are crucial in designing the device and assessing the performance, especially when the device dimensions shrink from micro- (MEMS) to nano- scale (NEMS). Note that the actual (g / h) ratio in most actual devices falls in the range of 0.5 to 5. The pull-in voltage in the plate-bending limit is consistent with literature [17, 27], but the bending-stretching transition and the stretching limit are virtually unavailable in current literature. Table 3 compares the present work with various existing models. It is remarkable that the celebrated lumped model predicts the smallest (w_0^*/g) = 1/3 and predicts "pull-in" to occur before the actual critical applied voltage is reached. Our new model essentially covers the entire range of literature values (besides the lumped model) and shows bending-stretching transition is the main cause of inconsistencies in the literature values. Most existing models do not allow bridge profile change (w/w_0) as the gap widens and are therefore incapable of predicting the bending-stretching in the electromechanical behavior. Thirdly, when an AC voltage is applied to the electrode-pad, the resonance frequency of the bridge is determined by the governing constitutive relation, $\rho \propto (\omega_0)^n$, with $n = 1$ for thick and stiff bridge and $n = 3$ for thin and flexible bridge. In the linear bending region, resonance can be investigated using the simple harmonic motion equation, but deviation is expected as the gap widens. For

instance, the non-linear van der Pol equation will be needed to solve for $n = 3$ [28]. Failure to realize the bending-stretching transition in design will undermine the device performance.

The present model can be extended to include other important parameters not covered above. For instance, residual stress (σ_0) due to thermal mismatch is inevitable during device fabrication and operation. To accommodate its effect, the total membrane stress in equation (1) is rewritten as $\sigma = \sigma_0 + \sigma_m$ where σ_m is the concomitant stress due to change in bridge profile. Similarly, σ in equation (7) will be replaced by σ_m. The new constitutive relation and the subsequent pull-in parameters will yield useful information for switch design and can be checked against literature (e.g. [18, 19]), though it is beyond the present scope. Another interesting extension is that of "pull-off". When the electrostatic potential is turned off, the bridge adhered to the pad is expected to detach from the substrate and resume its undeformed geometry reversibly. However, in the presence of undesirable intersurface forces (e.g., capillary at high relative humidity, stray charges on surfaces), the bridge must overcome the energy barrier in order to delaminate from the substrate. The thin film delamination mechanics can be obtained using the present model. In fact, we have investigated the delamination mechanics of a clamped circular film earlier for an ideal zero-range surface force, and derived the critical mechanical force, bridge-pad gap and radius at "pull-off" [29]. The model can be modified to allow transformation from 2-D to 1-D.

Another related area alluded in Introduction is the measurement of long-range intrinsic surface forces such as van der Waals potentials, stray charges left at the interface etc. Such interactions can be incorporated into the present model by assigning an extra

term on the right hand side of (1) according to the Dugdale-Barenblatt-Maugis cohesive zone theory. In an earlier paper, we reported how a small graphite cylinder compelled a clamped silicone film into adhesive contact by means of a long-range surface force [30]. A solid-mechanics model was also constructed to account for the subsequent delamination and "pull-off". The present theoretical model here presents a thorough analysis for the "pull-in" event *prior* to the adhesion contact between the two adherends, and is capable of analyzing the magnitude and range of surface forces involved. Since the intersurface force potential is not tunable as the MEMS switch but a fixed function depending on the materials nature and the dielectric gap, one necessary modification to the present model is to allow the film-substrate gap to vary. Detailed analysis is beyond the scope of the present work.

4. Conclusion

Understanding the performance of a MEMS-RF-switch in terms of the device geometry, materials and structure is crucial in design criteria. In this study, a rigorous analytical elastic model is derived to account for the bridge deformed geometry and its effects on the pull-in voltage and other pull-in parameters. The ratio of bridge-pad gap to bridge thickness (g/h) is found to play a significant role in the device behavior.

Acknowledgements

Supports from NSF CMS-0527912 and University of Missouri Research Board (#2428) are gratefully acknowledged.

References

1. F. Najar, S. Choura, S. El-Borgi, E. Adbdel-Rahman and A. Nayfeh, "Modeling and design of variable-geometry electrostatic microactuators," *Journal of Micromechanics and Microengineering* **15**, 419-429, 2005.
2. G. Vogl and A. Nayfeh, "A reduced-order model for electrically actuated clamped circular plates," *Journal of Micromechanics and Microengineering* **15**, 684-690, 2005.
3. T.-B. Xu and J. Su, "Development, characterization, and theoretical evaluation of electroactive polymer-based micropump diaphragm," *Sensors and Actuators A* **121**, 267-274, 2005.
4. A. M. Prochaska, Y. Nemirovsky and U. Dinnar, "A membrane micropump electrostatically actuated across the working fluid," *Journal of Micromechanics and Microengineering* **15**, 2309-2316, 2005.
5. A. Ullmann, I. Fono and Y. Taitel, "A piezoelectric valve-less pump - dynamic model," *Journal of Fluids Engineering* **123**, 92-98, 2001.
6. W. K. Schomburg, Z. Rummler, P. Shao, K. Walff and L. Xie, "The design of metal strain gauges on diaphragms," *Journal of Micromechanics and Microengineering* **14**, 1101-1108, 2004.
7. J. Elders, V. Spiering and S. Walsh, "Microsystems Technology (MST) and MEMS applications: an overview," *Microelectromechanical Systems: Technology and Applications* **26** [4], 312-317, 2001.
8. G. M. Rebeiz and J. B. Muldavin, "RF MEMS switches and switch circuits," *IEEE Microwave Magazine* **2**, 59-71, 2001.
9. P. Osterberg and S. Senturia, "M-Test: a test chip for MEMS material property

measurement using electrostatically actuated test structures," *Journal of Microelectromechanical Systems* **6**, 107-118, 1997.

10. Y. Nemirovsky, "A methodology and model for the pull-in parameters of electrostatic actuators," *Journal of Microelectromechanical Systems* **10**, 601-615, 2001.
11. S. Chowdhury, M. Ahmadi and W. Miller, "A closed-form model for the pull-in voltage of electrostatically actuated cantilever beams," *Journal of Micromechanics and Microengineering* **15**, 756-763, 2005.
12. L. A. Rocha, E. Cretu and R. F. Wolffenbuttel, "Behavioural analysis of the pull-in dynamic transition," *Journal of Micromechanics and Microengineering* **14**, S37-S42, 2004.
13. X. Rottenberg, S. Brebels, W. De_Raedt, B. Nauwelaers and H.A.C. Tilmans, "RF-power: driver for electrostatic RF-MEMS devices," *Journal of Micromechanics and Microengineering* **14**, S43-S48, 2004.
14. M. Gretillat, F. Gretillat and N. Rooij, "Micromechanical relay with electrostatic actuation and metallic contacts," *Journal of Micromechanics and Microengineering* **9**, 324-331, 1999.
15. C. O'Mahony, M. Hill, R. Duane and A. Mathewson, "Analysis of electromechanical boundary effects on the pull-in of micromachined fixed-fixed beams," *Journal of Micromechanics and Microengineering* **13**, S75-S80, 2003.
16. H. Lee, R. A. Coutu_Jr, S. Mall and P. E. Kladitis, "Nanoindentation technique for characterizing cantilever beam style RF microelectromechanical systems (MEMS) switches," *Journal of Micromechanics and Microengineering* **15**, 1230-1235, 2005.
17. H. Rong, Q.-A. huang, M. Nie and W. Li, "An analytical model for pull-in voltage of

clamped-clamped multilayer beams," *Sensors and Actuators A* **116**, 15-21, 2004.

18. B. Schauwecker, J. Mehner, K.M. Strohm, H. Haspeklo and J.-F. Luy, "Investigations of rf shunt airbridge switches among idfferent environmental conditions," *Sensors and Actuators A* **114**, 49-58, 2004.
19. Y. Zhang and Y.-p. Zhao, "Numerical and analytical study on the pull-in instability of microstructure under electrostatic loading," *Sensors and Actuators A* **127**, 366-380, 2006.
20. P. L. Gould, *Analysis of Shells and Plates*, New York, Springer, 1988.
21. R. Gupta, *Electrostatic pull-in test structure design for in-situ mechanical property measurements of Micro-Electro-Mechanical Systems (MEMS), Ph.D. Thesis, MIT, USA*, 1997.
22. D. Maugis, *Contact, Adhesion and Rupture of Elastic Solids*, New York, Springer, 2000.
23. K.-T. Wan and J. Duan, "Adherence of a rectangular flat punch onto a clamped plate-Transition from a rigid plate to a flexible membrane," *Journal of Applied Mechanics* **69**, 104-109, 2002.
24. S. P. Timoshenko and S. Woinowsky-Krieger, *Theory of Plates and Shells*, 2nd ed. New York, McGraw-Hill, 1959.
25. K.-T. Wan, "Fracture mechanics of a V-peel adhesion test - Transition from a bending plate to a stretching membrane," *Journal of Adhesion* **70**, 197-207, 1999.
26. M. F. Ashby, *Materials selection in mechanical design*, 3rd ed. Woburn, MA, Butterworth- Heinemann, 2005.
27. M. R. Begley, "The impact of materials selection and geometry on multi-functional

bilayer micro-sensors and actuators," *Journal of Micromechanics and Microengineering* **15**, 2379-2388, 2005.

28. J. Stoker, *Nonlinear vibrations in mechanical and electrical systems*, New York, Wiley-Interscience, 1992.
29. K.-T. Wan and L. Kogut, "The coupling effect of interfacial adhesion and tensile residual stress on a thin membrane adhered to a flat punch," *Journal of Micromechanics and Microengineering* **15**, 778-784, 2005.
30. B. F. Ju, K.-T. Wan and K. K. Liu, "Indentation of a square elastomeric thin film by a flatended cylindrical punch in the presence of long-range intersurface forces," *Journal of Applied Physics* **96** [11], 6159-6163, 2004.

Table 1. Normalized parameters for the 1-D model.

Coordinates and profile	$\xi = \left(\frac{1}{\ell}\right)x,\ \omega = \left(\frac{1}{h}\right)w,\ \omega_0 = \left(\frac{1}{h}\right)w_0,\ \vartheta = \left(\frac{1}{h\ell}\right)V$
Device geometry (bridge-pad gap)	$\gamma = \left(\frac{1}{h}\right)g$
Electrostatic potential (applied voltage)	$\upsilon_0 = \left(\frac{\varepsilon_0 \ell^4}{2\kappa h^3}\right)^{1/2} V_0,$
Membrane stress	$\beta = \left(\frac{\ell^2 h}{\kappa}\right)^{1/2} \sigma^{1/2}$
Mathematical equivalent pressure	$\rho = \left(\frac{\ell^4}{\kappa h}\right)p$
Energies involved	$\Sigma_E = \left(\frac{\ell^3}{\kappa h^2}\right)U_E,\ \Sigma_C = \left(\frac{\ell^3}{\kappa h^2}\right)U_C,\ \Sigma_T = \left(\frac{\ell^3}{\kappa h^2}\right)U_T$

Table 2. Normalized parameters for the 2-D model.

Coordinates and profile	$\xi = \left(\frac{1}{a}\right)r, \omega = \left(\frac{1}{h}\right)w, \omega_0 = \left(\frac{1}{h}\right)w_0, \vartheta = \left(\frac{1}{\pi a^2 h}\right)V$
Device geometry (film-pad gap)	$\gamma = \left(\frac{1}{h}\right)g$
Electrostatic potential (applied voltage)	$\upsilon_0 = \left(\frac{\varepsilon_0 a^4}{2\kappa h^3}\right)^{1/2} V_0$
Membrane stress	$\beta = \left(\frac{a^2 h}{\kappa}\right)^{1/2} \sigma^{1/2}$
Equivalent pressure	$\rho = \left(\frac{a^4}{2\kappa h}\right)p$
Energies involved	$\Sigma_E = \left(\frac{a^2}{2\pi\kappa h^2}\right)U_E, \Sigma_C = \left(\frac{a^2}{2\pi\kappa h^2}\right)U_C, \Sigma_T = \left(\frac{a^2}{2\pi\kappa h^2}\right)U_T$

Table 3. Comparison of the pull-in parameter (w_0^*/g).

Methods	**Pull-in (w_0^*/g)**
1-D and 2-D Lumped model [12, 13] Assumption: rigid plates with one attached to an elastic spring and another stationary	1/3 = 0.3333
1-D Variational method [15] Trial function: $\omega = \omega_0 \cos^2(\pi\xi)$	1/3 = 0.3333
1-D Variational method [18] Trial function: $\omega = \omega_0 \xi^2 (\xi - 1)^2$	~ 0.45
1-D Energy Method for multi-layered bridge [17] Trial function: $\omega = (\omega_0 / 2)\ [1 + \cos(2\pi\xi)]$	0.40 – 0.67
1-D Galerkin Method [19]	0.55 (zero residual stress) 0.42 – 0.63 (range of residual stress)
1-D Present Work	0.4545 – 0.6791 (Force balance) 0.3970 – 0.6583 (Energy balance)
2-D Variational Method [2] Trial function: $\omega = C_1 J_0(\Omega m^{1/2} r) + C_2 I_0(\Omega m^{1/2} r)$	~ 0.40
2-D Present Work	0.5723 – 0.7500 (Force balance) 0.4633 – 0.7135 (Energy balance)

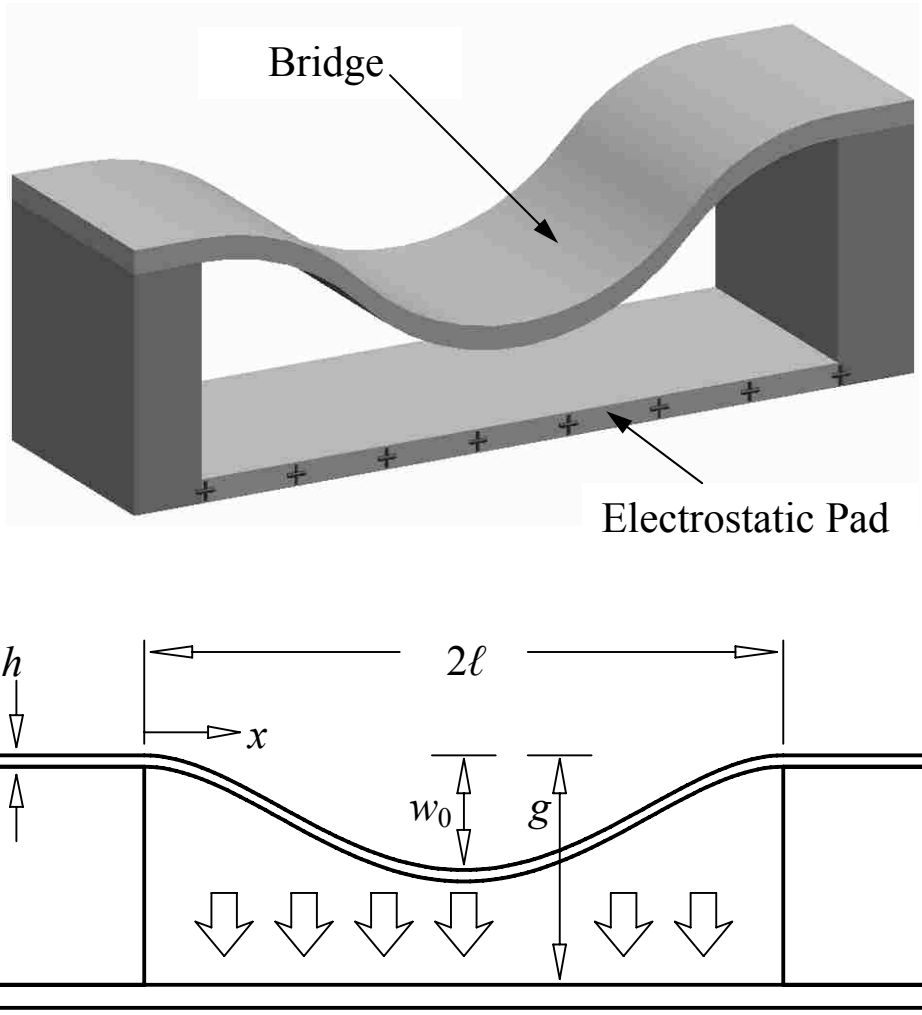

Figure 1 Sketch of a typical MEMS-RF-switch. The suspended bridge deforms in the presence of an electrostatic force induced by the electrode-pad directly underneath.

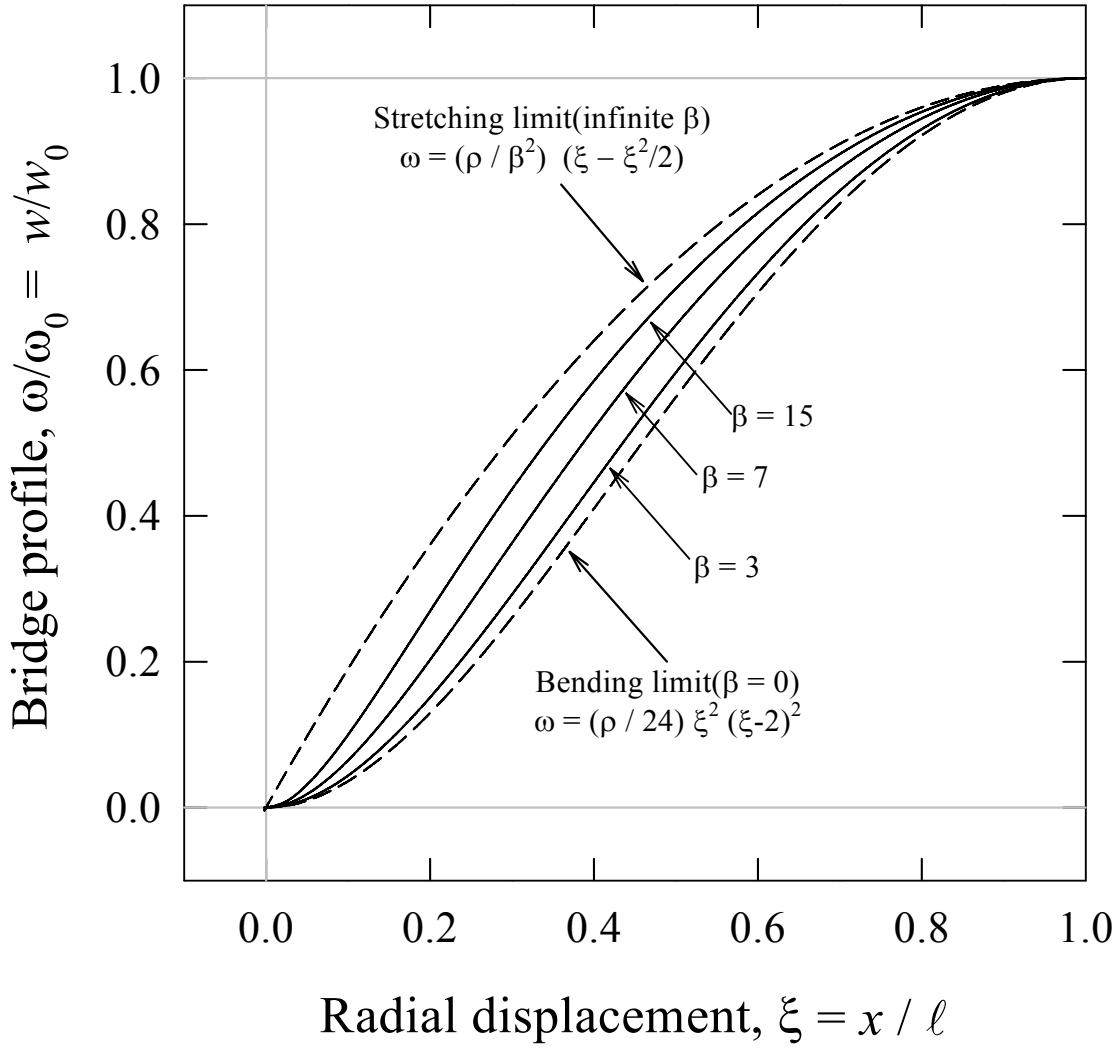

Figure 2 Normalized bridge deformed profile as a function of membrane stress. The bridge anchors at $\xi = 0$ and has its mid-span at $\xi = 1$. The dashed curves show the plate-bending and membrane-stretching limits.

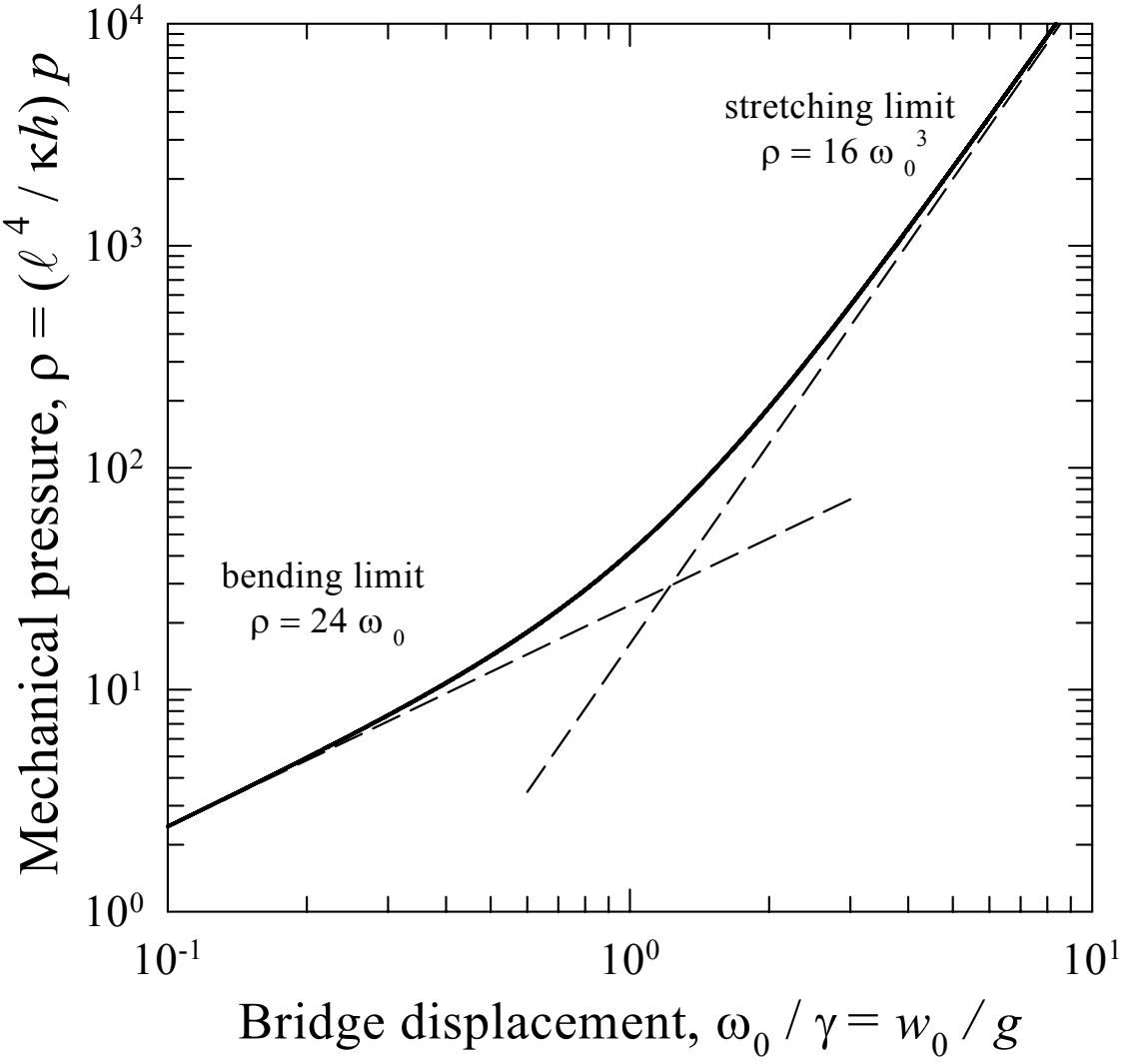

Figure 3 Mechanical response of the bridge under a uniform pressure across the span. The dashed curves show the plate-bending and membrane-stretching limits.

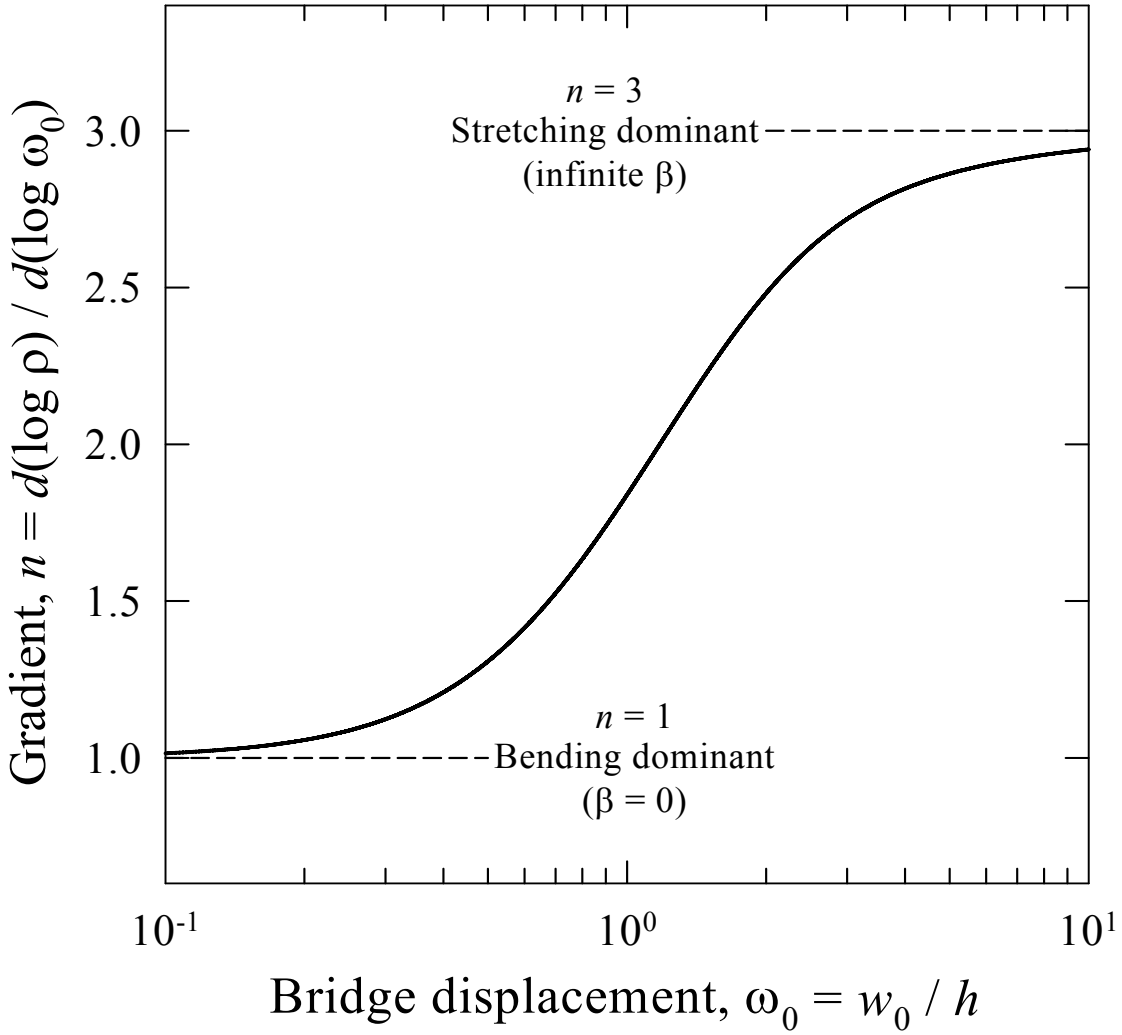

Figure 4 The gradient $n(\omega_0)$ of the mechanical response $\rho(\omega_0)$.

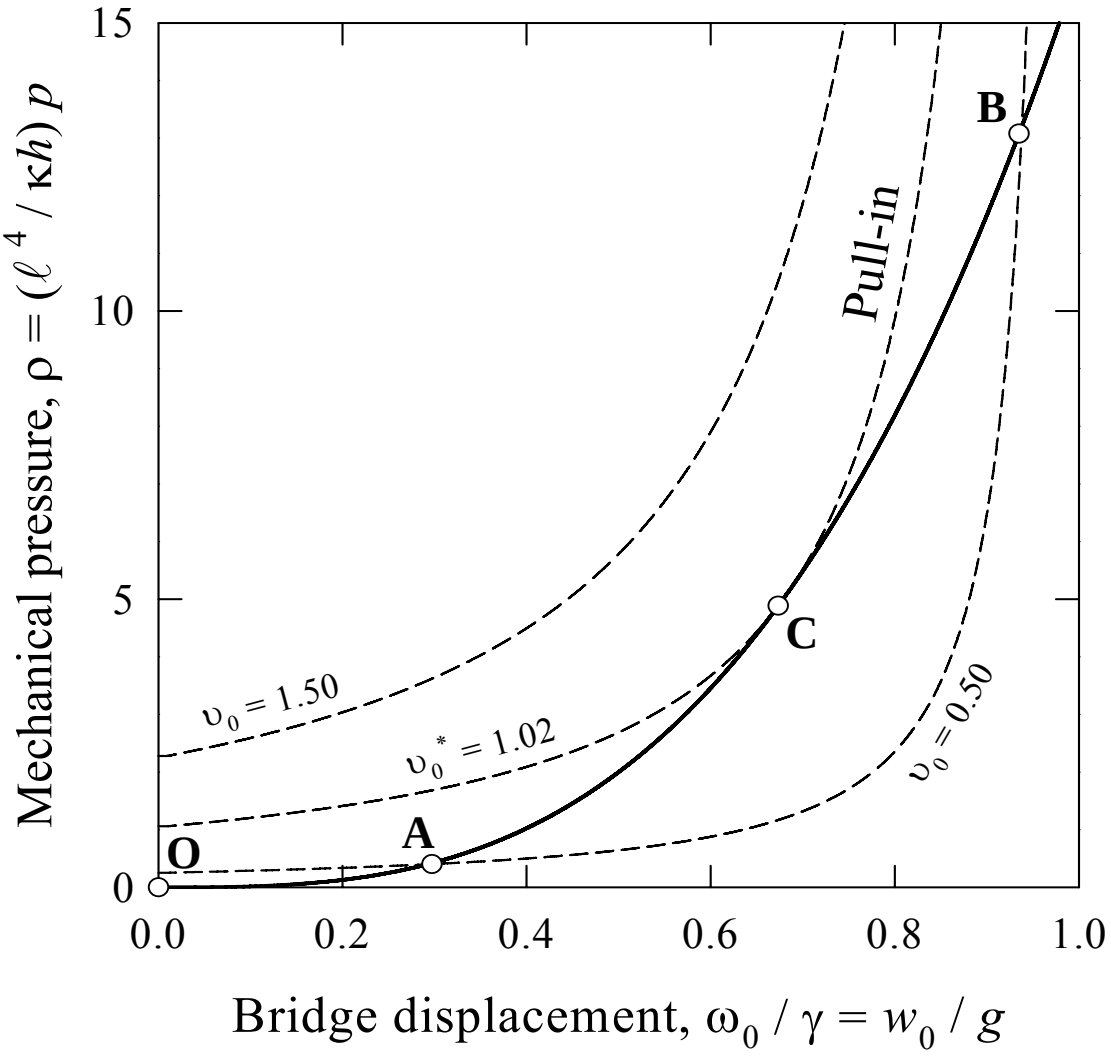

Figure 5 Forces acting on the bridge in the stretching limit. With the attractive electrostatic force shown as dashed curves for a range of applied voltage, and the cubic mechanical force on the bridge shown as dark curve (OACB). Stable equilibrium is maintained along the path OAC. "Pull-in" occurs at C.

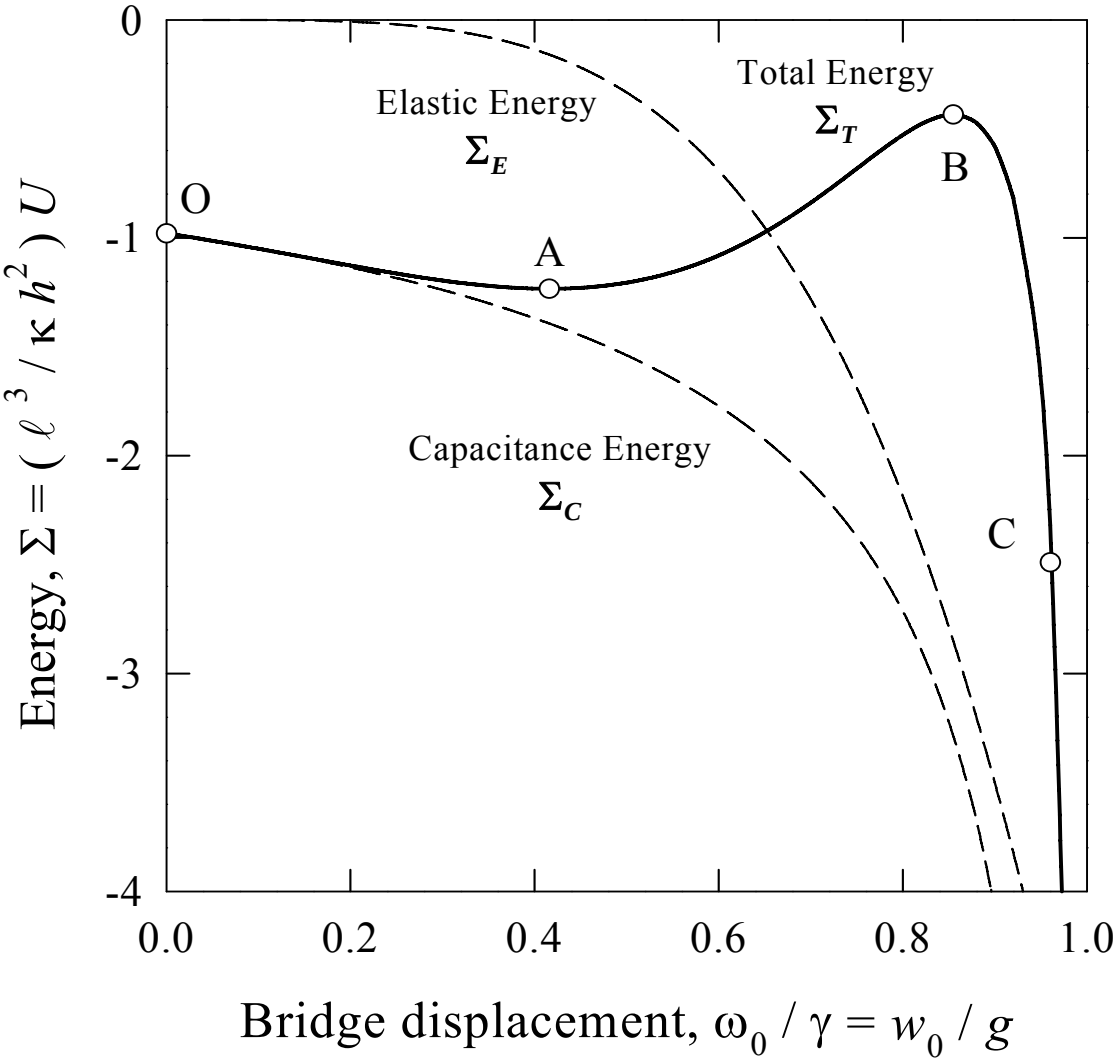

Figure 6 Energetics of the MEMS-RF-switch with υ_0 = 1.00 in the stretching limit. Various energy terms as functions of bridge central displacement are shown.

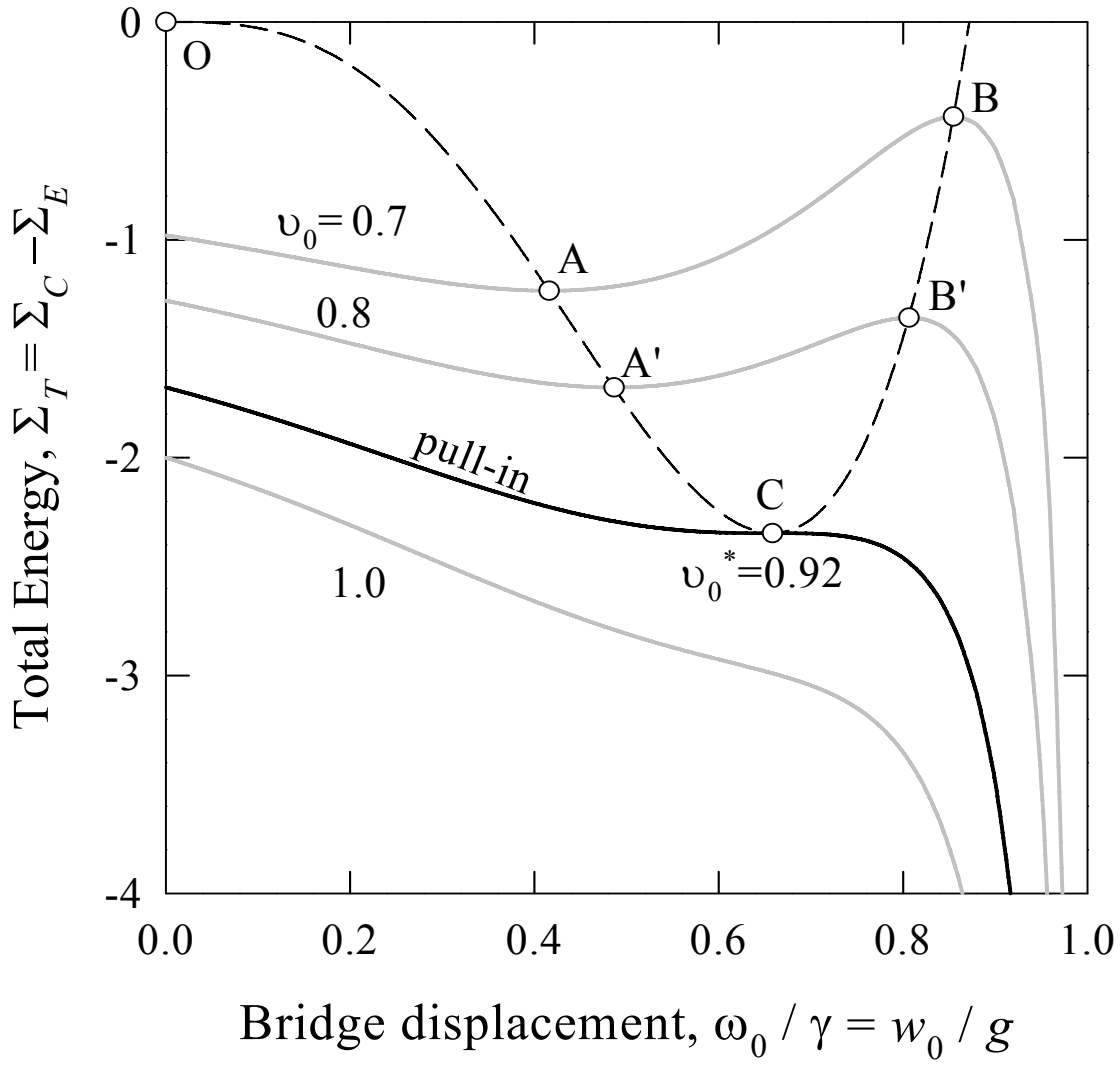

Figure 7(a) Total energy as a function of central bridge displacement for a range of applied voltage in the stretching limit. Stable equilibrium is maintained along the path OAA′C. Path CB′B is unstable and physically inaccessible. “Pull-in” occurs at C.

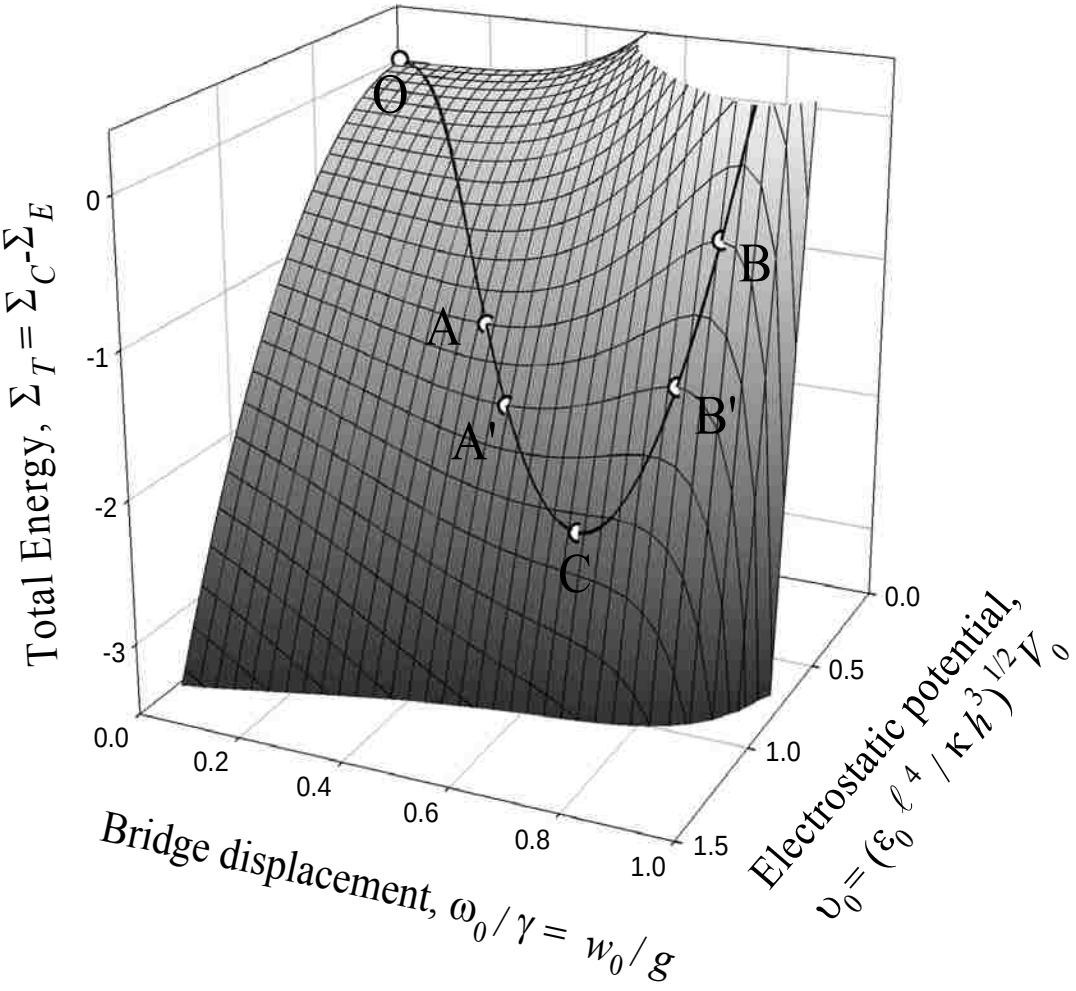

Figure 7(b) Total energy as a function of both central bridge displacement and applied voltage.

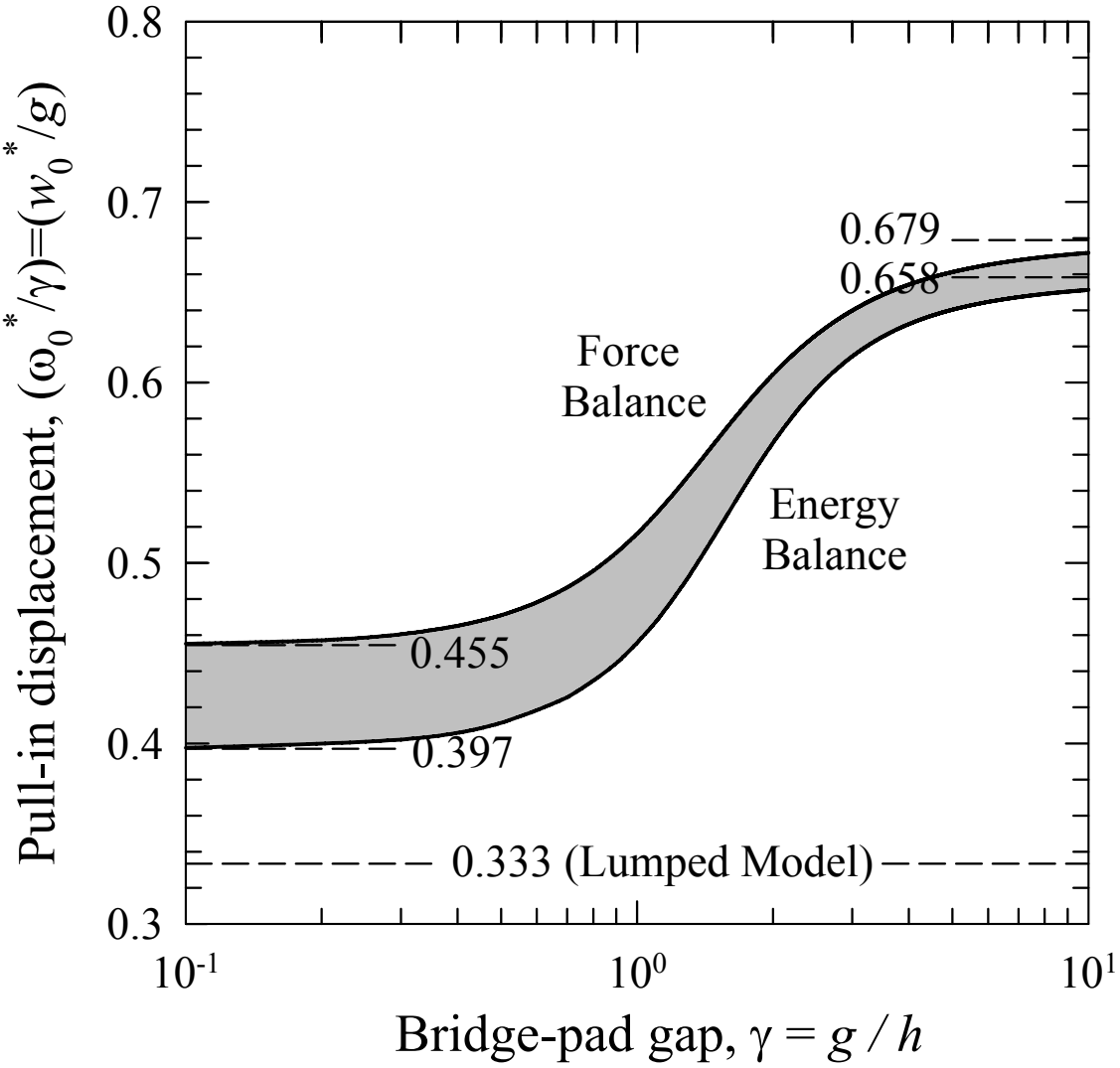

Figure 8 Pull-in (w_0^*/g) as a function of the bridge-pad gap. Both force and energy balances are shown. Pull-in occurs within the shaded area.

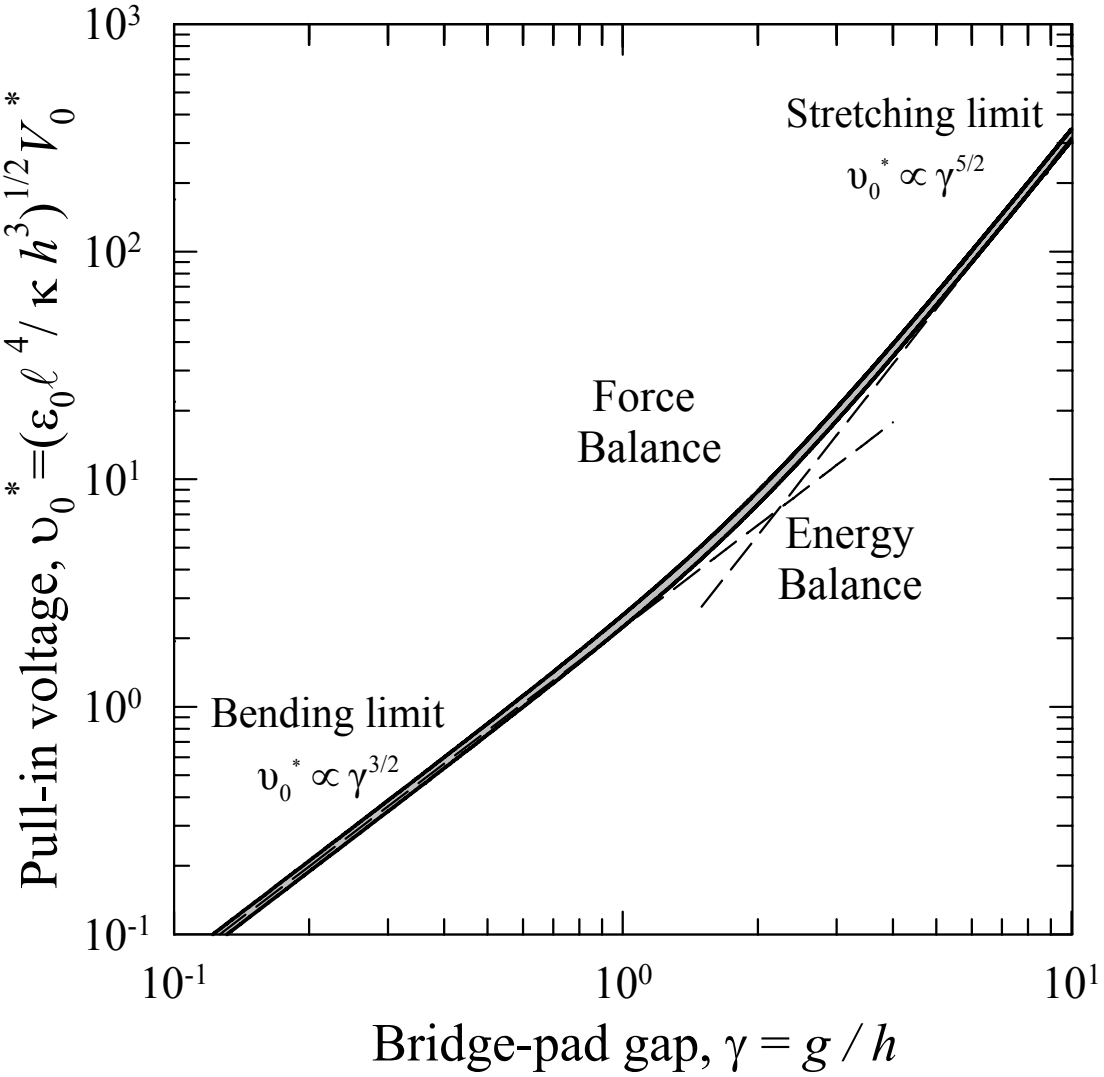

Figure 9 Pull-in voltage as a function of the bridge-pad gap. Both force and energy balances are shown. Pull-in occurs within the shaded area. The dashed lines show the plate-bending and membrane-stretching limits.

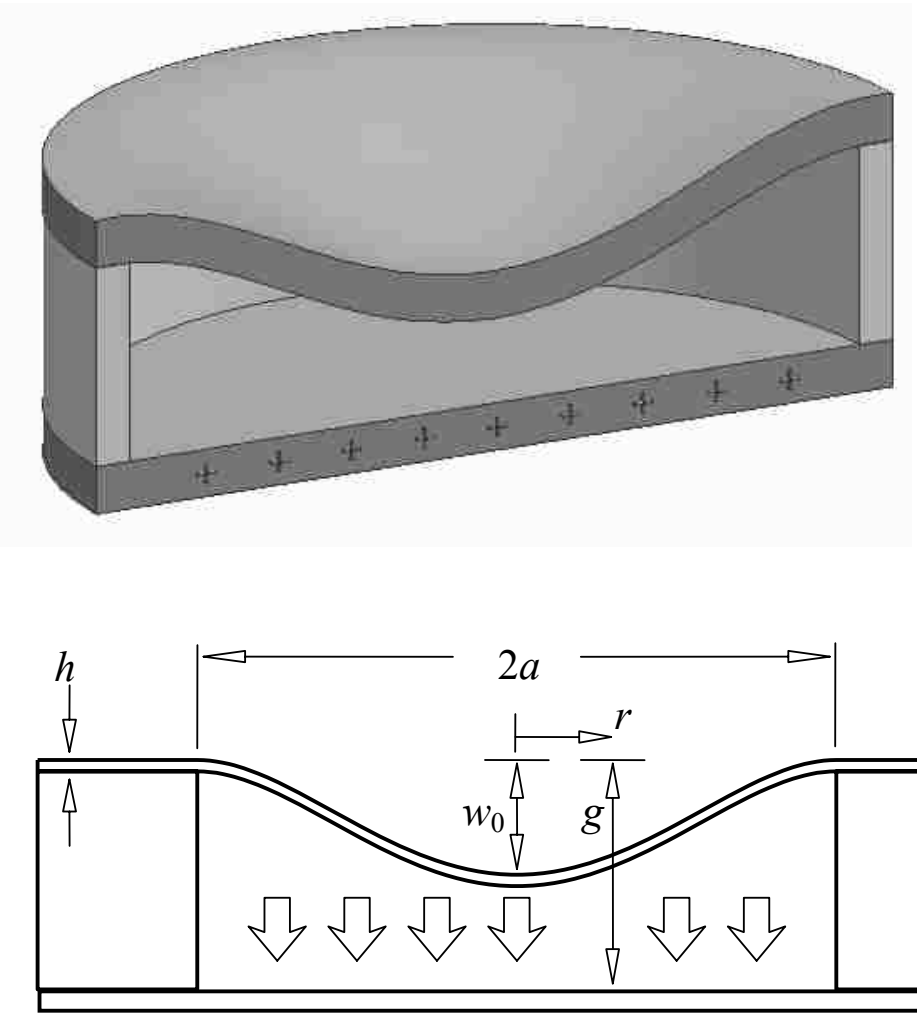

Figure 10 Sketch of a 2-D axisymmetric MEMS-RF-switch.

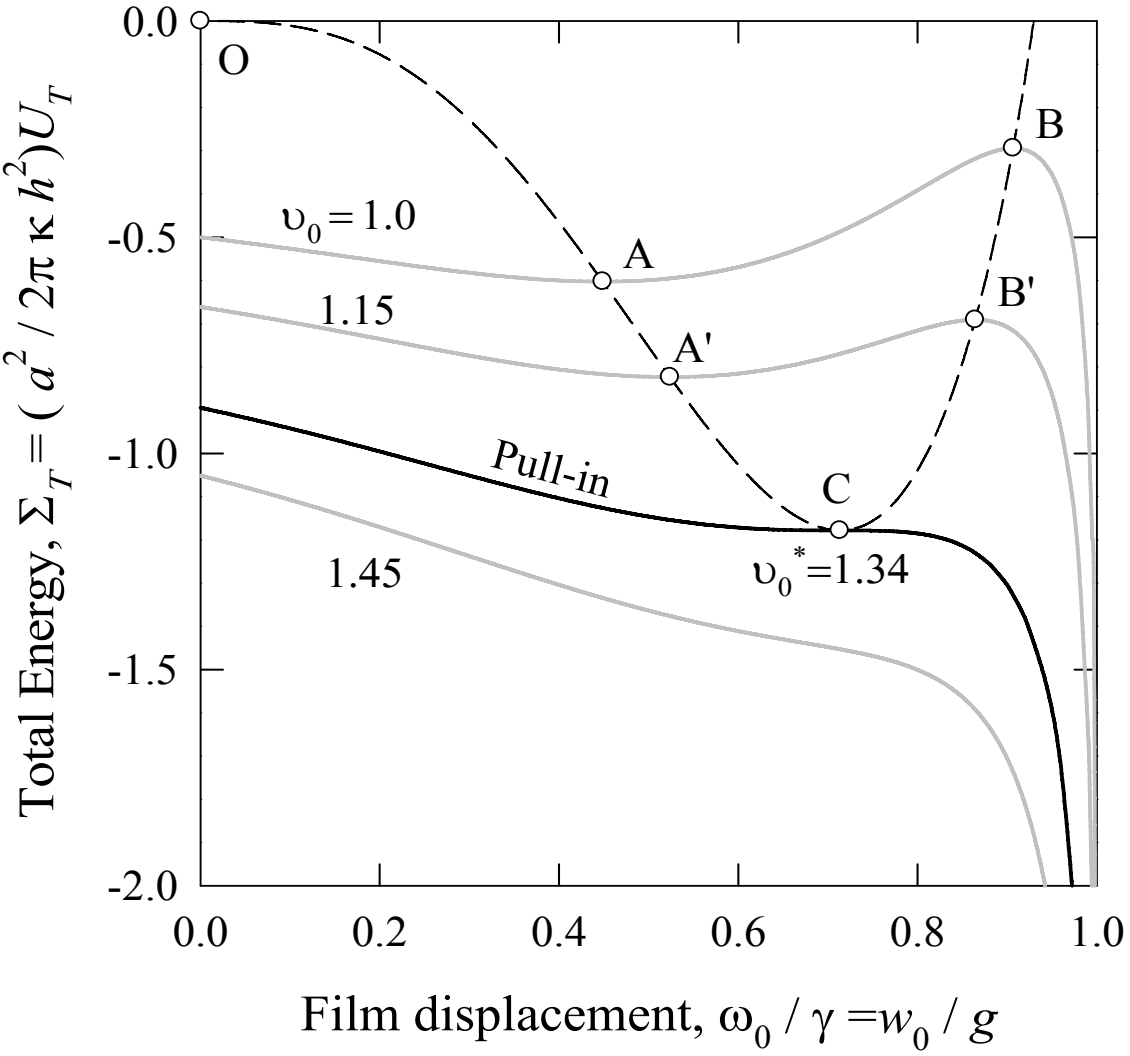

Figure 11(a) Total energy $\Sigma T(\omega_0, \upsilon_0)$ for fixed υ_0 in the stretching limit. "Pull-in" occurs at C.

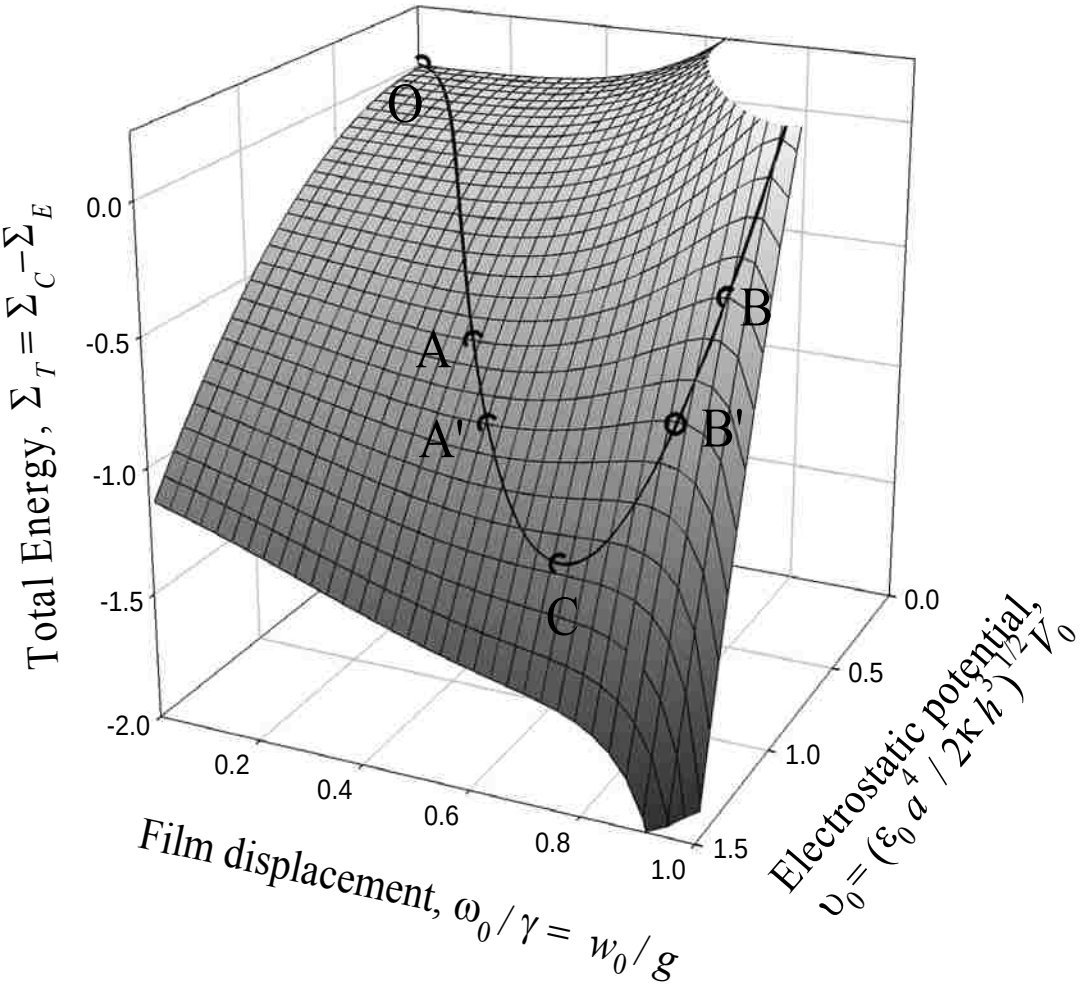

Figure 11(b) Total energy $\Sigma T(\omega_0, \upsilon_0)$.

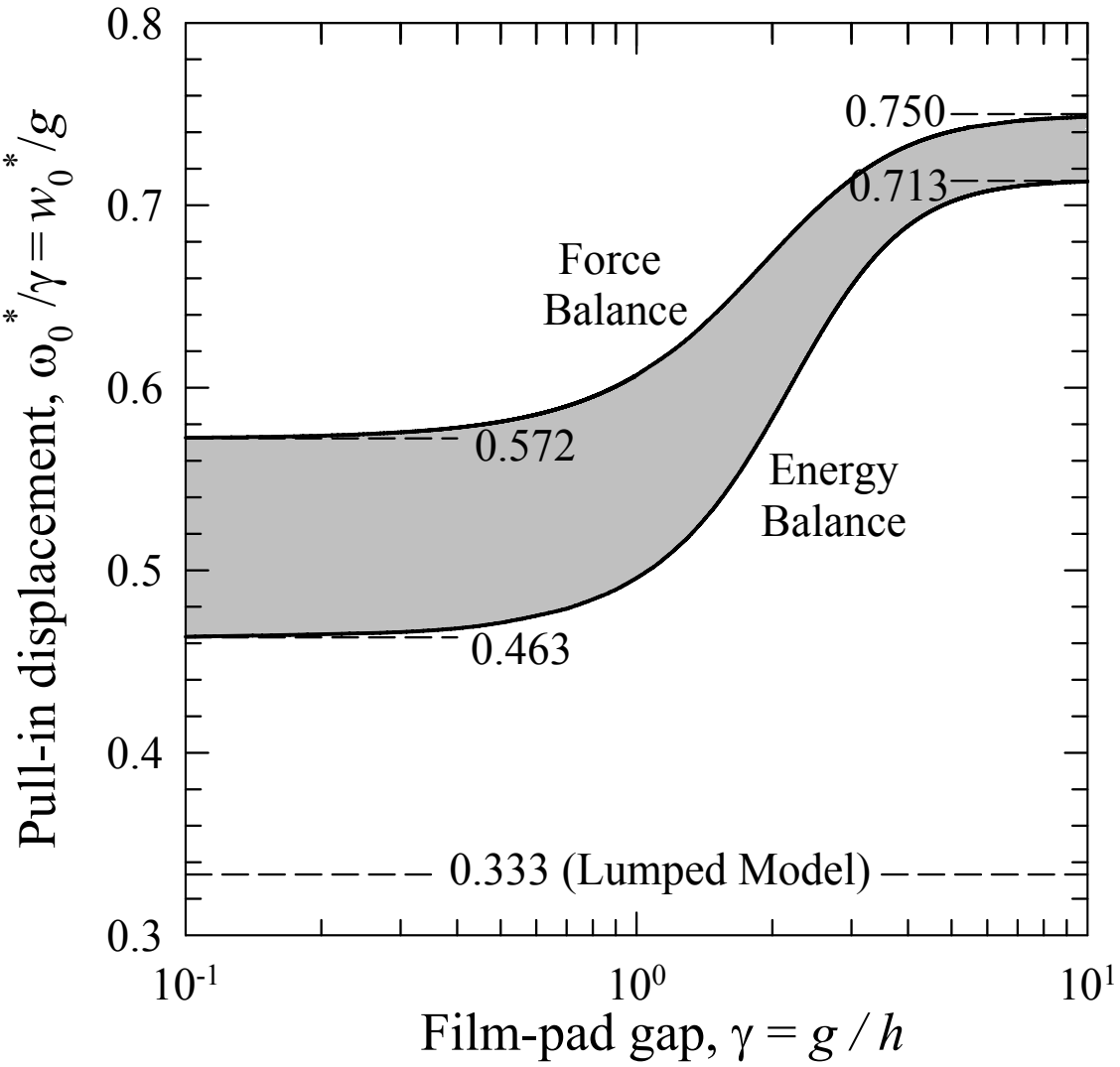

Figure 12 Pull-in (w_0^*/g) as a function of the film-pad gap.

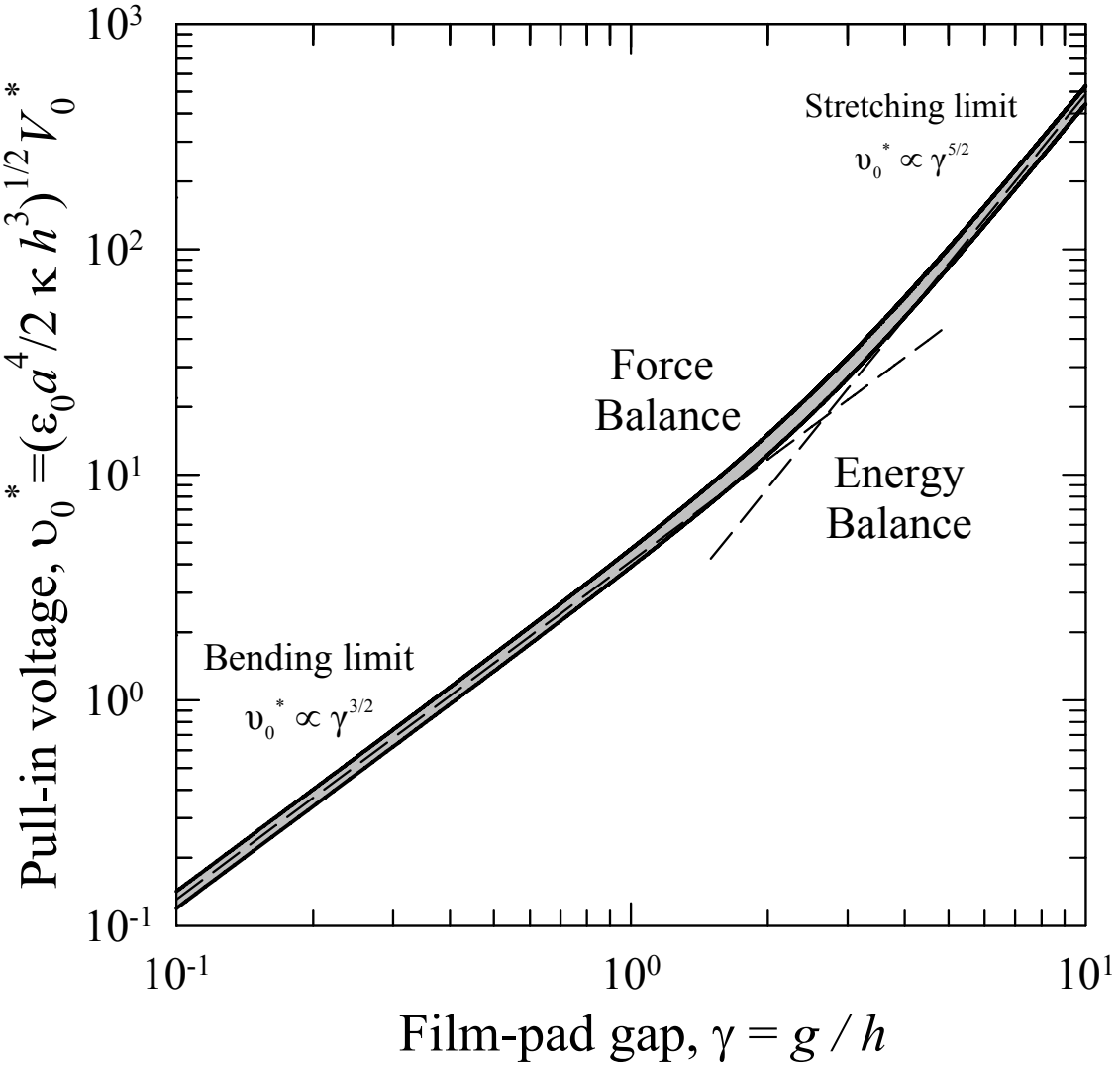

Figure 13 Pull-in voltage as a function of the film-pad gap. Pull-in occurs within the shaded area.

PAPER II

"Pull-in" of a Pre-stressed Thin Film by an Electrostatic Potential: A 2-D Axisymmetric Plate

Gang Duan [1], Kai-tak Wan [1, 2,]

[1] Mechanical Engineering, [2] Chemical & Biological Engineering, University of Missouri-Rolla, Rolla, MO 65409-0050, USA

Abstract

A 2-D axisymmetric pre-stressed film clamped at the periphery is loaded by an electrostatic potential applied to a pad directly underneath. Upon a critical applied potential, "pull-in" occurs and the film is compelled to make direct contact with the pad. An elastic model is constructed to account for "pull-in" in terms of the applied voltage, the residual stress, and the film-pad gap based on two complementary methods, namely, the force balance and the energy balance. The new model determines the validity range of the classical solution and accounts for the deviation for large elastic strain and high tensile membrane stress. Both tensile and compressive residual stresses are allowed. New design criteria are derived for MEMS devices.

Keywords: thin film, residual stress, pull-in, electrostatic potential

1. Introduction

Electric actuated thin films are widely used in micro-electromechanical systems (MEMS) such as radio frequency switches (RF-switches)[1-3], micro-pumps and valves[4-7], and electrostatic actuators [8, 9]. Moveable parts in the form of thin films oftentimes suffer from tensile / compressive residual stress due to mismatch of the thermal expansion coefficients (CTE) of the film and the substrate during fabrication processes and device operation. Extreme residual stresses in ultra-thin films can lead to buckling, cracking, and even failure of the device. In a typical 2D RF-switch (Figure 1), an electrostatic potential applied to a pad compels the mechanically suspended thin film directly above to contact leading to a film-pad interface and thus "pull-in". In our previous study [13], "pull-in" of a 1D bridge and 2D circular film free of residual stress was investigated using two complementary methods: (i) force balance and (ii) energy balance. In this paper, we reexamine the "pull-in" phenomenon for a 2D film subject to an intrinsic residual stress. The trends and graphs discussed will be useful in formulating design criteria and in assessing the device performance.

2. Theory

2.1. Mechanical deformation of the film

Figure 1 shows an axisymmetric film clamped at the periphery with radius, a, thickness, h, elastic modulus, E, Poisson's ratio, v, flexural rigidity, $\kappa = Eh^3/12(1-v^2)$, subjected to an intrinsic equibiaxial residual stress, σ_0, with $\sigma_0 > 0$ corresponding to tensile stress and $\sigma_0 < 0$ compressive stress. The electrostatic pad with the same radius as the film is separated from the film by a distance, g. An electrical potential, V_0, applied to

the pad sets up a uniform electric field in the gap and compels the film to deform to a profile, $w(r)$. A concomitant longitudinal stress, σ_m, arising from the film deformation leads to a total stress of

$$\sigma = \sigma_m + \sigma_0 \tag{1}$$

For simplicity, a set of normalized variables listed in Table 1 is adopted hereafter. Depending on the relative magnitude of σ_m and σ_0, the resultant stress can be either tensile ($\sigma > 0$ and $\beta^2 > 0$) or compressive ($\sigma < 0$, $\beta^2 < 0$ and $\beta = i\,|\beta|$ with $i = \sqrt{-1}$). Based on linear elasticity, the film profile is governed by [10-12]

$$-\kappa\,\nabla^4 w \;+\; (\sigma h)\,\nabla^2 w \;=\; -\left(\frac{\varepsilon_0 V_0^{\,2}}{2}\right)\frac{1}{(g-w)^2} \tag{2}$$

where ε_0 is the permittivity of free space and ∇^2 is the Laplacian operator in cylindrical coordinates. The left-hand side denotes the mechanical deformation of the film, and the right-hand side is the electrostatic attraction. The nonlinear equation (2) forbids an analytical solution because w appears on both sides. Following the theoretical framework in our previous paper, the electromagnetic and mechanical components are decoupled by the Dugdale-Barenblatt-Maugis cohesion zone approximation [13]. The electrostatic force is replaced by an equivalent uniform pressure, p, which is taken to be the average traction on the film. The boundary conditions are given by $w\big|_{r=a} = 0$, $(\partial w/\partial r)\big|_{r=a} = 0$, and $(\partial w/\partial r)\big|_{r=0} = 0$. Equation (2) is integrated with respect to r once, yielding (3), where $\theta = \partial\omega/\partial\xi$ is the profile gradient.

$$\xi^2 \frac{\partial^2\theta}{\partial\xi^2} + \xi\,\frac{\partial\theta}{\partial\xi} - (1+\beta^2\xi^2)\,\theta \;=\; \rho\,\xi^3 \tag{3}$$

The boundary conditions are rewritten as $\omega\big|_{\xi=1} = 0$, $(\partial\omega/\partial\xi)\big|_{\xi=1} = 0$, and $(\partial\omega/\partial\xi)\big|_{\xi=0} = 0$.

The average mechanical pressure is related to the electric field by

$$\rho = \upsilon_0^2 \int_0^1 \frac{\xi}{[\gamma - \omega(\xi)]^2}\, d\xi \tag{4}$$

An analytical solution to (3) is found to be

$$\omega^t = \rho \left(\frac{1}{\beta^3 I_1(\beta)}\right)\left\{\frac{\beta}{2}(1-\xi^2) I_1(\beta) + I_0(\beta\xi) - I_0(\beta)\right\} \tag{5a}$$

$$\omega^c = \rho \left(\frac{1}{\beta^3 J_1(\beta)}\right)\left\{\frac{\beta}{2}(-1+\xi^2) J_1(\beta) + J_0(\beta\xi) - J_0(\beta)\right\} \tag{5b}$$

where the superscripts *t* and *c* denote tensile and compressive stresses, respectively, and $J_n(\xi)$ and $I_n(\xi)$ are the n^{th} order Bessel function and modified Bessel function of the first kind, respectively. The central deflection, $\omega_0 = \omega\big|_{\xi=0}$, is given by

$$\omega_0^t = \rho \left(\frac{1}{\beta^3 I_1(\beta)}\right)\left\{\frac{\beta}{2} I_1(\beta) - I_0(\beta) + 1\right\} \tag{6a}$$

$$\omega_0^c = \rho \left(\frac{1}{\beta^3 J_1(\beta)}\right)\left\{-\frac{\beta}{2} J_1(\beta) - J_0(\beta) + 1\right\} \tag{6b}$$

The concomitant stress on the film is found by integrating the radial and circumferential elastic strains, and is given by

$$\beta_m^{\,2} = 6\int_0^1 \left(\frac{\partial\omega}{\partial\xi}\right)^2 \xi\, d\xi = [\rho . f(\beta)]^2 \tag{7}$$

with $$f^t(\beta) = \frac{\{(9\beta/2)\, I_1(\beta)^2 - 3 I_2(\beta)\, [\beta\, I_0(\beta) + 4 I_1(\beta)]\}^{1/2}}{\beta^{5/2}\, I_1(\beta)} \tag{8a}$$

and

$$f^{c}(\beta) = \frac{\{(9\beta/2)\,J_1(\beta)^2 - 3J_2(\beta)\,[\beta\,J_0(\beta) - 4J_1(\beta)]\}^{1/2}}{\beta^{5/2}\,J_1(\beta)} \tag{8b}$$

In the case of a large compressive residual stress, the film buckles according to the Euler criterion (denoted by the superscript † hereafter), $\sigma_0 \le \sigma_0^{\dagger}$, with

$$\sigma_0^{\dagger} = -j_1^{\,2}\left(\frac{\kappa}{a^2 h}\right) \quad \text{or} \quad (\beta_0^{\dagger})^2 = -j_1^{\,2} \approx -14.7 \tag{9}$$

where $j_1 = 3.8317$ is the first zero of J_1 with $J_1(j_1) = 0$ [14]. As $\beta_0 \to \beta_0^{\dagger}$, f^{c} approaches infinity and buckling occurs. In fact, intrinsic buckling is inevitable even in the absence of an electric field when $\beta_0^2 < -j_1^{\,2}$. The elastic solution does not specify a positive or negative curvature of the buckled film, but the film is taken here to buckle towards the electrostatic pad.

Figure 2 shows the film profile for a range of stress. Figure 3 shows the mechanical response, $\rho(\omega_0)$. There are two relevant limiting cases. In the case of a thick and stiff film, the deformation is small ($\omega_0 < 0.5$), the concomitant stress is negligible ($\beta_m \approx 0$), and the pre-stressed film is dominated by plate-bending. In such limit, the mechanical response (6a) and (6b) reduces to a linear relation,

$$\rho^{t} = \left[\frac{2\beta_0^{\,3} I_1(\beta_0)}{2 - 2I_0(\beta_0) + \beta_0 I_1(\beta_0)}\right]\omega_0^{t} \tag{10a}$$

$$\rho^{c} = \left[\frac{2\beta_0^{\,3} J_1(\beta_0)}{2 - 2J_0(\beta_0) - \beta_0 J_1(\beta_0)}\right]\omega_0^{c} \tag{10b}$$

respectively. The square brackets in (10a) and (10b) are constants for fixed residual stress, but increase with an increasing β_0 alluding to strain hardening. It can be easily

shown that our solution is consistent with the Timoshenko solution for $\beta_0 = 0$ [10]. Another limiting case is that of a thin and flexible film with $\kappa \approx 0$. Here the film stress virtually approaches infinity, $\beta \to \infty$, and membrane-stretching dominates. Both (6a) and (6b) reduce to

$$\rho = 12\ \omega_0^{\,3} + 2\ \beta_0^2\ \omega_0 \tag{11}$$

where the first cubic term is the direct consequence of the concomitant stress, and the second linear term arises from the residual stress. There is no distinction here between tensile and compressive residual stress because the concomitant stress dominates. For $\beta_m \gg \beta_0$ and $\beta \approx \beta_m$, the linear term in (11) vanishes, $\rho \approx 12\omega_0^{\,3}$, and $\rho(\omega_0)$ approaches the membrane-stretching limit independent of residual stress. The linear (10) and cubic (11) asymptotes are shown in Figure 3. The transition from pure bending to pure stretching is discussed as follows. For $\beta_0^2 > -j_1^{\,2}$, an increasing residual stress requires the linear-cubic transition to occur at a larger ω_0. At the critical buckling limit $\beta_0^2 = -j_1^{\,2}$, the linear-cubic transition is pushed to $\omega_0^{\dagger} = 0$ with the linear part of (11) completely eliminated. For $\beta_0^2 < -j_1^{\,2}$, buckling occurs spontaneously even in the absence of the applied field, and the central deflection becomes

$$\omega_0^{\dagger} = \left[\frac{J_0(j_1)-1}{\sqrt{3}\ j_1\ J_0(j_1)}\right]\sqrt{\left|\beta_0\right|^2 - \left|\beta_0^{\dagger}\right|^2} \quad \approx 0.5248\sqrt{\left|\beta_0\right|^2 - j_1^{\,2}} \tag{12}$$

which is a monotonic increasing function of $\left|\beta_0^2\right|$. If the film-pad gap falls below this critical value ($\gamma < \omega_0^{\dagger}$), then the film spontaneously touches the pad below and the device fails. The maximum compressive residual stress a working device can tolerate is found by

rearranging (12) to yield $\left|(\beta_0^2)_{\max}\right| \approx 3.6309\gamma^2 + 14.6819$. Increasing the external load requires the mechanical response to approach $\rho = 12\omega_0{}^3$. Figure 4 shows a contour plot of $\omega_0(\beta_0^2)$ for fixed ρ as indicated. The curve $\rho = 0$ intersects the β_0^2–axis at $(\beta_0^\dagger)^2 = -j_1{}^2$, which defines the physically inaccessible region due to buckling (shaded area). All $\omega_0(\beta_0^2)$ curves are monotonic decreasing, because the presence of residual stress stiffens the film and reduces the central displacement.

2.2. Coupled electromagnetic and mechanical behavior

The electromechanical behavior of the device can be derived by two methods: (i) an electromagnetic attraction and mechanical force balance, or (ii) a thermodynamic energy balance. The limiting case of a thin and flexible film is chosen to demonstrate both methods. Figure 5 shows the mechanical restoring force, F_M (solid curve), and electrostatic force, F_C (dashed curves), for a range of applied voltage at fixed residual stress (β_0^2 = 25). When the applied voltage increases from null, the two force curves intersect at A which corresponds to a stable configuration with $(\partial F_M / \partial w_0) > (\partial F_C / \partial w_0)$, and at B which corresponds to an unstable and physically inaccessible configuration with $(\partial F_M / \partial w_0) < (\partial F_C / \partial w_0)$. When the external voltage reaches υ_0^* (with the asterisk denoting "pull-in" hereafter), the F_M and F_C curves intersect only at one point, C, with $(\partial F_M / \partial w_0) = (\partial F_C / \partial w_0)$, corresponding to the last stable configuration. Further increase beyond υ_0^* leads to "pull-in" and the film spontaneously collapses onto the pad. Force balance is maintained along the stable path OAC.

An alternative way to derive the electromechanical behavior is an energy balance. The total energy of the film-pad system can be written as

$$U_T = -\frac{\varepsilon_0 V_0^2}{2}\int_0^a \frac{r}{g-w}\,dr + \int p\,dV \quad \text{or} \quad \Sigma_T = -\upsilon_0^2 \int_0^1 \frac{\xi}{\gamma-\omega}\,d\xi + \int \rho\,d\vartheta \qquad (13)$$

with V as the volume of the film-pad gap. The first term on the right-hand side denotes the energy stored in the capacitive dielectric film-pad gap, and the second term represents the elastic energy stored in the deformed film. Figure 6 shows a family of $\Sigma_T(\omega_0)$ for a fixed residual stress β_0^2 = 25 and a range of υ_0. The curve OAA′C joining the local minima represents the stable path, while CB′B is unstable and physically inaccessible. At C, $\upsilon_0 = \upsilon_0^*$, the local minimum and maximum merge to form an inflexion with $(\partial\Sigma_T/\partial\omega_0) = [\partial^2\Sigma_T/\partial(\omega_0)^2] = 0$, corresponding to a neutral equilibrium. "Pull-in" occurs once υ_0^* is exceeded.

In theory, the force and energy balances should yield identical results. However, the cohesive zone approximation leads to a small inconsistency, υ_0^* = 5.1565 from the force balance and υ_0^* = 4.6585 from the energy balance, as shown in figures 5 and 6. This discrepancy cannot be resolved by the present model, as actual pull-in occurs between these two limits. Figures 7-10 show the coupling effects of the residual stress and the film-pad gap for both the force balance (grey) and energy balance (dark). Figures 7 and 8 show the pull-in displacement (ω_0^*/γ) and the corresponding pull-in voltage υ_0^* as a function of the film-pad gap, respectively. Figures 9 and 10 show the same quantities as functions of residual stress.

In Figure 7, the two families of curves do not coincide but are close to each other. A small gap ($\gamma \leq 0.1$) requires $\beta_m \approx 0$ and $\beta \approx \beta_0$, and (ω_0^*/γ) tends to a constant depending on the magnitude of β_0. Numerical computation shows that force balance yields $0.5278 \leq (\omega_0^*/\gamma) \leq 0.8007$ and energy balance yields $0.4458 \leq (\omega_0^*/\gamma) \leq 0.7349$. Conversely, a large gap ($\gamma \geq 10$) requires $\beta_m \gg \beta_0$ and $\beta \approx \beta_m$, and therefore all curves converge at a large γ. At $\gamma = 10$, force balance requires $0.7105 \leq (\omega_0^*/\gamma) \leq 0.7552$, and energy balance requires $0.6639 \leq (\omega_0^*/\gamma) \leq 0.7215$. Figure 8 shows the corresponding $\upsilon_0^*(\gamma)$. Two asymptotes are also shown as dashed curves: (i) $\upsilon_0^* \propto \gamma^{3/2}$ for plate-bending dominated films with $\beta_0 = 0$ and small gaps with $\gamma \leq 0.1$, and (ii) $\upsilon_0^* \propto \gamma^{5/2}$ for membrane-stretching dominated films with $\beta_0 = 0$ and large gaps with $\gamma \geq 10$. Non-buckled films with $\beta_0^2 > -j_1^2$ experience the bending-stretching transition at a larger γ as β_0^2 increases. The critically buckled film with $\beta_0^2 = -j_1^2$ does not have a bending-stretching transition, and $\upsilon_0^* \propto \gamma^{5/2}$ always holds. Intrinsically buckled films with $\beta_0^2 < -j_1^2$ possess a monotonic increasing υ_0^*, and they approach the $\upsilon_0^* \propto \gamma^{5/2}$ asymptote at a high γ. Figure 9 shows the monotonic decreasing (ω_0^*/γ) as a function of film-stiffening residual stress. Films with a large γ show the least dependency on the residual stress because the concomitant stress dominates, and (ω_0^*/γ) tends to be constant at a large γ. For instance, at $\gamma = 10$, (ω_0^*/γ) only varies from 0.7728 to 0.7263 (force balance) and from 0.7407 to 0.6867 (energy balance) in the range of $-50 < \beta_0^2 < 50$. In case of a smaller gap, intrinsic buckling at a large compressive residual stress forces the film to

touch the pad ($\omega_0^* = \gamma$) even in the absence of an electric field ($\upsilon_0^* = 0$). Such involuntary pull-in is seen at $\gamma = 2$ with $\beta_0^2 = -29$ and at $\gamma = 0.1$ with $\beta_0^2 \approx -j_1^2$. Figure 10 shows the monotonic increasing function of pull-in voltage versus residual stress. Films with a small γ are dominated by the residual stress, while a large γ (e.g., $\gamma = 10$) has less dependency on β_0 because $\beta_m \gg \beta_0$. Involuntary pull-in is again expected for large enough compressive stress.

3. Discussion

The proposed model has distinct advantages over some existing models in framing the design criteria for microdevices. For example, Osterberg and Senturia [8] proposed a formula, $\upsilon_0^* \approx 3.6987\gamma^{3/2}$, for the pull-in voltage of a circular plate without residual stress based on both theoretical modeling and experimental data. Juillard and Colinet [15] argued that the formula was invalid for a large film-pad gap γ, but did not suggest an exact solution. For a small gap and stress free film, our model predicts $\upsilon_0^* = 4.4836\gamma^{3/2}$ (force balance) and $\upsilon_0^* = 3.7730\gamma^{3/2}$ (energy balance), which is essentially consistent with Osterberg. On the other hand, a large gap requires $\upsilon_0^* = 1.5910\gamma^{5/2}$ (force balance) and $\upsilon_0^* = 1.3375\gamma^{5/2}$ (energy balance), which is vastly different from the small gap behavior. Transitional behavior from "small" to "large" gap is found to occur at $\gamma \approx 3$ by our model, which sets an upper validity limit to the classical Osterberg solution. Apart from the influence of gap dimension, our model further allows a non-zero residual stress to be incorporated. The maximum compressive stress susceptible to plate buckling is found to be $\beta_0^2 = -j_1^2$ and the pull-in voltage obeys

$\upsilon_0^* \propto \gamma^{5/2}$ exclusively and $\omega_0^\dagger = 0$. Increasing residual stress in the tensile mode strain hardens the plate and shifts the transition to $\upsilon_0^* \propto \gamma^{5/2}$ at a larger gap.

It is worthwhile to note some application of our model in other micro-devices. In an electrostatic driven micro-pump or strain gauges with circular diaphragms, some authors assumed a central point load to represent the nonlinear electrostatic force, while others assume a uniform pressure [5-7, 16]. The circular films are usually modeled to undergo either pure plate-bending or pure membrane-stretching but never mixed bending-stretching mode. Typical profiles and volume of a bending plate is given by $\omega = \omega_0 (1 - \xi^2)^2$ and $\vartheta = 1/3$, and a stretching membrane $\omega = \omega_0 (1 - \xi^2)$ and $\vartheta = 1/2$. Our model yields a profile that spans the full bending-stretching spectrum and also predicts a continuous volume change from 1/3 to 1/2 [13]. Further correction as a result of non-zero residual stress can also be derived easily from the current model. These results are important parameters in designing and evaluating fluid flow rate especially in a micro-fluidics channel.

The proposed model can also be used to characterize a capacitive Micromachined Ultrasonic Transducers (cMUT). Nikoozadeh et al. [17] proposed a model for the axisymmetric thin film in cMUT based on the classical Timoshenko plate-bending solution. Caliano et al. [18] assumed the standard Bessel function for the film profile as in a drum head undergoing either pure plate-bending or pure membrane-stretching but not bending-stretching. Vogl et al. [19-20] considered a reduced-order Galerkin model for a vibrating bending plate with non-zero residual stress and derived the film profile to be

$$w(r) = \sum_{s=1}^{N} c_s \, \phi_s(r) \qquad \text{with} \qquad \phi_s(r) = \frac{J_0(\Omega_s{}^{1/2} r)}{J_0(\Omega_s{}^{1/2})} - \frac{I_0(\Omega_s{}^{1/2} r)}{I_0(\Omega_s{}^{1/2})}$$

where ϕ_s is the s^{th} shape function and $\Omega_s^{\,2} = (\rho h a^4 / \kappa)\ \omega_s^{\,2}$ is the s^{th} eigenvalue with ω_s the natural frequency of vibration and ρ the mass density of the film. For a small film-pad gap ($\gamma = 0.3$), the series solution leads to a pull-in displacement, $\omega_0^* / \gamma \approx 0.4750$, which falls in the range of $\omega_0^* / \gamma \approx 0.4661$ (energy balance) to 0.5756 (force balance) in our model. Note that all of the aforementioned models in the literature do not consider the concomitant stress and are therefore incapable to portray the bending-stretching transition. On the other hand, our model accounts for neither film vibration triggered by an AC signal nor air-cushion in the film-substrate gap, though the Dugdale-Barenblatt-Maugis cohesion zone approximation adopted here could lead to better analytical solutions and thus better design criteria.

4. Conclusion

An analytical elastic model is derived for a pre-stressed 2-D axisymmetric film that is applicable to MEMS-RF-switch and micro-pumps in terms of the measurable quantities. The coupling effects of residual stress and the ratio of the film-pad gap to film thickness (*g/h*), or γ, are found to play a significant role in the device behavior. A small film-pad gap with $\gamma < 0.5$ requires $\upsilon_0^* \propto \gamma^{3/2}$, and the residual stress effects dominate due to a small concomitant stress ($\beta_0 \gg \beta_m$). In contrary, a large film-pad gap with $\gamma > 5$ requires $\upsilon_0^* \propto \gamma^{5/2}$, and the residual stress effects diminish as a result of a large concomitant stress ($\beta_m \geq \beta_0$). The results obtained are crucial to improve the design criteria.

Acknowledgements

Support from the NSF CMS-0527912 is acknowledged.

References

1. J. Elders, V. Spiering and S. Walsh, "Microsystems Technology (MST) and MEMS applications: an overview," *Microelectromechanical Systems: Technology and Applications* **26**[4], 312-317, 2001.
2. G.M. Rebeiz and J.B. Muldavin, "RF MEMS switches and switch circuits," *IEEE Microwave Magazine* **2**, 59-71, 2001.
3. X. Rottenberg, S. Brebels, W. De Raedt, B. Nauwelaers and H.A.C. Tilmans, "RF-power: driver for electrostatic RF-MEMS devices," *Journal of Micromechanics and Microengineering* **14**, S43-S48, 2004.
4. W. Oh Kwang and H. Ahn Chong, "A Review of Microvalves," *Journal of Micromechanics and Microengineering* **16**, R13-R39, 2006.
5. Amos Ullmann, Ilan Fono, and Yehuda Taitel, "A Piezoelectric Valve-Less Pump-Dynamic Model," *Transactions of ASME, Journal of Fluids Engineering*, **123**, 92-98, 2001.
6. Tian-Bing Xu and Ji Su, "Development, Characterization, and Theoretical Evaluation of Electroactive Polymer-based Micropump diaphragm," *Sensors and Actuators A* **121**, 267-274, 2005.
7. Olivier Francais and Isabelle Dufour, "Enhancement of Elementary Displaced Volume with Electrostatically Actuated Diaphragms: Application to Electrostatic Micropumps," *Journal of Micromechanics and Microengineering* **10**, 282-286, 2000.
8. P. Osterberg and S. Senturia, "M-Test: a test chip for MEMS material property measurement using electrostatically actuated test structures," *Journal of Microelectromechanical Systems* **6**, 107-118, 1997.

9. Y. Nemirovsky, "A methodology and model for the pull-in parameters of electrostatic actuators," *Journal of Microelectromechanical Systems* **10**, 601-615, 2001.

10. P.L. Gould, *Analysis of Shells and Plates*, Springer, New York, 1988.

11. R. Gupta, *Electrostatic pull-in test structure design for in-situ mechanical property measurements of Micro-Electro-Mechanical Systems (MEMS)*, *Ph.D. Thesis*, *MIT*, *USA*, 1997.

12. S.P. Timoshenko and S. Woinowsky-Krieger, *Theory of Plates and Shells*, 2 ed, McGraw-Hill, New York, 1959.

13. G. Duan and K.-T Wan, "Analysis of 1-D and 2-D Thin Film 'pull-in' Phenomena under the Influence of an Electrostatic Potential," *Journal of Applied Mechanics*, in press, 2007.

14. S.P. Timoshenko and J.M. Gere, *Theory of Elastic Stability*, 2 ed, McGraw-Hill, New York, 1961.

15. J Juillard and E Colinet, "Modelling of Nonlinear Circular Plates using Modal Analysis: Simulation and Model Validation," *Journal of Micromechanics and Microengineering* **16**, 448-656, 2006.

16. W K Schomburg, Z Rummler, P Shao, K Wulff, and L Xie "The Design of Metal Strain Gauges on Diaphragms," *Journal of Micromechanics and Microengineering* **14**, 1101-1108, 2004.

17. Amin Nikoozadeh, Baris Bayram, Goksen G. Yaralioglu, and Butrus T. Khuri-Yakub, "Analytical Calculation of Collapse Voltage of CMUT Membrane," 2004 *IEEE Ultrasonics Symposium*, 256-259.

18. A. Caronti, G. Caliano, A. Iula and M. Pappalardo, "An Accurate Model for Capacitive Microachined Ultrasonic Transducers," *IEEE Transactions on Ultrasonics, Ferroelectrics, and Frequency Control* **49**, 159-168, 2002.

19. G. Vogl and A. Nayfeh, "A reduced-order model for electrically actuated clamped circular plates," *Journal of Micromechanics and Microengineering* **15**, 684-690, 2005.

20. A H Nayfeh and P F Pai, *Linear and Nonlinear Structural Mechanics*, Wiley, New York, 2004.

Table 1. Normalized parameters.

Coordinates and profile	$\xi = \left(\frac{1}{a}\right) r \, , \omega = \left(\frac{1}{h}\right) w \, , \omega_0 = \left(\frac{1}{h}\right) w_0 \, , \vartheta = \left(\frac{1}{\pi a^2 h}\right) V$
Device geometry (film-pad gap)	$\gamma = \left(\frac{1}{h}\right) g$
Electrostatic potential (applied voltage)	$\upsilon_0 = \left(\frac{\varepsilon_0 a^4}{2\kappa h^3}\right)^{1/2} V_0$
Membrane stress	$\beta_m = \left(\frac{a^2 h}{\kappa}\right)^{1/2} \sigma_m{}^{1/2} , \beta_0 = \left(\frac{a^2 h}{\kappa}\right)^{1/2} \sigma_0{}^{1/2} , \beta^2 = \beta_m{}^2 + \beta_0{}^2$
Equivalent pressure	$\rho = \left(\frac{a^4}{2\kappa h}\right) p$
Energies involved	$\Sigma_T = \left(\frac{a^2}{2\pi\kappa h^2}\right) U_T$

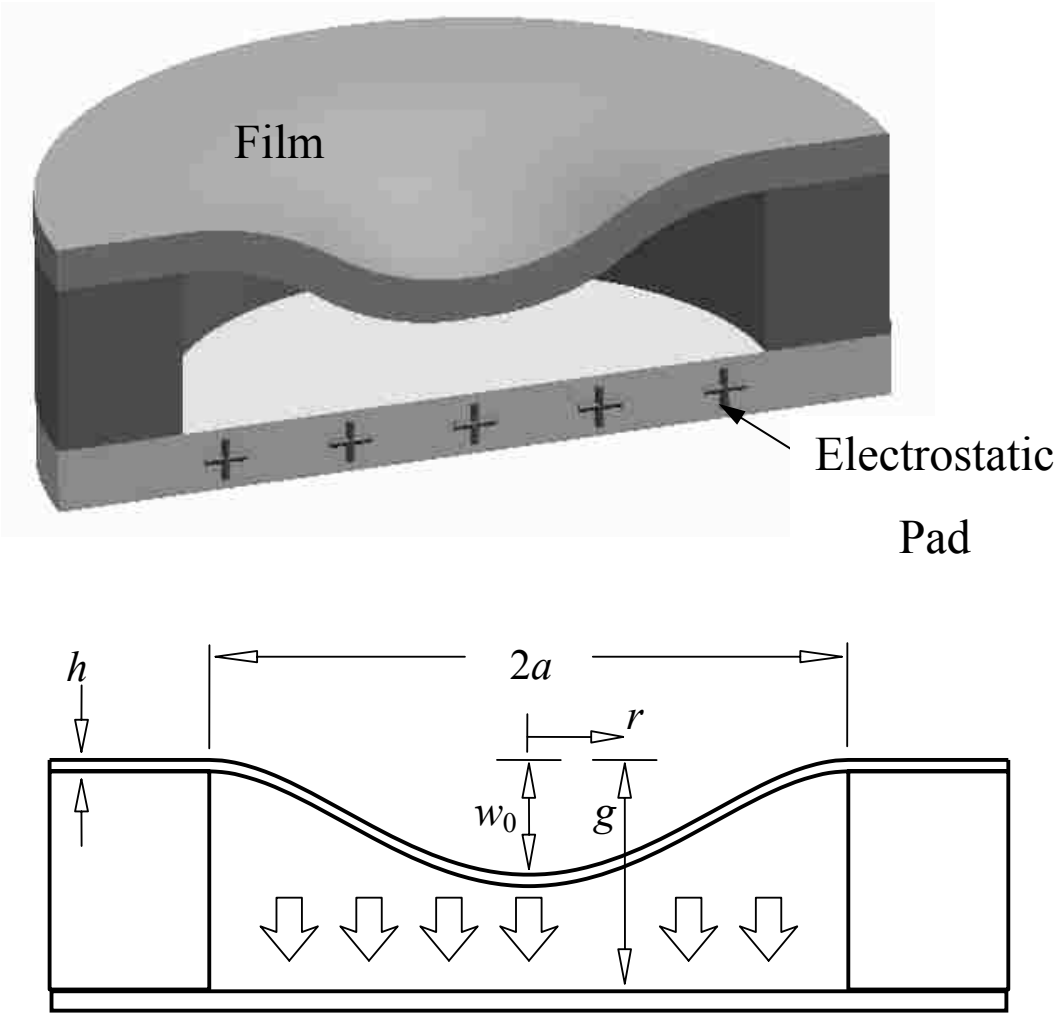

Figure 1 Sketch of a 2-D axisymmetric MEMS-RF-switch. The deformed profile of the film under an electrostatic force induced by the pad directly underneath is shown.

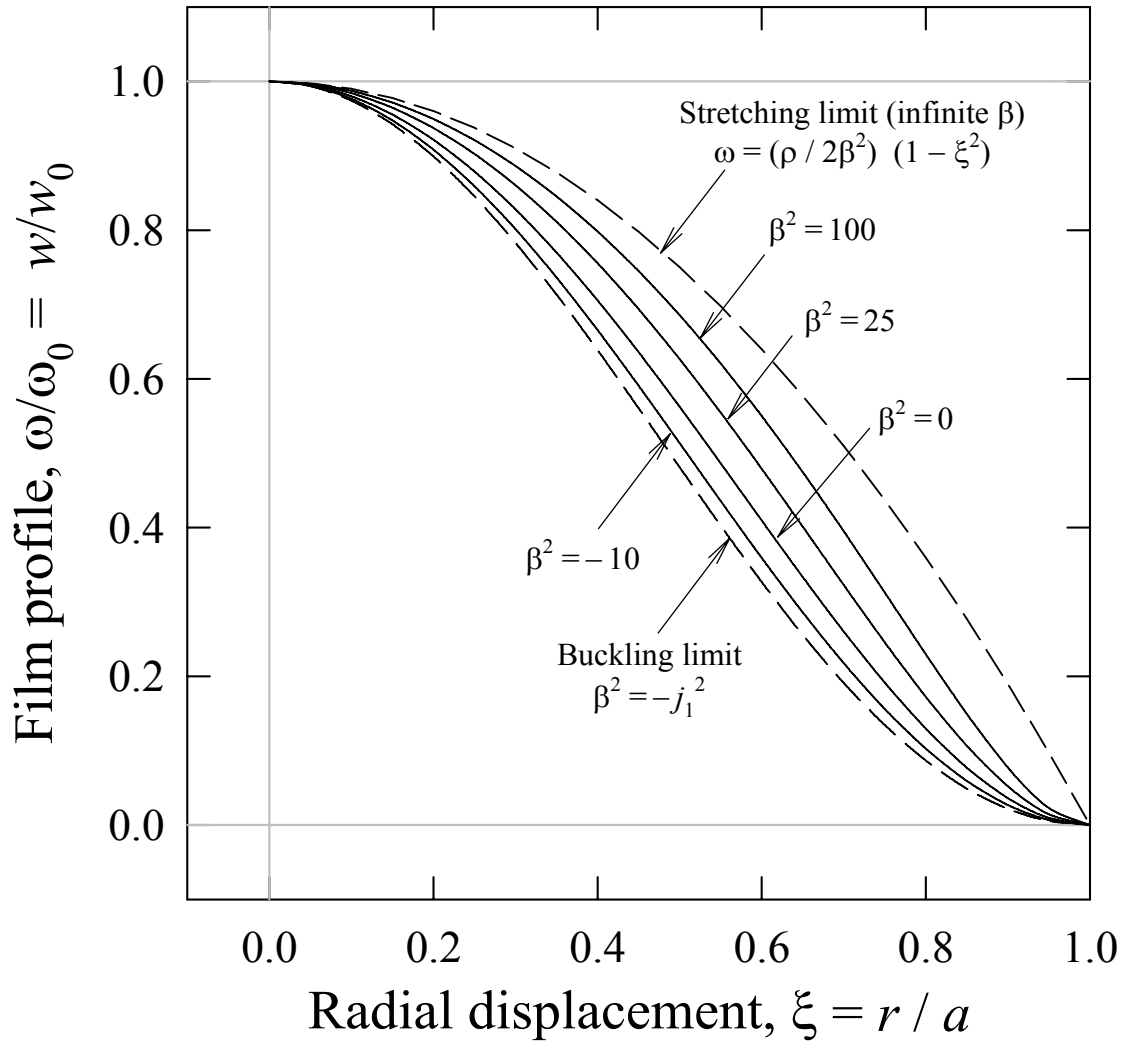

Figure 2 Normalized deformed profiles for a range of total stress. The circular film, centered at $\xi = 0$, is clamped at $\xi = 1$. The dashed curves show the limits of pure membrane-stretching and spontaneous buckling.

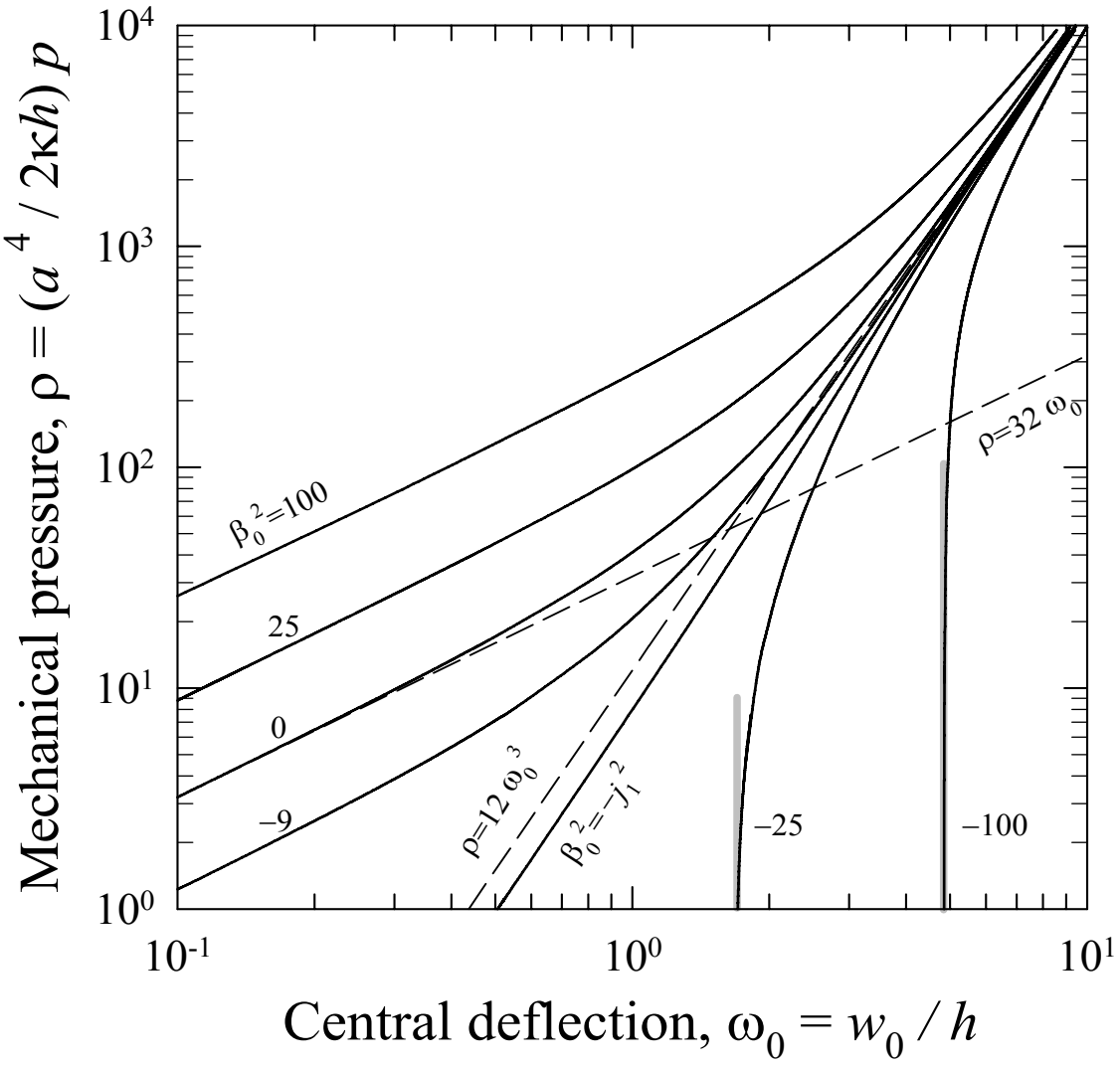

Figure 3 Mechanical response of a pre-stressed film deformed by a uniform pressure. The dashed curves show the limiting cases of pure plate-bending and pure membrane-stretching with zero residual stress. Grey lines show the central deflection of spontaneous buckling.

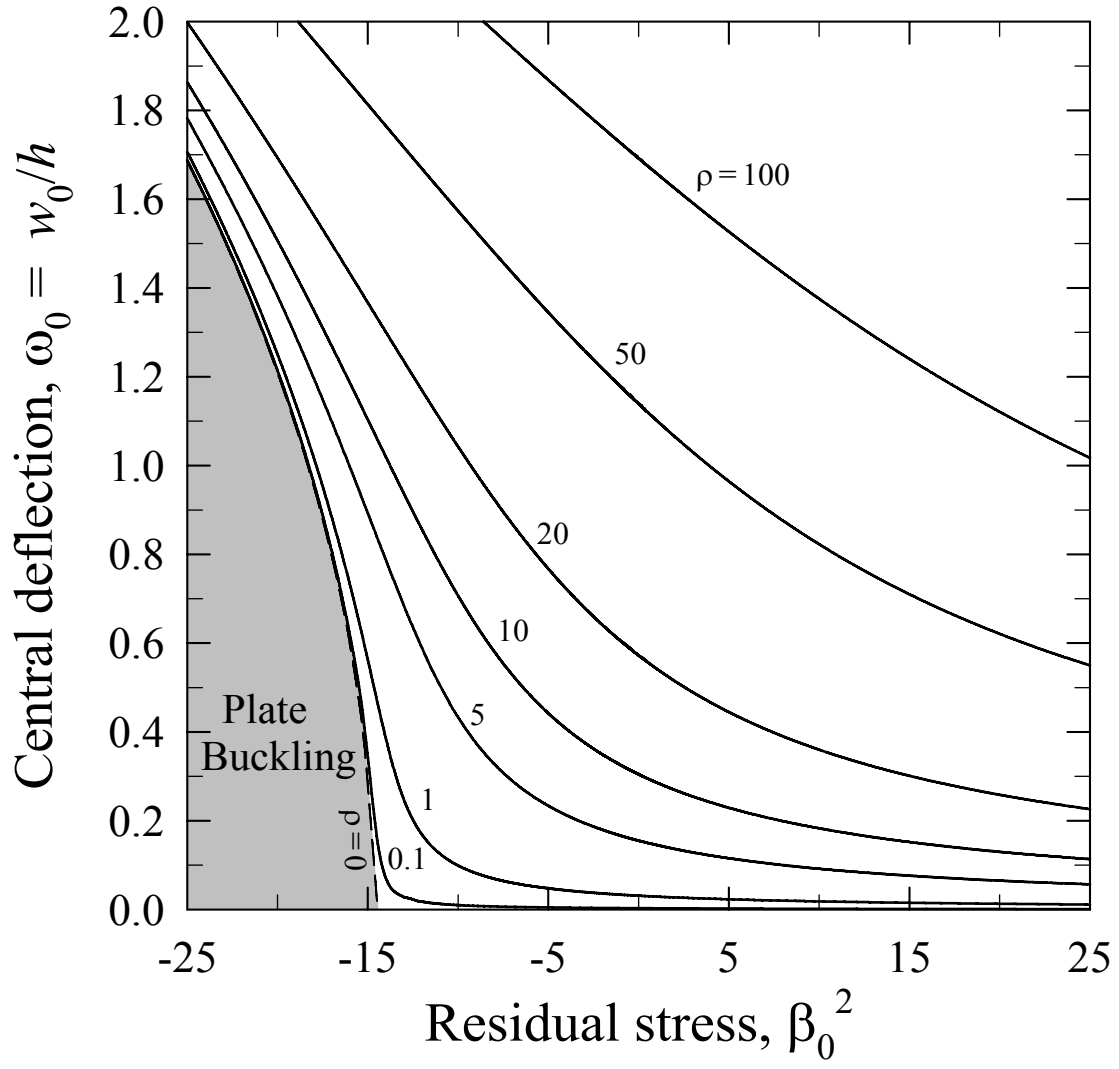

Figure 4 Central deflection of film under a uniform pressure for a range of residual stress. The dashed curve shows the spontaneous buckling limit ($\rho = 0$).

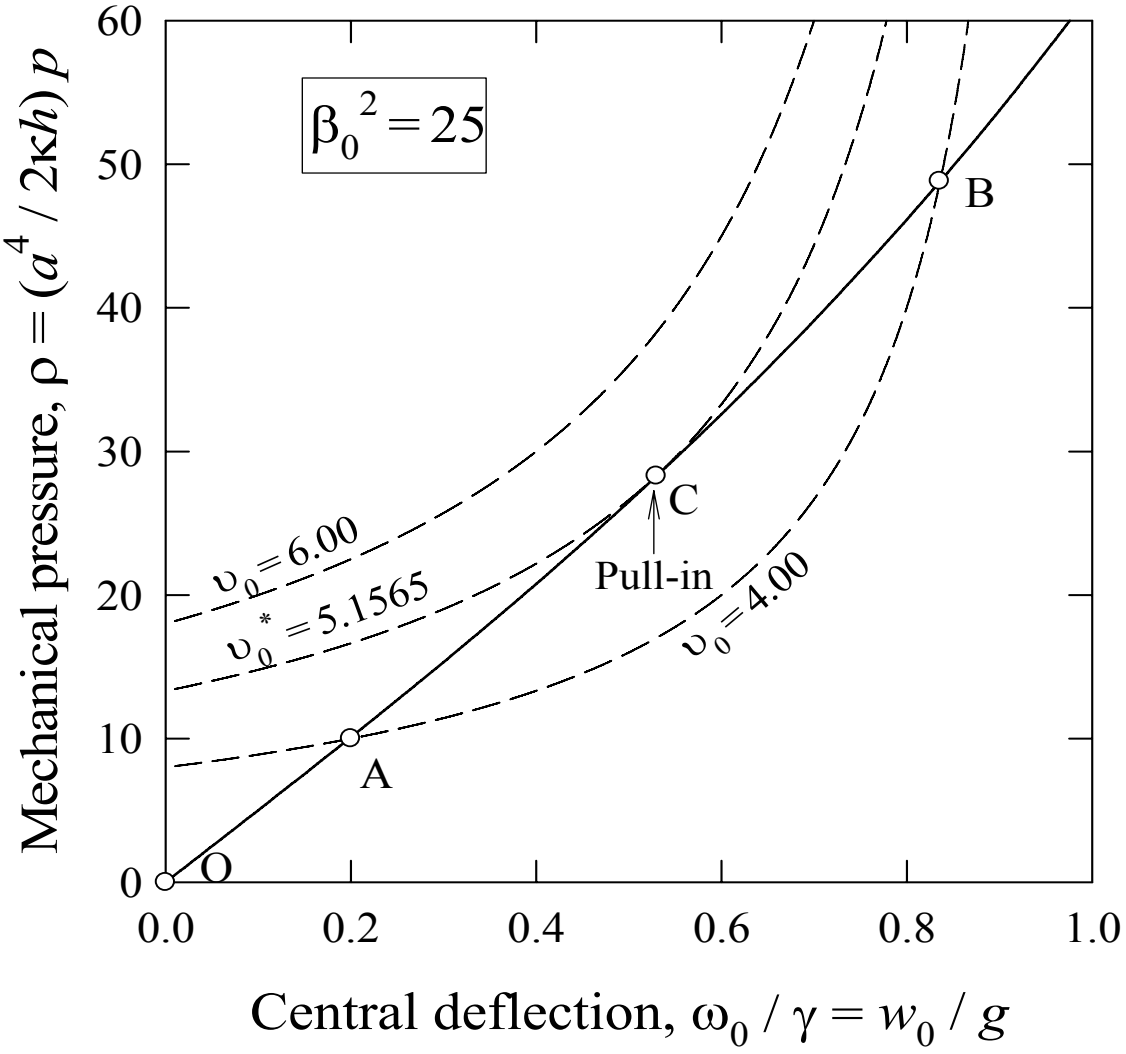

Figure 5 A film subjected to the attractive electrostatic force. Stable equilibrium is maintained along OAC, and "pull-in" occurs at C.

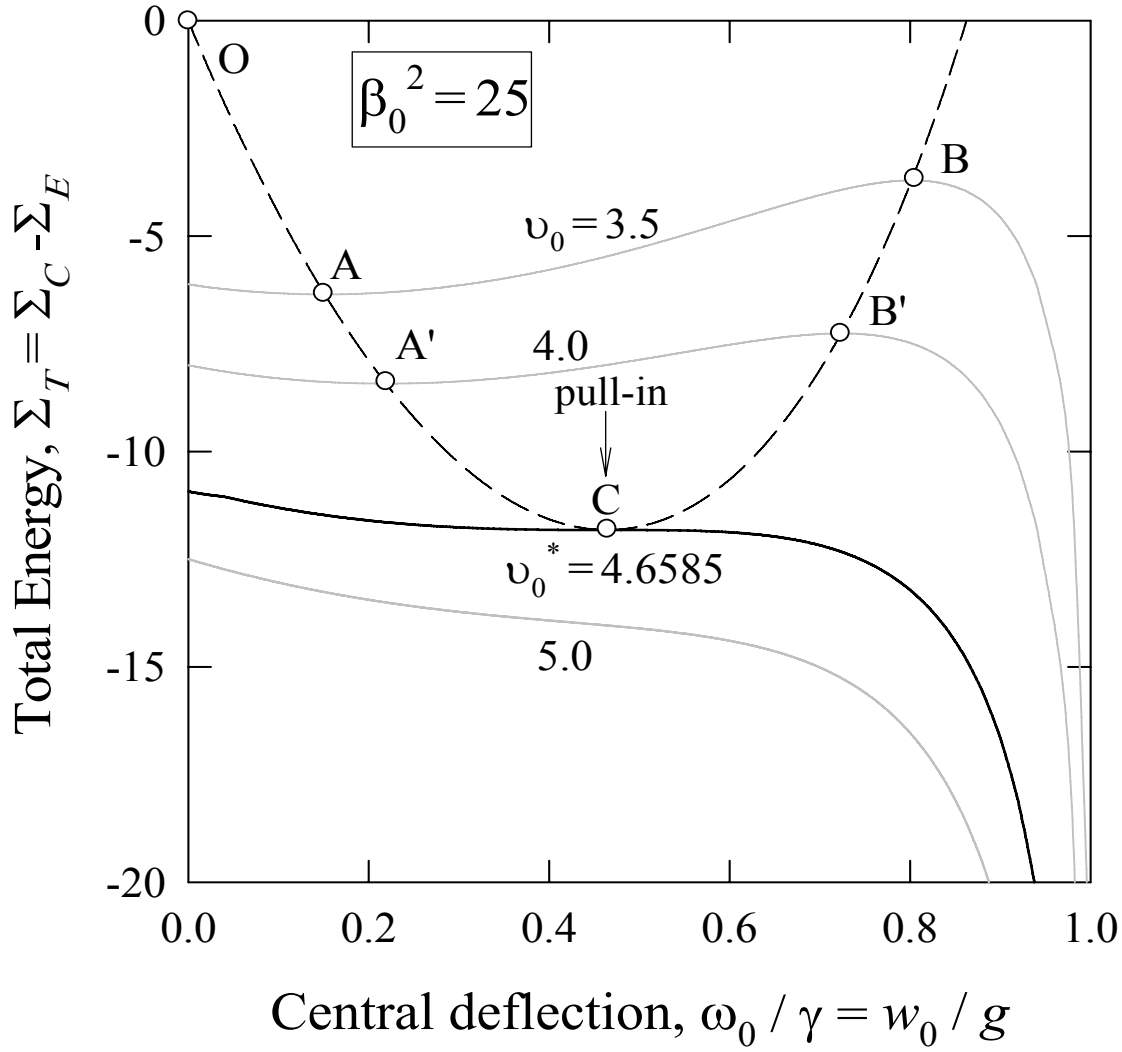

Figure 6 Total energy as a function of film central deflection for fixed residual stress and a range of applied voltage. Stable equilibrium is maintained along OAA′C, and "pull-in" occurs at C. Path CB′B is unstable and physically inaccessible.

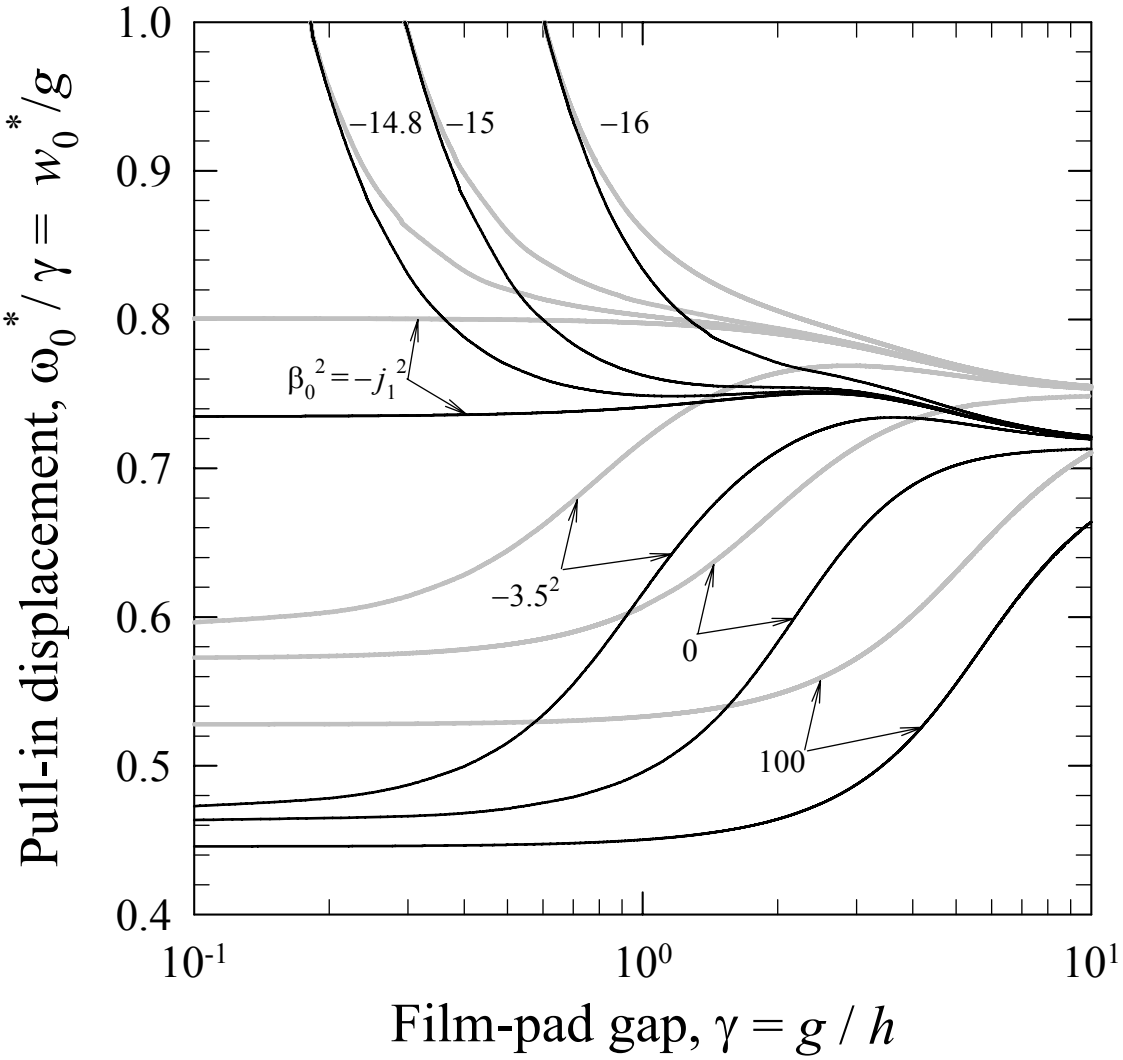

Figure 7 Pull-in displacement as a function of the film-pad gap for a range of residual stress. With force balance (grey curves) and energy balance (dark curves).

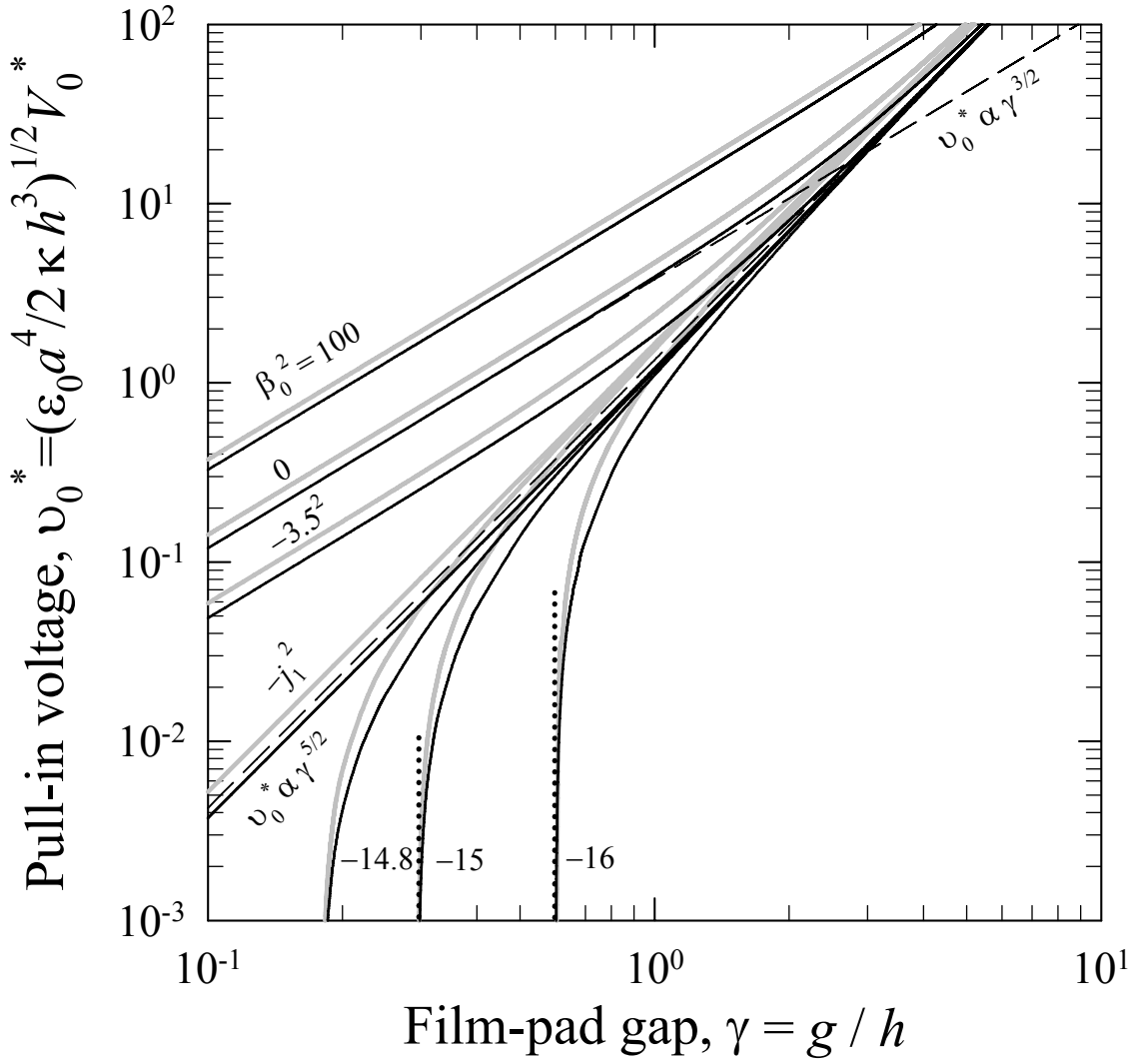

Figure 8 Pull-in voltage as a function of the film-pad gap for a range of residual stress. With force balance (grey curves) and energy balance (dark curves). Dashed lines show the plate-bending and membrane-stretching limits with zero residual stress. Dotted lines show the central deflection of spontaneous buckling.

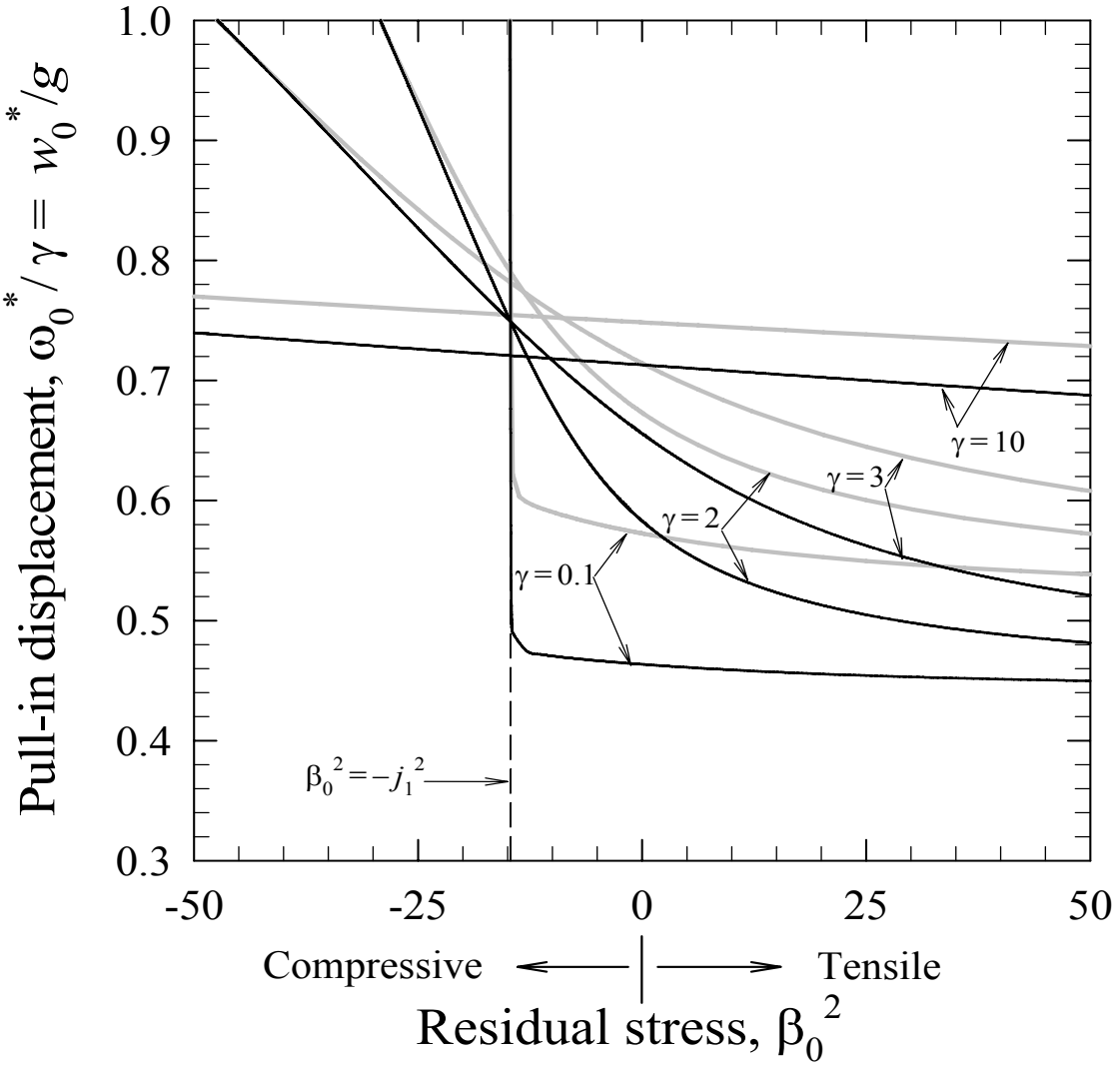

Figure 9 Pull-in displacement as a function of the residual stress for a range of film-pad gap. With force balance (grey curves) and energy balance (dark curves).

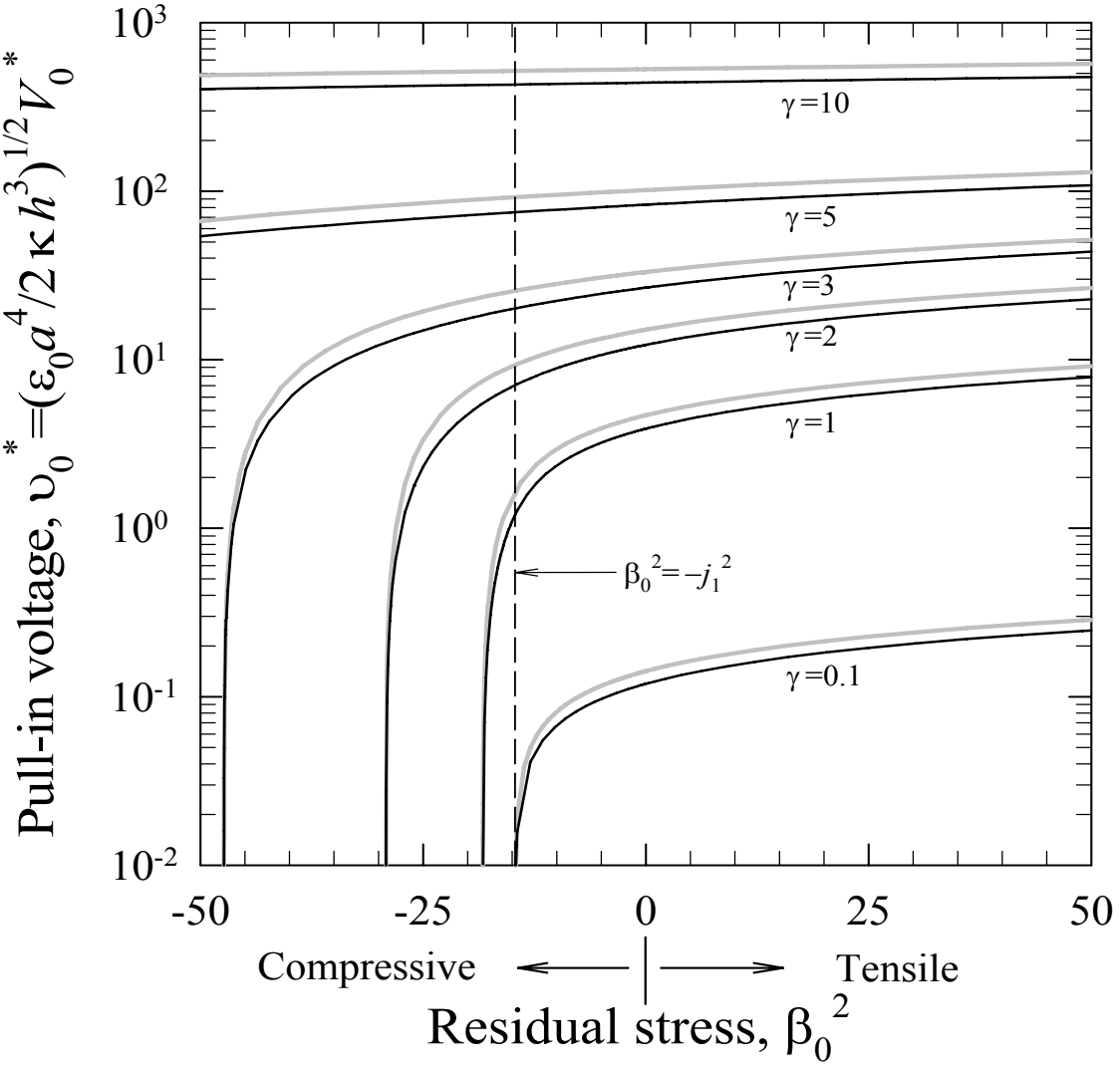

Figure 10 Pull-in voltage as a function of the residual stress for a range of film-pad gap. With force balance (grey curves) and energy balance (dark curves).

PAPER III

"Pull-in" of a Pre-stressed Thin Film by an Electrostatic Potential: A 1-D Rectangular Bridge

Gang Duan, Kai-tak Wan

Mechanical Engineering, University of Missouri-Rolla, Rolla, MO 65409-0050

Abstract

A 1-D rectangular pre-stressed thin film clamped at two opposite ends is loaded by an electrostatic potential applied to a pad directly underneath. The pre-stress is allowed to be either tensile or compressive in nature. At a critical applied potential, the film becomes unstable and makes direct contact with the pad, leading to "pull-in". A simple elastic model is constructed to account for the phenomenon for ranges of film-pad gap and residual stress. The results compare favorably with finite element analysis (FEA) in the literature and possess some advantages over other available closed-form solutions.

Keywords: thin film, residual stress, pull-in, electrostatic potential

1. Introduction

In our previous paper [1], we derived the electromechanical behavior of a 2-D axisymmetric membrane clamped at the periphery, and discussed a number of applications in RF-switches and micro-pumps. The present paper is an extension to a 1-D bridge, i.e. rectangular membrane, clamped at the opposite ends with an electrostatic pad

directly underneath. Results from this model, especially the "pull-in" behavior, are rigorously compared with the literature. In addition to our previous work, tensile / compressive membrane stress and the fringing field effects due to finite bridge width are also considered.

2. Theory

2.1. Mechanical deformation of the film

Figure 1 shows a bridge of thickness, h, width, b, and length, 2ℓ, clamped at two opposite ends. An electrostatic pad of the same width and same length lies directly underneath with a bridge-gap separation, g. The bridge possesses a longitudinal residual stress, σ_0 ($\sigma_0 > 0$ for tensile and $\sigma_0 < 0$ for compressive). The bridge, possessing an elastic modulus, E, Poisson's ratio, ν, and flexural rigidity, $\kappa = Ebh^3/12(1-\nu^2)$, is compelled by a pad voltage, V_0, deforming it into a profile, $w(x)$. A concomitant membrane stress, σ_m, as a result of the bridge deformation, results in a total membrane stress, $\sigma = \sigma_m + \sigma_0$. For simplicity, a list of normalized variables given in Table 1 is used hereafter. The total membrane stress, β^2, can be either tensile ($\beta^2 > 0$) or compressive ($\beta^2 < 0$ or $\beta = i|\beta|$ with $i = \sqrt{-1}$). Linear elasticity requires [2-5]

$$-\kappa \nabla^4 w + (\sigma hb) \nabla^2 w = -\left(1+0.65\frac{w}{b}\right)\left(\frac{\varepsilon_0 V_0^{\,2}}{2}\right)\frac{b}{(g-w)^2} \qquad (1)$$

where ε_0 is the permittivity of free space and $\nabla^2 \equiv \partial^2 / \partial x^2$ is the Laplacian operator. The mechanical deformation of the bridge (LHS) is balanced by the electrostatic attraction (RHS) with the fringing field effects governed by the first bracket. The nonlinear differential equation (1) can be solved using the Dugdale-Barenblatt-Maugis cohesion

zone approximation as in our previous work [6]. The electrostatic force in (1) is replaced by a uniform pressure, p, yielding

$$\omega'''' - \beta^2\omega'' = \rho \tag{2}$$

where $' = d/d\xi$. If pressure leading to bridge deformation is given by ρ_M and that as a result of electromagnetic attraction is ρ_C, then $\rho_M = \rho_C = \rho$ at equilibrium. The electromagnetic pressure is averaged over the bridge span and is given by

$$\rho_C = \upsilon_0^{\,2} \int_0^1 \left(1 + 0.65\frac{\omega(\xi)}{\tau}\right)\frac{1}{[\gamma - \omega(\xi)]^2}\,d\xi \tag{3}$$

The boundary conditions are given by $\omega|_{\xi=0} = 0$, $(\partial\omega/\partial\xi)|_{\xi=0} = 0$, and $(\partial\omega/\partial\xi)|_{\xi=1} = 0$. In case of tensile residual stress, an analytical solution to (2) is found to be

$$\omega = \rho_M\left(\frac{1}{\beta^3}\right)\left\{\frac{1}{\tanh\beta}[\cosh(\beta\xi) - 1] - \sinh(\beta\xi) + \beta\left(\xi - \frac{\xi^2}{2}\right)\right\} \tag{4}$$

with a central deflection, $\omega_0 = \omega|_{\xi=1}$, given by

$$\omega_0 = \rho_M\left(\frac{1}{\beta^3}\right)\left\{\frac{1}{\tanh\beta}(\cosh\beta - 1) - \sinh\beta + \frac{\beta}{2}\right\} \tag{5}$$

The concomitant membrane stress is found to be

$$\begin{aligned}\beta_m^{\,2} &= 6\int_0^1 \left(\frac{\partial\omega}{\partial\xi}\right)^2 d\xi \\ &= \rho_M^{\,2}\left[\frac{(6+\beta^2)\cosh(2\beta) - 9\beta\sinh\beta\cosh\beta - 6 - 4\beta^2}{\beta^6\sinh^2\beta}\right]\end{aligned} \tag{6}$$

In case of compressive residual stress, all β's are replaced by $i\,|\beta|$ such that $\sinh(ix) = i\sin(x)$, $\cosh(ix) = \cos(x)$, and $\tanh(ix) = i\tan(x)$. When $\beta_0^2 = \left(\beta_0^{\dagger}\right)^2 = -\pi^2$, β_m approaches infinity and the bridge intrinsically buckles towards the pad even in the absence of external field. The superscript † denotes buckling. This is in consistent with the Euler

criterion, $\sigma_0^{\dagger} = -\pi^2(\kappa/\ell^2 bh)$ which sets an upper bound for the compressive residual stress [7].

2.2. The electro-mechanical behavior

The coupled electromagnetic and mechanical behavior of the bridge is here derived by (i) a force balance and (ii) a thermodynamic energy balance. As stated in our previous work [6], the two approaches are expected to yield the same result, but the cohesive zone approximation leads to some differences. In the force balance, the electromagnetic pressure obtained from (3) equals to the mechanical pressure from (6), yielding a stable equilibrium configuration, $\rho_M = \rho_C$. At "pull-in", $\upsilon_0 = \upsilon_0^*$ and $\partial\rho_M/\partial\beta_m = \partial\rho_C/\partial\beta_m$. An incremental increase with $\upsilon_0 > \upsilon_0^*$ leads to "pull-in" and the bridge spontaneously collapses onto the pad. Alternatively, in an energy balance, total energy of the device is written as the sum of energy stored in the capacitive dielectric medium at the bridge-pad gap and the elastic energy stored in the bridge, such that

$$U_T = -\frac{\varepsilon_0 V_0^2}{2}\int_0^{2\ell}\left(1+0.65\frac{w}{b}\right)\frac{b\,dx}{g-w} + \int p\,dV$$

$$\text{or}\quad \Sigma_T = -2\upsilon_0^2\int_0^1\left(1+0.65\frac{\omega}{\tau}\right)\frac{d\xi}{\gamma-\omega} + \int \rho\,d\vartheta \qquad (7)$$

with V the volume of the bridge-pad gap. Stable equilibrium is maintained when $(\partial\Sigma_T/\partial\beta_m) = 0$ and $[\partial^2\Sigma_T/\partial(\beta_m)^2] < 0$. At $\upsilon_0 = \upsilon_0^*$, $(\partial\Sigma_T/\partial\beta_m) = [\partial^2\Sigma_T/\partial(\beta_m)^2] = 0$, i.e. neutral equilibrium.

The bridge width plays a significant role in the device behavior because of the fringing effects. We will first discuss the limit of an infinite width $\tau \to \infty$ before addressing finite τ. Figures 2-3 show graphically the device behavior according to force balance (grey) and energy balance (dark) with a large film width $\tau \to \infty$. Figure 2 shows the bridge deformation as a function of applied voltage for a fixed gap ($\gamma = 1$) and a range of residual stresses as indicated. As υ_0 increases from null, stable equilibrium is maintained until "pull-in" occurs when $\omega_0(\upsilon_0)$ meets the "pull-in" curve $\omega_0^*(\upsilon_0^*)$, i.e. curve OABCDE. It is interesting to note that $\omega_0^* \approx 0.4$ is virtually independent of tensile residual stress ($\beta_0^2 \geq 0$), but ω_0^* increases sharply for an increasing compressive stress ($\beta_0^2 < 0$). Involuntary "pull-in" and device failure occur at point O with $\beta_0^2 = \left(\beta_0^\dagger\right)^2$. Figure 3 shows $\upsilon_0^*(\gamma)$. Deformation of a thick and stiff bridge and small gap ($\gamma \leq 0.1$) is dominated by plate-bending and $\upsilon_0^* \propto \gamma^{3/2}$. In contrary, in a thin and flexible bridge with a large gap ($\gamma \geq 10$) membrane-stretching prevails and $\upsilon_0^* \propto \gamma^{5/2}$. Non-buckled bridge with $\beta_0^2 > -\pi^2$ exercises a bending-stretching transition at larger γ as β_0^2 increases. When the bridge buckles with $\beta_0^2 = -\pi^2$, the bending-stretching transition disappears such that $\upsilon_0^* \propto \gamma^{5/2}$. A finite bridge width causes the device behavior to deviate from the infinite τ-limit. Figures 4 and 5 show $\omega_0^*(\gamma)$ and $\upsilon_0^*(\gamma)$ for a range of τ based on force balance, respectively. The $\tau \to \infty$ limit serves as upper bound in both cases. Significant deviation is expected for larger gaps ($\gamma > 0.1$).

3. Discussion

It is worthwhile to compare our model with closed-form models, FEA results, and experimental data in literature. Osterberg and Senturia [2] reported CoventorWare FEA data for a range of device dimension, which were experimentally verified. Six device specifications for wide bridge and small gap are listed in Table 2. The pull-in voltage from our model and other published closed-form models are listed in Table 3 for comparison. All models other than Osterberg's [8-10] are derived from the classical lumped-model where a stiff and non-deformable bridge is attached to a theoretical spring to supply the mechanical restoring force. The effective spring constant accounts for the intrinsic elastic properties, residual stress and membrane stretching. Such simple model has a number of significant shortcomings. For instance, the non-deformable bridge leads to a "pull-in" deflection of $\omega_0^* / \gamma = 1/3$, independent of membrane stress and bridge-pad gap, which is clearly counterintuitive and contradictory to experimental measurements. Another consequence is the error in estimating the "pull-in" voltage. Some authors introduce a correction coefficient to minimize the deviation from FEA, e.g. $\upsilon_0^* = \alpha \times (\upsilon_0^*)_{\text{model}}$ with α = 1.09 obtained by curve-fitting for wide film with small gap [10]. Comparison can also be made for bridges with large gap shown in Table 4. The pull-in voltage predicted from FEA, closed-form models, and our model are listed in Table 5. Osterberg's empirical model [2] and O'Mahony's model [9] do not account for concomitant stress especially in case of large deflection and thus deviate significantly from FEA in case 9. Tilmans' model [11] considers neither the fringing field nor the concomitant stress and thus leads to large deviation in cases 7 and 9. Chowdhury's model [10], though allowing nonlinear stretching for large deflection and fringing field, is essentially an

extension of the lumped model and thus requires introduction of a correction factor to minimize the deviation. Pamidighantam's model [8], also based on the lumped-model, seems to predict a better pull-in voltage (Table 5), but a different correction factor is chosen for individual device dimension. A distinct advantage of the present model is the rigorous derivation of the deformed bridge profile and the associated "pull-in" from the first principles. It is clear from Table 3 that the energy method yields consistent results comparable to FEA. The force method leads to a large deviation at roughly 11% in all cases, due to the fact that the pressure variation along the bridge span is wiped out. Another important consequence of the present model is that the "pull-in" deflection and voltage are expressed in terms of (i) materials parameters: stiffness, flexural rigidity, and residual stress of the bridge, (ii) geometrical parameters: film length, width, thickness, and bridge-pad gap, and (iii) structural index: mixed bending-stretching deformation mode. These provide important design criteria for the device performance and reliability.

Recently, Zhang and Zhao [12] elegantly expressed the deformed bridge profile in terms of a Taylor series and adopted the Galerkin method to solve the nonlinear differential equation (1). While ignoring the fringing field, the pull-in central deflection is found to be $0.42 < (\omega_0^* / \gamma) < 0.68$, which falls into the range predicted by the present model. Besides the consistency, our model explains the physical cause of the spread, namely, the transition from plate-bending to membrane-stretching in the presence of residual stresses. The relation between pull-in displacement and residual stress $\omega_0^*(\beta_0^2)$ computed by Zhang are also consistent with the present model as shown in Figure 6. Most of Zhang's data fall within the window bounded by force balance and energy balance, and are in fact in the vicinity of the force balance. The small deviation is

likely the consequence of round-up errors and the bending-stretching transition. The buckling limit is $\beta_0^2 = -\pi^2$. The contact limit represents the critical compressive residual stress required to force the bridge to touch the pad in the mid-span, and is here given by $\beta_0^2 = -14.4$. The data point for $\beta_0^2 = -25$ by Zhang falls out of the allowable range.

4. Conclusion

A rigorous analytical elastic model is derived to account for the electromechanical behavior of a pre-stressed 1-D rectangular bridge in terms of the device geometry, materials, and structure. The coupling effects of residual stress and the ratio of the film-pad gap and film width to film thickness, (*b/h*) and (*g/h*), are found to play a significant role in the device behavior. A small film-pad gap, $\gamma < 0.5$, requires $\upsilon_0^* \propto \gamma^{3/2}$ and the residual stress effects dominates due to a small concomitant membrane stress ($\beta_0 >> \beta_m$) and fringing field effect. A large film-pad gap, $\gamma > 5$, requires $\upsilon_0^* \propto \gamma^{5/2}$ for wide film, and the behavior approaches $\upsilon_0^* \propto \gamma^{3/2}$ with a decreasing film width because of a large concomitant membrane stress ($\beta_m \geq \beta_0$). The results are consistent with published data in the public domain. The trends and graphs obtained are crucial in designing MEMS switches.

Acknowledgements

Support from the NSF CMS-0527912 is acknowledged.

References

1. G. Duan and K.-T Wan, "'Pull-in' of a Pre-stressed Thin Film by an Electrostatic Potential: A 2-D Axisymmetric Plate," *Journal of Applied Mechanics*, submitted.
2. P. Osterberg and S. Senturia, "M-Test: a test chip for MEMS material property measurement using electrostatically actuated test structures," *Journal of Microelectromechanical Systems* **6**, 107-118, 1997.
3. R. Gupta, *Electrostatic pull-in test structure design for in-situ mechanical property measurements of Micro-Electro-Mechanical Systems (MEMS). Ph.D. Thesis, MIT, USA*, 1997.
4. S.P. Timoshenko and S. Woinowsky-Krieger, *Theory of Plates and Shells*. 2 ed, McGraw-Hill, New York, 1959.
5. P.L. Gould, *Analysis of Shells and Plates*, Springer, New York, 1988.
6. G. Duan and K.-T Wan, "Analysis of 1-D and 2-D Thin Film "pull-in" Phenomena under the Influence of an Electrostatic Potential," *Journal of Applied Mechanics*, accepted.
7. S.P. Timoshenko and J.M. Gere, *Theory of Elastic Stability*. 2 ed, McGraw-Hill, New York, 1961.
8. S. Pamidighantam, R. Puers, K. baert, and H. A. C. Tilmans, "Pull-in voltage analysis of electrostatically actuated beam structures with fixed-fixed and fixed-free end conditions," *Journal of Micromechanics and Microengineering* **12**, 458-464, 2002.
9. C. O'Mahony, M. Hill, R. Duane and A. Mathewson, "Analysis of electromechanical boundary effects on the pull-in of micromachined fixed-fixed beams," *Journal of Micromechanics and Microengineering* **13**, S75-S80, 2003.

10. S. Chowdhury, M. Ahmadi, and W. C. Miller, "Pull-in voltage study of electrostatically actuated fixed-fixed beams using a VLSI on-chip interconnect capacitance model," *Journal of Microelectromechanical Systems* **15**, 639-651, 2006.
11. H. A.C. Tilmans and R. Legtenberg, "Electrostatically driven vacuum-encapsulated polysilicon resonators: Part II. Theory and performance," *Sensors and Actuators A* **45**, 67-84, 1994.
12. Y. Zhang and Y.-P. Zhao, "Numerical and analytical study on the pull-in instability of micro-structure under electrostatic loading," *Sensors and Actuators A* **127**, 366-380, 2006.

Table 1. Normalized parameters.

Coordinates and profile	$\xi = \left(\frac{1}{\ell}\right)x,\ \omega = \left(\frac{1}{h}\right)w,\ \omega_0 = \left(\frac{1}{h}\right)w_0,\ \vartheta = \left(\frac{1}{bh\ell}\right)V$
Device geometry (film-pad gap)	$\gamma = \left(\frac{1}{h}\right)g,\ \tau = \left(\frac{1}{h}\right)b$
Electrostatic potential (applied voltage)	$\upsilon_0 = \left(\frac{\varepsilon_0 b\ell^4}{2\kappa h^3}\right)^{1/2} V_0,$
Membrane stresses	$\beta_m^2 = \left(\frac{\ell^2 bh}{\kappa}\right)\sigma_m,\ \beta_0^2 = \left(\frac{\ell^2 bh}{\kappa}\right)\sigma_0,\ \beta^2 = \beta_m{}^2 + \beta_0{}^2$
Equivalent pressure	$\rho = \left(\frac{b\ell^4}{\kappa h}\right)p$
Total energy	$\Sigma_T = \left(\frac{\ell^3}{\kappa h^2}\right)U_T$

Table 2. Device with wide film and small gap ($E = 169$GPa, $\nu = 0.06$, width $b = 50\mu$m, $h = 3\,\mu$m, $g = 1\mu$m)

Specifications	**Case 1**	**Case 2**	**Case 3**	**Case 4**	**Case 5**	**Case 6**
Film length, 2ℓ (μm)	250	250	250	350	350	350
Residual stress, σ_0 (MPa)	0	100	–25	0	100	–25

Table 3. Pull-in voltage, V_0^*, for wide film and small gap indicated in Table 2. The parentheses are the percentage deviation from CW FEA.

Model	**Case 1**	**Case 2**	**Case 3**	**Case 4**	**Case 5**	**Case 6**
CW FEA	40.1	57.6	33.6	20.3	35.8	13.7
Ref. [2]	39.5 (1.5%)	56.9(1.2%)	33.7(0.3%)	20.2(0.5%)	35.4(1.1%)	13.8(0.7%)
Ref. [11]	39.31(2.0%)	57.45(0.3%)	33.26(1.0%)	20.06(1.2%)	36.02(0.6%)	13.35(2.6%)
Ref. [8]	40.38(0.7%)	58.87(2.2%)	34.12(1.5%)	20.6(1.5%)	36.77(2.7%)	13.63(0.5%)
Ref. [9]	39.1(2.5%)	56.85(1.3%)	33.22(1.1%)	19.95(1.7%)	35.6(0.6%)	13.45(1.8%)
Ref. [10]	39.6(1.3%)	57.4(0.3%)	33.71(0.3%)	20.2(0.5%)	35.91(0.3%)	13.71(0.1%)
Present Model						
Force balance	44.3(10.4%)	64.7(12.3%)	37.2(10.7%)	22.6(11.3%)	40.2(12.3%)	14.5(5.8%)
Energy balance	39.5(1.5%)	58.26(1.1%)	33.0(1.8%)	20.2(0.5%)	36.4 (1.7%)	13.6(0.7%)

Table 4. Device specifications for large gap ($2\ell = 300\mu m$ and $\nu = 0.33$)

Specifications	**Case 7**	**Case 8**	**Case 9**
Elastic modulus (GPa)	77	70	77
Film width (μm)	0.5	10	50
Film thickness (μm)	1	1	0.5
Film-pad gap (μm)	1	2	6
Residual stress (MPa)	0	60	0

Table 5. Pull-in voltage, V_0^*, for large gap indicated in Table 4.

Model	**Case 7**	**Case 8**	**Case 9**
CW FEA (standard)	2.81	39.7	90.0
Ref. [2]	2.63(6.4%)	35.5(10.6%)	18.1(79.8%)
Ref. [11]	3.54(26.0%)	38.6(2.8%)	18.4(79.5%)
Ref. [8]	2.87(2.1%)	37.7(5.0%)	75.8(15.4%)
Ref. [9]	2.57(8.5%)	36.2(8.8%)	19.5(78.2%)
Ref. [10]	2.16(23.1%)	43.9(10.6%)	67.9(24.2%)
Present Model			
Force balance	3.8(35.2%)	47.8(20.4%)	119.5(33.3%)
Energy balance	2.65(5.7%)	42.5(7.0%)	105.9(18.1%)

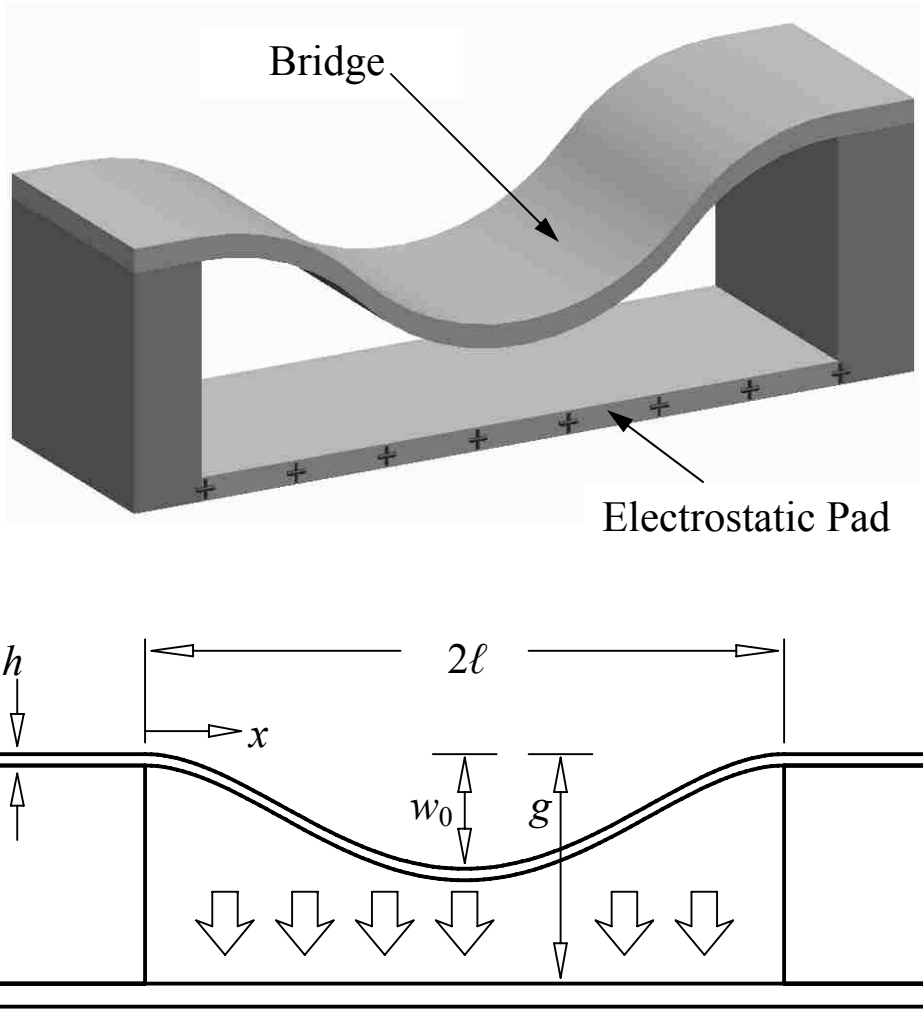

Figure 1 Sketch of the MEMS-RF-switch. The deformed profile of the film under an electrostatic force induced by the pad directly underneath is shown.

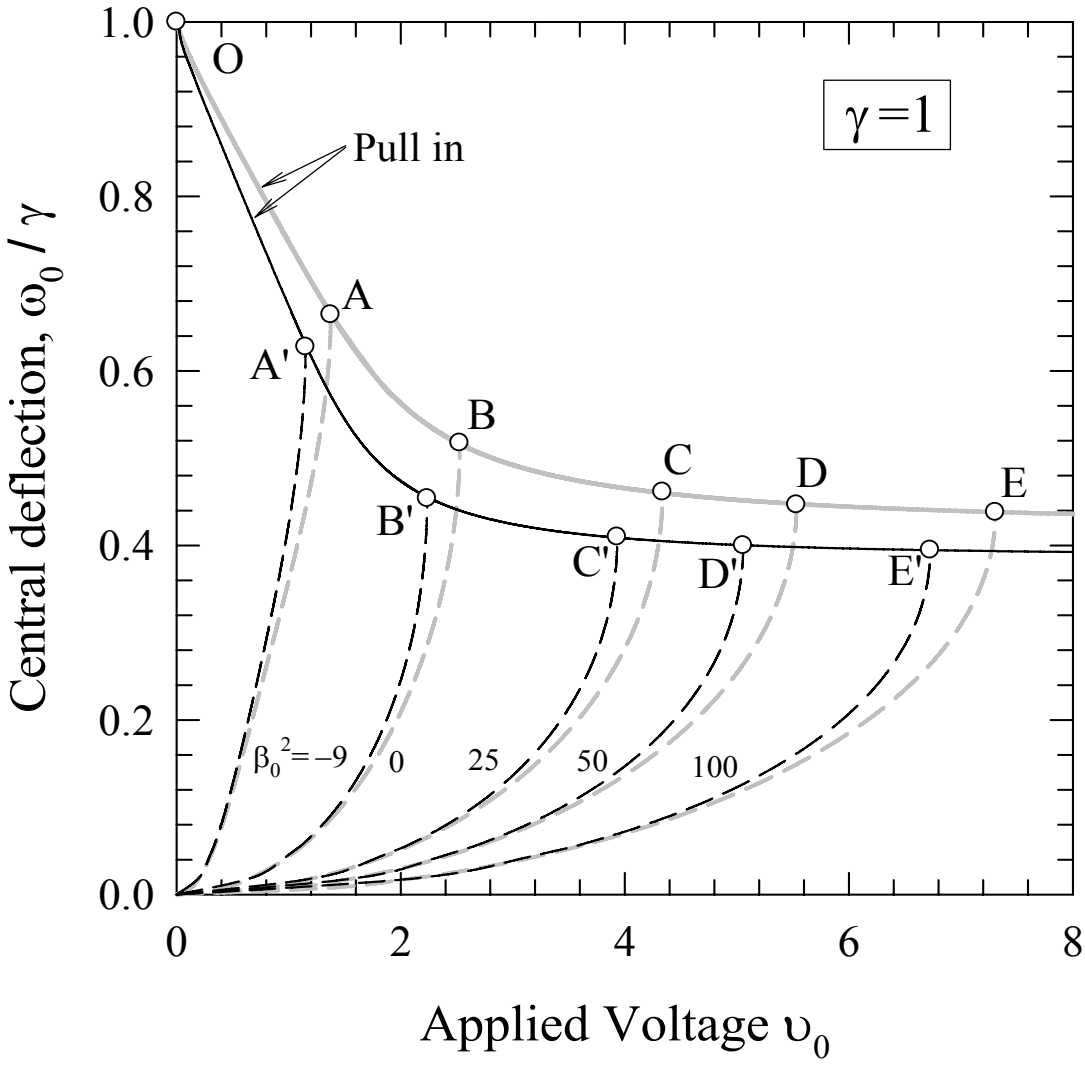

Figure 2 Film central deflection as a function of the applied electrostatic voltage. The dashed curves show the film behavior before pull-in, and the solid curves show the pull-in central deflection. Force balance (grey curves) and energy balance (dark curves).

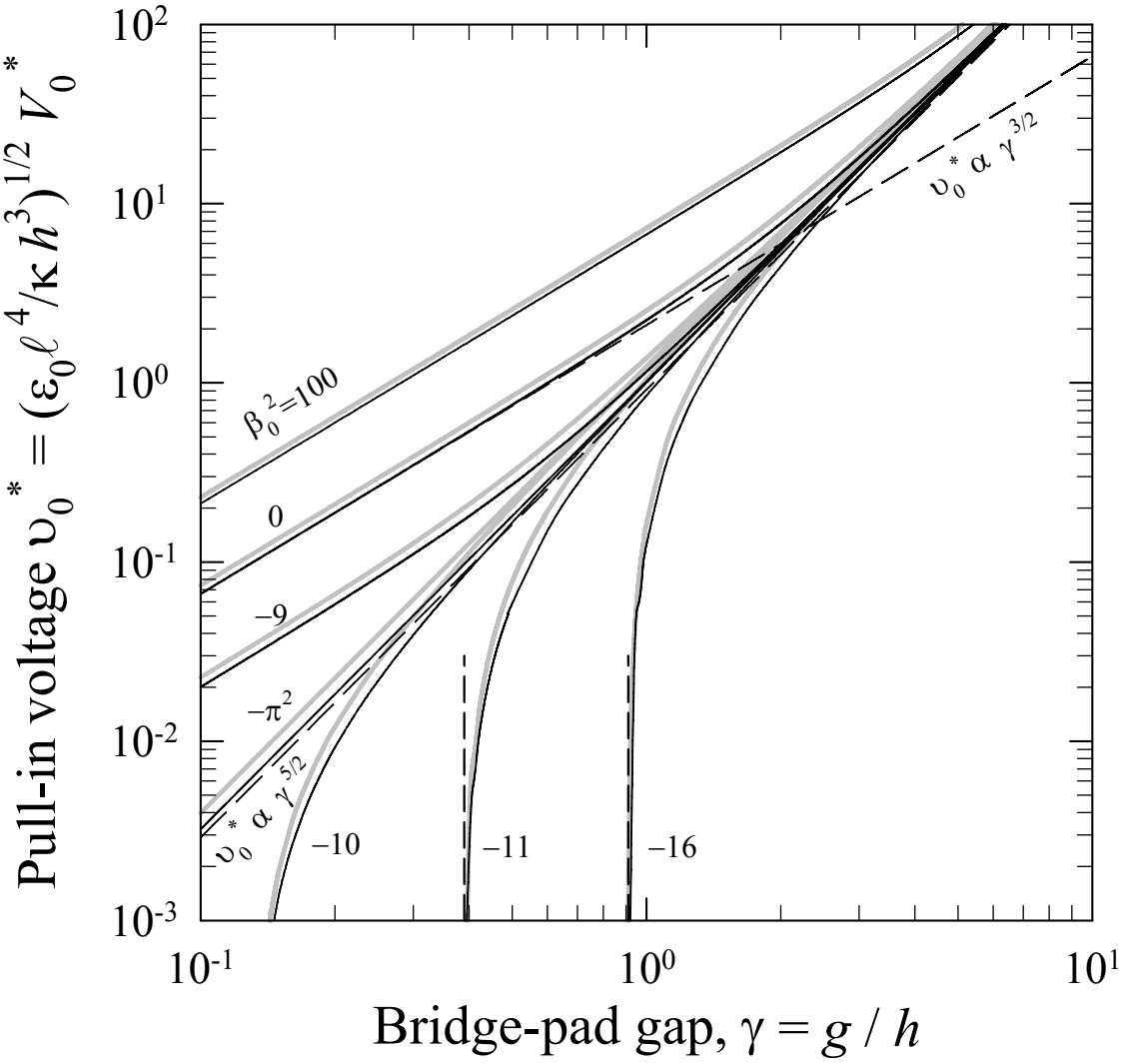

Figure 3 Pull-in voltage as a function of the film-pad gap with a range of residual stress. Force balance (grey curves) and energy balance (dark curves). The dashed curves show the plate-bending and membrane-stretching limits with zero residual stress.

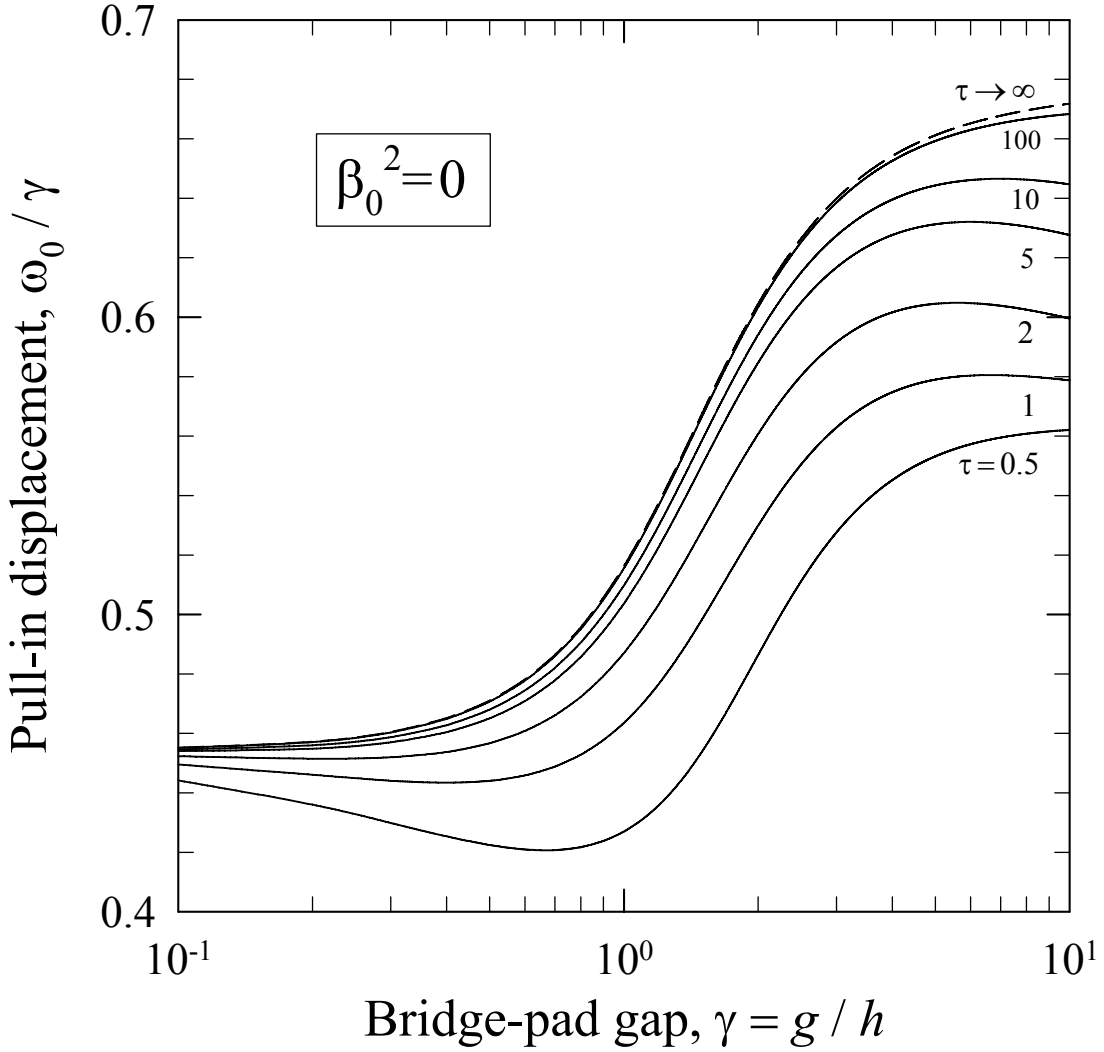

Figure 4 Pull-in displacement (w_0^*/g) as a function of the film-pad gap with a range of film width. Force balance (grey curves) and energy balance (dark curves).

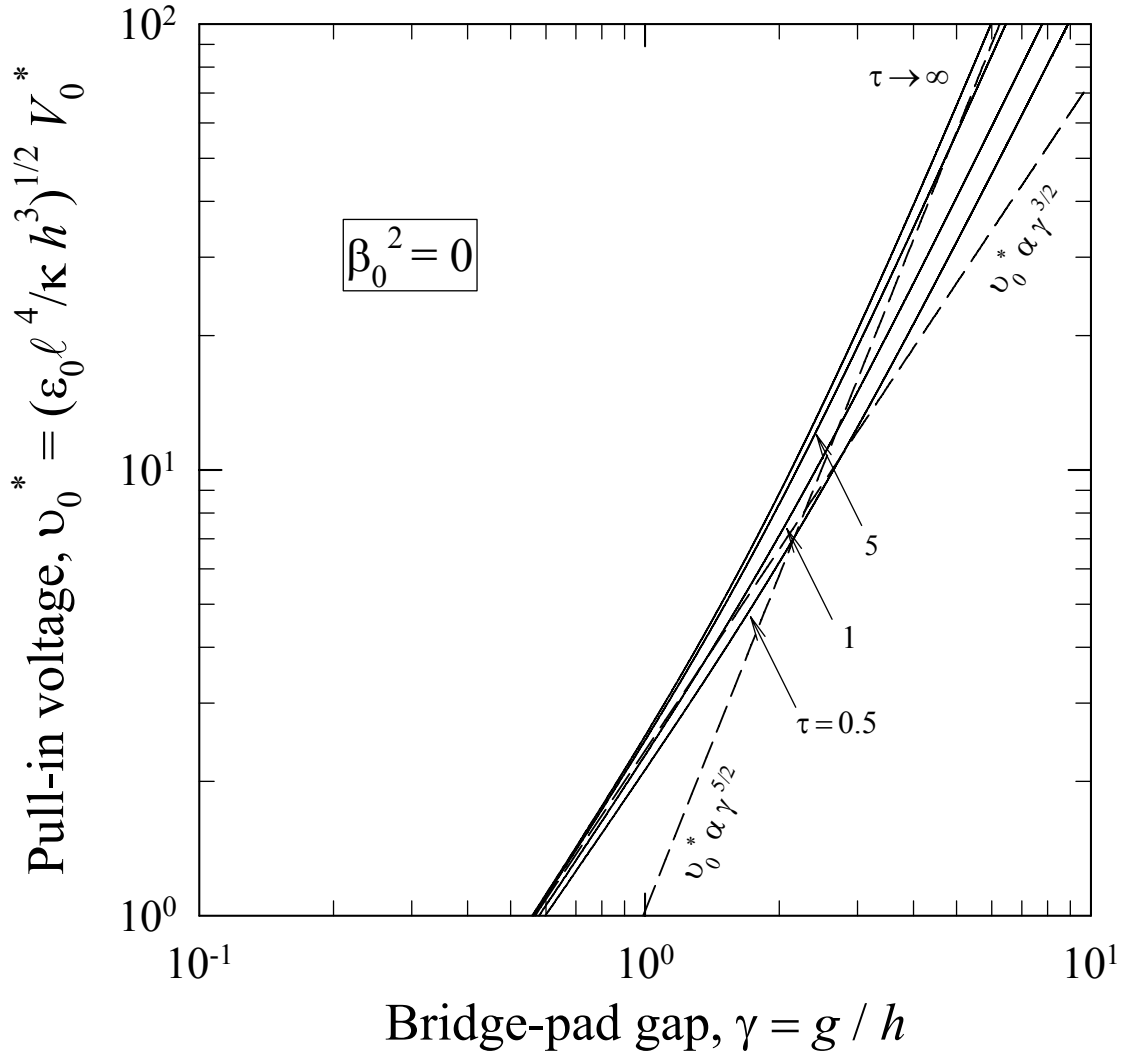

Figure 5 Pull-in voltage (υ_0^*) as a function of the film-pad gap with a range of film width. The dashed curves show the plate-bending and membrane-stretching limits with zero residual stress.

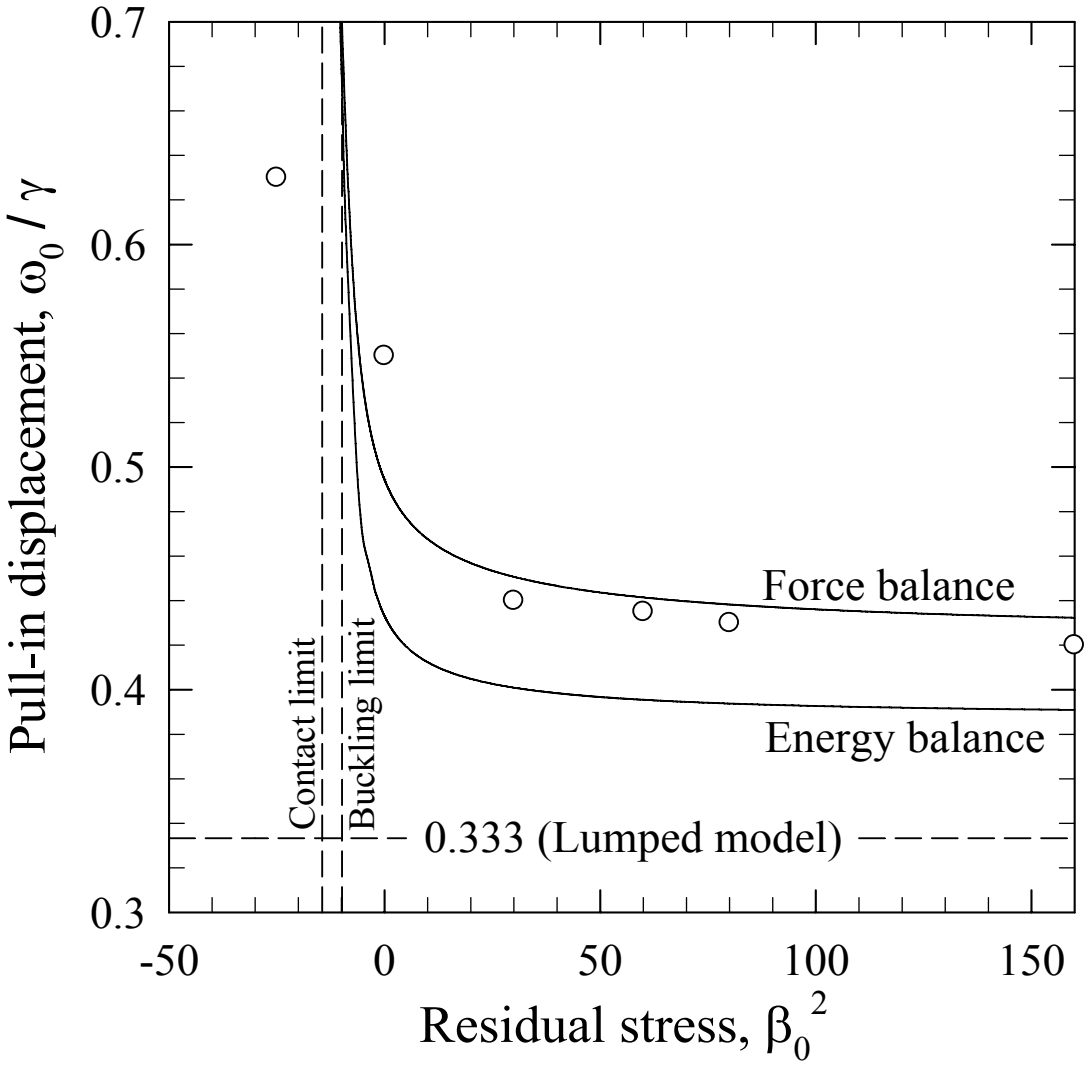

Figure 6 Pull-in displacement (w_0^*/g) as a function of residual stress. The two curves are derived using the present model, and the data points are given by Zhang et al [12].

APPENDIX A

THIN FILM ADHESION IN THE PRESENCE OF AN EXTERNAL ELECTRIC FIELD

Thin Film Adhesion in the Presence of an External Electric Field

Gang Duan and Kai-tak Wan

Department of Mechanical and Aerospace Engineering, University of Missouri-Rolla, Rolla, MO 65401, USA

1. Introduction

Electric actuated thin films are widely used in micro-electromechanical systems (MEMS) such as radio frequency switches (RF-switches), micropumps, and electrostatic actuators. In a typical MEMS-RF-switch, a rectangular thin film is clamped at both ends in the presence of an electrostatic potential (V_0) applied to a pad directly underneath the film. When the applied electrostatic potential exceeds a certain threshold, V_0^*, the film makes direct contact with the pad, leading to "pull-in". The critical "pull-in" voltage (V_0^*) & displacement (ω_0^*) were predicted in our previous work [1]. In this paper, a rigorous theoretical model is constructed for the contact mechanics of the transition from pre- to post- "pull-in" and the elastic recovery of the film at the removal of external electrostatic potential. The model provides (i) structural index of the film: mixed plate-bending and membrane-stretching; (ii) geometrical parameters: film-pad gap, film thickness and length span; and (iii) material parameters of the film: elastic modulus and Poisson ratio. A critical film-pad gap, $\gamma^\dagger$, is determined. Should the gap fall below $\gamma^\dagger$, the film can no longer return to the undeformed planar geometry due to the adhesion even at the removal of external electrostatic potential. The theoretical results have significant impacts on the design and fabrication of many MEMS devices and nano structures.

2. Theory

2.1. 1-D electromechanical RF-switch

Figure 1 shows a 1-D rectangular thin film clamped at the two opposite ends and suspended above an electrode-pad with a distance, g, and a dielectric layer coated on the pad with thickness, g_0. The film is assumed to be free of pre-stress and possesses a unit width, length, 2ℓ, thickness, h, elastic modulus, E, Poisson's ratio, v, flexural rigidity, $\kappa=Eh^3/12(1-v^2)$. A uniform electric field is set up by an electrical potential, V_0. The film is compelled and deformed to a profile, $w(x)$ with central displacement w_0.

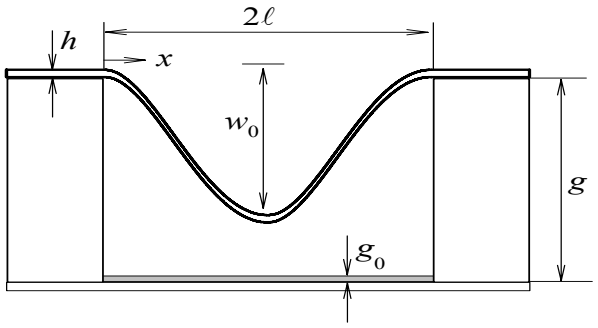

Fig.1. an RF-switch pre-"pull-in".

When the applied electrostatic potential exceeds a certain threshold, V_0^*, the film makes direct contact with the pad, leading to "pull-in", with contact length, $2c$, shown in Figure 2.

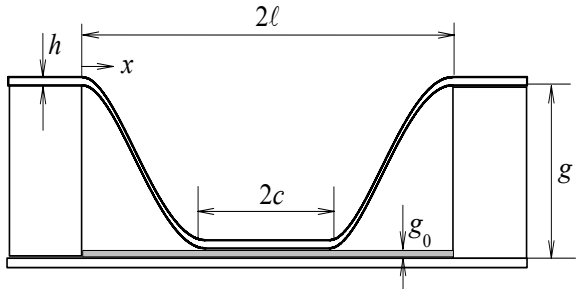

Fig.2. an RF-switch post-"pull-in".

After the "pull-in" phenomenon takes place, the thin film is compelled and deformed by bending and a longitudinal membrane stress, σ, to a profile, $w(x)$, governed by [2,3]

$$\underbrace{-\kappa\,\nabla^4 w}_{\substack{\text{Plate-}\\\text{bending}}} + \underbrace{(\sigma h)\,\nabla^2 w}_{\substack{\text{Membrane-}\\\text{stretching}}} = \underbrace{-\left(\frac{\varepsilon_0 V_0^{\,2}}{2}\right)\frac{1}{(g-w)^2}}_{\text{Electrostatic force}} \tag{1}$$

With boundary conditions: $w_{x=0} = 0$, $(\partial w/\partial x)_{x=0} = 0$, and $(\partial w/\partial x)_{x=\ell-c} = 0$. The coupled electro-mechanical behavior leads to nonlinearity of (1) and therefore forbids an analytical solution. The Dugdale-Barenblatt-Maugis cohesive zone model is adopted to decouple the two components and the electrostatic force (RHS of (1)) is replaced by a uniform mechanical pressure, p, given by

$$p = \frac{\varepsilon_0 V_0^{\,2}}{2(\ell-c)} \int_0^{\ell-c} \frac{1}{[g-w(x)]^2}\, dx \tag{2}$$

Solving (1) analytically, the film profile becomes

$$\omega = \rho\left(\frac{1}{\beta^3}\right)\left\{\frac{\lambda\cosh[\beta(\lambda-\xi)]}{\sinh(\beta\lambda)} - \frac{\lambda}{\tanh\beta\lambda} + \beta\left(\lambda\xi - \frac{\xi^2}{2}\right)\right\} \tag{3}$$

The normalized parameters are defined as $\xi = x/\ell$, $\omega = w/h$, $\gamma = g/h$, $\alpha = g_0/g$, $\lambda = 1 - c/\ell$, $\rho = (\ell^4/\kappa h)\,p$, $\beta = (\ell^2 h/\kappa)^{1/2}\sigma^{1/2}$, $\upsilon_0 = (\varepsilon_0\ell^4/2\kappa h^3)^{1/2} V_0$, and $\Sigma = (\ell^3/\kappa h^2)U$. A simple energy balance is constructed as follows. The total energy of the system is given by $U_T = U_C - U_E$, where U_C is energy stored in the dielectric gap, and U_E is elastic energy stored in the film. With

$$U_C = -\frac{\varepsilon_0 V_0^{\,2}}{2} \int_0^{\ell-c} [g-w(x)]^{-1}\, dx \tag{4}$$

and

$$U_E = \underbrace{-\frac{\kappa}{2}\int_0^{\ell-c}\left(\frac{\partial^2 w}{\partial x^2}\right)^2 dx}_{\text{Bending Energy}} \underbrace{-\frac{Eh}{4}\int_0^{\ell-c}\left(\frac{\partial w}{\partial x}\right)^4 dx}_{\text{Stretching Energy}} \tag{5}$$

The stable equilibrium can be found by putting $(\partial U_T / \partial c) = 0$ and $[\partial^2 U_T / \partial c^2] < 0$, or $(\partial \Sigma_T / \partial \lambda) = 0$ and $[\partial^2 \Sigma_T / \partial \lambda^2] < 0$. The general behavior of the thin film requires numerical integration. The bending limit is chosen in this section to demonstrate the general behavior that is applicable also to mixed bending-stretching films. At equilibrium, λ can be found by

$$\lambda = \frac{(2\gamma)^{3/4}\left(\alpha - 2\alpha^2 + \alpha^3\right)^{1/4}}{\sqrt{\upsilon_0}} \tag{6}$$

The pull-in voltage for energy balance is $\upsilon_0^* = 2.1008\gamma^{3/2}$ from our previous work. [1] So the pull-in λ^* is given by

$$\lambda^* = 1.1603\left(\alpha - 2\alpha^2 + \alpha^3\right)^{1/4} \tag{7}$$

At the critical applied voltage υ_0^*, "pull-in" occurs and the film slams onto the pad. The pull-in λ^* only depends on the dielectric layer thickness, α, and λ^* increases with the increases of α, as shown in Figure 3. When the applied voltage υ_0 is larger than the "pull-in" voltage υ_0^*, the contact length between film and pad increases, or λ decreases. The critical pull-in λ^* (point A, B, and C) separates physically inaccessible region (grey dash line) from the pull-in phenomenon.

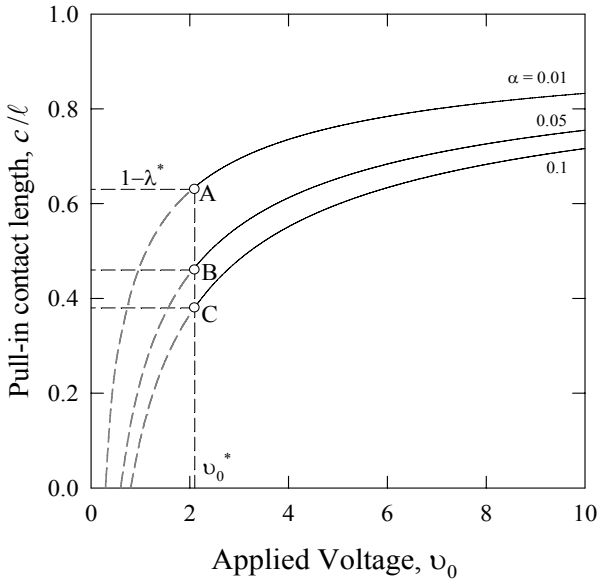

Fig.3. "Pull-in" non-contact length.

2.2. Interfacial adhesion of a 1-D rectangular thin film

The above 1-D model predicts the "pull-in" contact length for a certain applied voltage. In this section, we discuss the contact mechanics between the film and the pad post- "pull-in". Adhesion occurs when the film makes contact with the pad. Upon grounding the pad, the adhesive interface is supported by short-range attractions such as van der Waals interaction and water meniscus due to relative humidity in the environment. When the electrostatic potential is removed, the total energy of the system thus becomes $U_T = U_E - U_S$, where U_E and $U_S = \gamma_s (2c)$ are the elastic and surface energy, with γ_s, or $\Gamma = (\ell^4/\kappa h^2)\,\gamma_s$, the film-pad interfacial adhesion energy. The system total energy is illustrated in Figure 4 for a RF-switch with film-pad gap γ=1, α=0.05, and Γ=200, following the trajectory ABC.

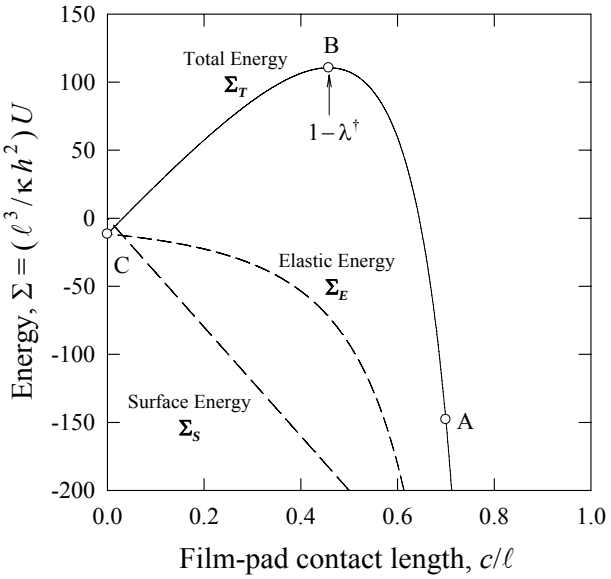

Fig.4. post- "Pull-in" system energy.

The unstable equilibrium (point B) can be found by putting $(\partial U_T / \partial c) = 0$ and $[\partial^2 U_T / \partial c^2] > 0$, or $(\partial \Sigma_T / \partial \lambda) = 0$ and $[\partial^2 \Sigma_T / \partial \lambda^2] > 0$. At equilibrium, "pull-off" $\lambda^\dagger$ becomes

$$\lambda^\dagger = \frac{2(6/5)^{1/4}\left[(1-\alpha)\gamma\right]^{1/2}}{\Gamma^{1/4}} \tag{8}$$

When $\lambda < \lambda^\dagger$, the system total energy increases with the increase of λ, so the system is stable. While λ goes beyond the unstable equilibrium point B, a spontaneous delamination between film and pad begins, the delamination is unstable, in that, the contact length shrinks spontaneously to zero and the film snaps from the pad. The critical film-pad gap $\gamma^\dagger$ leading to a spontaneous "pull-off" can be obtained by putting the "pull-in" λ^* equals the "pull-off" $\lambda^\dagger$,

$$\gamma^\dagger = \frac{12\upsilon_0^{\,2}}{5\alpha\Gamma} \tag{9}$$

3. Discussion

From the elastic model derived for the post- "pull-in" behavior of a thin film in a 1-D rectangular RF-switch, it is shown the critical "pull-in" λ^* only depends on the dielectric layer thickness, so a smaller dielectric layer can increase the "pull-in" contact length, leading to a larger film-pad contact area, thus a larger adhesion energy between the film and pad. When the film-pad gap, γ, is designed such that $\gamma < \gamma^\dagger$, removal of the electrostatic potential does not detach the film but leaves it in adhesive contact with the pad with a contact length given by (6). The critical film-pad gap $\gamma^\dagger$ is crucial in designing the device and assessing the performance, especially when the device dimensions shrink from micro- (MEMS) to nano- scale (NEMS). Failure to realize critical "pull-off" $\gamma^\dagger$ in design might render the device incapable to perform [4].

The results shown can be used to formulate certain design criteria: a larger "pull-in" contact length as a result of a higher operation potential or a smaller dielectric layer thickness will increase the adhesion energy between the film and pad, this implies a larger film-pad gap is needed for the film to obtain enough elastic energy to overcome the adhesion energy and return to "pull-off" state.

4. Conclusions

The post- "pull-in" behaviors of MEMS-RF-switch are derived. The trends and graphs given here will have significant impacts on the design and fabrication of many MEMS devices; especially those involve moveable rectangular thin films.

5. Acknowledgements

Supports from NSF CMS-0527912 and University of Missouri Research Board (#2428) are acknowledged.

References

1. G. Duan and K. T. Wan, J. Appl. Mech., in press.
2. K. T. Wan, J. Appl. Mech., 2002, 69, pp 110-116.
3. S. P. Timoshenko and S. Woinowsky-Krieger, Theory of Plates and Shells, 1959, 2nd Ed., McGraw Hill, New York.
4. MF Wong, G. Duan, and K. T. Wan, J. Appl. Physics, 2007,101, 024903, pp 1-7

APPENDIX B

ADHESION-DELAMINATION MECHANICS: APPLICATION TO MICRO BEAM NETWORK AND NANO STRUCTURES

The following is an extension of my work towards nano structures, and is already published in J Appl Phys [1]. The journal paper comprises contributions from me and another graduate student in Dr. Wan's research group, Ming-Fung Wong. Following is my own contribution in the paper, excluding Wong's work. The theoretical model is a rigorously constructed for the delamination mechanics of a pre-stressed rectangular film adhered to a rigid punch using a thermodynamic energy balance shown in Figure 1.

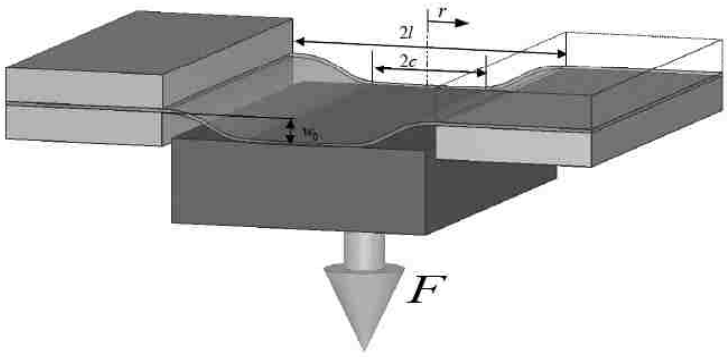

Fig.1. Sketch of the punch-film system

The total energy of the film-punch system is given by $U_T = U_P + U_E + U_S$, where the potential energy of the applied load, $U_P = F\ w_0$; the elastic energy stored in the overhanging non-contact film, $U_E = -(½)\ U_P = -(½)\ F\ w_0$, as a result of the linear $F(w_0)$; and the surface energy at the adhesive contact interface, $U_S = \gamma\ c$. Delamination occurs when $\partial U_T / \partial c > 0$. At equilibrium, the equal sign holds. As delamination proceeds, the contact area shrinks from both contact edges until equilibrium condition is satisfied. At every equilibrium stage of delamination, the punch displacement is related to the contact length $w_0(c)$. When the punch displacement reaches a critical value, a "pinch-off" (stable shrinking of the contact area to a line) is predicted.

Wu et al. [2] constructed micro beam network free of residual stress. The structure is prone to collapse if the individual beam length exceeds the detachment length, l_d, the maximum beam length to avoid stiction. When two adjacent beams separated by $2w_0^*$ adhere (Figure 2), Wu assumes a parabolic deformed beam profile.

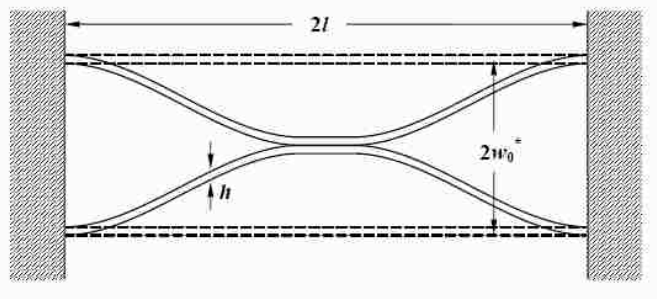

Fig.2. Sketch of two adjacent adhered micro-beams adhered

An energy method similar to the model [1] is used to derive

$$l_d = C\left[\frac{Eh^3}{\gamma}\right]^{1/4} (w_0^*)^{1/2} \tag{1}$$

with $C = (128/5)^{1/2} \approx 2.25$. Dimension analysis shows that the square bracket in (1) is a correct scaling parameter. There are, however, a number of minor inconsistencies when compared with the model [1]. Assuming a parabolic beam profile, the energy balance using the formulation [1] yields (1) with $C = 2$, and E is replaced by $E / (1 - \nu^2)$. The parabolic profile, in fact, posts difficulty because it does not satisfy the boundary condition at the clamped edge, $dw/dx = 0$ at $x = l$. If the correct profile (2) is used [1]

$$\omega = \varphi \left[\frac{1}{4}(1-\lambda)\,(1-\xi)^2 - \frac{1}{6}\,(1-\xi)^3\right] \tag{2}$$

the energy method requires $C = (48)^{1/4} \approx 2.632$. If the beams are subject to tensile residual stress as a result of thermal mismatch, shrinkage, or swelling, (1) remains valid as long as the residual stress σ_0 is smaller than

$$\sigma_0^{\dagger} = \left[\frac{2Eh\gamma}{27(1-\nu^2)}\right]^{1/2} \frac{1}{w_0^*} \tag{3}$$

For $\sigma_0 > \sigma_0^{\dagger}$, the beam stretching solution serves as a better solution. The profile is given by $\omega = \varphi(1-\xi)/\beta^2$ [1] and the detachment length becomes

$$l_d = \left[\frac{12Eh}{\gamma}\right]^{1/4} w_0^* \tag{4}$$

The detachment length scales as $l_d \propto (w_0^*)^{1/2}$ when the deformation is small and bending is dominant, and becomes $l_d \propto w_0^*$ when the deformation is large and beam stretching prevails. It is doubtful that a stretching-dominant deformation will occur, because the micro structure needs some degree of rigidity to retain its integrity and geometry.

References

1. M. F. Wong, G. Duan, and K. T. Wan, "Adhesion-Delamination Mechanics of a Pre-stressed Rectangular Film Adhered onto a Rigid Substrate." *Journal of Applied Physics*, **101**, 024903 2007.
2. D. Wu, N. Fang, C. Sun and X. Zhang, "Stiction problems in releasing of 3D microstructures and its solution." *Sensors and Actuators A: Physical* **128**, 109-115, 2006.

VITA

Gang Duan was born on December 20, 1978 in He County, Anhui, P. R. China. His pre-college education was taken in Ma'anshan, Anhui, P. R. China. He attended Hefei University of Technology where he received his B.S. and M.S. in Mechanical Engineering in 2000 and 2003, respectively.

Since August 2003, he joined Dr. Kai-tak Wan's group for his PhD program in Mechanical Engineering at University of Missouri-Rolla, Rolla, MO, USA. He has held a Graduate Research Assistantship and Graduate Teaching Assistantship during his study at University of Missouri-Rolla. In December 2007, he received his PhD in Mechanical Engineering from University of Missouri-Rolla.